약학박사 학위논문

Self-assembled nanoparticles of chitosan oligosaccaride derivatives for targeted delivery of anticancer drugs

2015년 8월

서울대학교 대학원

약학과 약제과학 전공

Termsarasab Ubonvan

Abstract

Self-assembled nanoparticles of chitosan oligosaccaride derivatives for targeted delivery of anticancer drugs

Termsarasab Ubonvan

Department of Pharmaceutical Science

College of Pharmacy

The Graduate School

Seoul National University

Chitosan oligosaccharide (CSO) derivatives were successfully synthesized and used for the development of self-assembled nanoparticles for targeted delivery of doxorubicin (DOX) as a model of anticancer drug. The novel amphiphilic polymer, arachidyl chistosan oligosaccharide (CSOAA), was firstly synthesized in this study. In addition, CSOAA was further developed by grafting polyethylene glycol (PEG) (CSOAA-PEG) and diethylenetriaminepentaacetic dianhydride (DTPA)-Gadolinium (III) (CSOAA-DTPA-Gd) on the CSOAA backbone for a prolonged drug circulation time in blood stream and improving intensity of contrast agent for

magnetic resonance imaging (MRI) of neoplastic lesions, respectively. The CSOAA formed self-assembled nanoparticles with nano-sized less than 200 nm in diameter, narrow particle size distribution, and low critical aggregation concentration (CAC) that could imply to stability of the nanoparticles. DOX-loaded CSOAA nanoparticles exhibited sustained drug released profile and improved drug releasing in acidic condition. *In vitro* cellular uptake of DOX in FaDu cells of the NPs-treated group were higher than free DOX group. *In vivo* antitumor efficacy of DOX-loaded CSOAA NPs was also verified in FaDu tumor xenografted mouse model. In the CSOAA-DTPA-Gd studies, the amount of Cy5.5-labled nanoprobes taken-up by FaDu and Hep-2 cells, as observed by confocal laser scanning microscopy (CLSM), increasing according to incubation time (up to 12 h). A phantom study of CSOAA-DTPA-Gd nanoprobes showed a T_1-positive contrast-enchancing effect, compared to that of the commercial formulation (Gd-DTPA; Magnevist®). In the CSOAA-PEG studies, the stability of nanoparticles were investigated that the mean diameter both of CSOAA and CSOAA-PEG nanoparticles remain in DDW over 72 h, but the mean diameter of CSOAA-PEG nanoparticles remained relatively constant in serum over 72 h, compared with CSOAA nanoparticles (changed of 20.92% and 223.16%, respectively). The uptake of DOX in the nanoparticles by K562 human leukemia cells was higher than DOX solution. From the pharmacokinetic studies in rats, *in vivo* clearance rate of DOX in the CSOAA-PEG nanoparticles group was slower than other groups (CSOAA nanoparticles and DOX solution groups), subsequently extending the circulation period. All of the results suggested that the synthesized CSO derivatives could be used for preparation in self-assembeld

nanoparticles as an effective candidate for targeted anticancer drug delivery and neoplastic diagnosis system. They could be applied for the other anticancer drugs to improve the specificity uptake of drugs at tumor site, thereny optimizing pharmacokinetics, antitumor efficacy, and side effect.

Keywords: Arachidyl chitosan, Gadolinium, Polyethylene glycol, Doxorubicin, nanoparticles, antitumor efficacy

Student Number: 2012-30774

Contents

List of Tables

PART I. Chitosan oligosaccharide–arachidic acid-based nanoparticles for anticancer drug delivery

PART II. Self-assembled magnetic resonance imaging nanoprobes based on arachidyl chitosan for cancer diagnosis

PART III. Polyethylene glycol-modified arachidyl chitosan-based nanoparticles for prolonged blood circulation of doxorubicin

List of Figures

PART I. Chitosan oligosaccharide–arachidic acid-based nanoparticles for anticancer drug delivery

PART II. Self-assembled magnetic resonance imaging nanoprobes based on arachidyl chitosan for cancer diagnosis

PART III. Polyethylene glycol-modified arachidyl chitosan-based nanoparticles for prolonged blood circulation of doxorubicin

PART I. Chitosan oligosaccharide–arachidic acid-based nanoparticles for anticancer drug delivery

1. Introduction

Polymeric nanoparticles have been widely investigated as drug carriers for anti-cancer agents (Cho et al., 2011; Choi et al., 2012; Kaida et al., 2010; Kolishetti et al., 2010; Yoon et al., 2012). Self-assembly based on amphiphilic polymer has been widely investigated because it has many interesting properties. Amphiphilic polymers can form stable nanoparticles composed of a hydrophobic core and a hydrophilic shell in an aqueous environment. Poorly water-soluble drugs can be encapsulated in the internal hydrophobic cavity, which can improve their solubility and bioavailability (Alibadi et al., 2005; Kwon, 2003; Li and Tan, 2008). The nano-size and hydrophilic shell of these self-assembled nanoparticles can impede elimination by the reticuloendothelial system (RES) and have an enhanced permeability and retention (EPR) effect as a passive targeting strategy, leading to effective accumulation of drugs at the tumor region (Maeda et al., 2000).

Doxorubicin (DOX) is an anthracycline antibiotic that is commonly used in the treatment of various types of cancer, such as hematological malignancies, breast carcinomas, ovarian carcinomas, bronchogenic carcinomas, and soft-tissue sarcomas. DOX has also exhibited therapeutic effects for head and neck cancer (Airoldi et al., 2008), which includes several types of tumor localized in the oral cavity, nose, throat, sinuses, and salivary glands (Cho et al., 2012a). The response rate for anti-cancer therapeutics is known to be relatively low in head and neck cancer, with a survival

benefit of about 10 weeks for patients with recurrent/metastatic disease (Reuter et al., 2007). Although DOX shows high potential anti-cancer efficacy, its clinical application is limited because of its severe side effects, especially cardiotoxicity and myelosuppression (Kratz et al., 2007; Wildiers et al., 2008). Therefore, it is thought that tumor-targeting strategy can minimize these side effects (Cho et al., 2012b).

Chitosan (CS) is a linear cationic polysaccharide composed of randomly distributed β-(1-4)–linked D-glucosamine and N-acetyl–D-glucosamine units, produced by the deacetylation of chitin. CS has been regarded as an attractive material for the development of drug delivery systems due to its biocompatibility, biodegradability, and low toxicity (Kumar et al., 2004; Muzzarelli and Muzzarelli, 2005). Moreover, CS has free primary amino groups, allowing for further chemical modification. However, the major drawback of CS is its poor solubility at physiological pH. Recently, many researchers have investigated chitosan oligosaccharide (CSO), a low-molecular-weight CS, because it can be soluble in water and several organic solvents under physiologically relevant conditions (Vishu Kumar et al., 2004). CSO has been modified with hydrophobic residues, such as alkyl groups, cholesterol, tocopherol, and deoxycholic acid (Chae et al., 2005). These hydrophobically modified CSOs can form self-assembled nanoparticles, which can be used as carriers for tumor-targeted drug and gene delivery.

In this study, arachidic acid (AA), as a fatty acid, was conjugated to a CSO backbone to make an amphiphilic CSO derivative. DOX was loaded into the self-assembled nanoparticles based on chitosan oligosaccharide–arachidic acid

(CSOAA). The physiochemical properties of DOX-loaded CSOAA-based nanoparticles, such as particle size, zeta potential and morphology, and *in vitro* drug release behavior were investigated. *In vitro* cytotoxicity and cellular uptake efficiency were evaluated in head and neck cancer cells, and *in vivo* anti-tumor efficacy were also assessed in the head and neck cancer xenografted mouse model.

2. Materials and methods

2.1. Materials

Chitosan oligosaccharide (CSO; average molecular weight = 5 kDa, degree of deacetylation > 90%) was purchased from Kitto Life Co., Ltd. (Seoul,Korea). Arachidic acid (AA), 1-ethyl-3-(3-dimethylaminopropyl) carbodiimide (EDC), N-hydroxysuccinimide (NHS), and deuterium oxide were purchased from Sigma-Aldrich Co. (St. Louis, MO, USA). Dimethylsulfoxide-d_6 (DMSO-d_6) was purchased from Cambridge Isotope Laboratories Inc. (Andover, MA, USA). Doxorubicin hydrochloride (DOX HCl) was obtained from Boryung Pharmaceutical Co. (Seoul, Korea). Minimum essential medium (MEM), penicillin, streptomycin, and fetal bovine serum (FBS) were obtained from Gibco Life Technologies, Inc. (Grand Island, NY, USA). All other chemicals were of reagent grade and were used without further purification.

2.2. Synthesis and characterization of CSOAA

Amphiphilic CSOAA was synthesized from CSO and AA. Briefly, CSO (0.2 mmol) and AA (0.6 mmol) were dissolved separately in 20 ml DMSO each at 50°C for 15 min and cooled down at room temperature. Carboxyl groups of AA were activated by adding EDC and NHS (1.5 mol/mol AA) and it was stirred at room temperature for 30 min. Then, activated AA solution was dripped into the CSO solution for 5 min. The coupling reaction was conducted for a further 12 h, and then 4 ml of deionized distilled water (DDW) was added. The pH of the mixture was adjusted to 3.5 with 1 N HCl and stirred for 30 min. The mixture was precipitated by adding acetone (ten times the volume of mixture) and centrifuged (8,608 × *g*, 30 min) to remove unreacted AA. The precipitation step was repeated three times. Next, the precipitate was dispersed with DDW and dialyzed with dialysis membrane (molecular weight cut-off = 1 kDa; Spectrum Laboratories, Laguna Hills, CA, USA) against DDW for 24 h. The dialyzed products were lyophilized.

The conjugation of CSOAA was confirmed by Fourier transform infrared spectroscopy (FTIR) and ^{1}H–nuclear magnetic resonance (NMR) analyses. FTIR spectra were obtained with a JASCO FTIR 4200 spectrometer (JASCO Company Ltd., Hachioji, Japan) by KBr method. The ^{1}H-NMR spectra were obtained using a Varian FT500-MHz NMR spectrometer (Varian Inc., Palo Alto, CA, USA). Samples (15 mg/ml) were dissolved in DMSO-d_6. The molar substitution (MS) of CSOAA,

which is total number of moles of reacted AA per one mole of CSO, was determined by integration of the values of the proton peaks from the ^{1}H-NMR spectra. MS of CSOAA was obtained using a linear regression line generated from standard samples with various molar ratios between AA and CSO (0.5:1, 1:1, 2:1, 3:1, and 4:1). The standard samples were prepared by homogeneously mixing CSO and AA in DDW/tetrahydrofuran (THF) mixture (1:1, v/v). THF was removed by evaporation and the resultant was lyophilized. The ratio of integration are a (1.23/1.81 ppm) of each standard sample was calculated.

2.3. Preparation and characterization of nanoparticles

To investigate the self-assembly behavior of CSOAA, the critical micelle concentration (CMC) of CSOAA was determined by using pyrene as a fluorescence probe. The fluorescence emission spectrum of pyrene (6×10^{-7} M) was recorded at 360–450 nm in the CSOAA concentration range from 10^{-4} to 1 mg/ml. The excitation wavelength was 334 nm and the slit openings for excitation and emission were set at 10 and 3 nm, respectively. The intensity ratio of the first peak (I_1, 373 nm) to the third peak (I_3, 384 nm) was calculated to determine the CMC.

Blank (without drug loading) self-assembled nanoparticles were prepared by dissolving CSOAA in DDW, vortexing for 15 min, and filtering through a 0.2-μm syringe filter (Minisart RC 15; Sartorius Stedim Biotech GmbH, Goettingen,

Germany).

DOX base was used as a hydrophobic drug and encapsulated into the CSOAA nanoparticles by a solvent evaporation method. To prepare DOX base according to a reported method (Cho et al., 2012b), DOX HCl was reacted with triethylamine in DMSO for 12 h, and then lyophilized. To make DOX-loaded nanoparticle, DOX base (1 mg) was dissolved in 1 ml DMSO and DDW mixture (1:1 v/v). CSOAA (7.5 mg) was added to that mixture and vortexed for 10 min. The solvent was evaporated under a nitrogen gas stream for 4 h at 70°C. DOX-loaded CSOAA-based self-assembled nanoparticles were obtained by resuspending the polymer and drug composite film with 1 ml DDW. That suspension was gently stirred for 15 min and further heated at 70°C for 15 min. Unloaded drug was eliminated with a 0.22-μm syringe filter.

Encapsulation efficiency (EE) of the DOX in nanoparticles was determined by disrupting DOX-loaded nanoparticles with 100× the volume of DMSO. DOX was analyzed quantitatively by Waters high-performance liquid chromatography (HPLC) system (Waters Co., Milford, MA, USA), equipped with a reversed-phase C-18 column (Xbridge RP18, 250 × 4.6 mm, 5 μm; Waters Co.), a separation module (Waters e2695), and a fluorescence detector (Waters 2475). The mobile phase consisted of 0.1 M sodium acetate buffer (pH 4.0, adjusted with acetic acid) and acetonitrile (71:29 v/v), and the eluent was monitored at excitation and emission wavelengths of 470 nm and 565 nm, respectively, with a flow rate of 1.0 ml/min. The injection volume for drug analysis was 20 μl. The EE value was calculated using

the following equation:

$$EE\ (\%) = \frac{actual\ amount\ of\ DOX\ in\ nanoparticle}{theoretical\ amount\ of\ DOX\ in\ nanoparticle} \times 100 \qquad (1)$$

Mean diameter and zeta potential values of the blank nanoparticles and DOX-loaded nanoparticles were measured by a dynamic light scattering (DLS) method (ELS-Z, Photal; Otsuka Electronics Co. Ltd., Osaka, Japan). The morphological shapes of self-assembled nanoparticles were observed under transmission electron microscopy (TEM; LIBRA 120; Carl Zeiss, Oberkochen, Germany). The samples were placed on a copper grid coated with carbon film, dried at 20°C, and photographed.

2.4. In vitro DOX release

In vitro release studies were performed in phosphate-buffered saline (PBS; pH 5.5, 6.8, and 7.4, adjusted with phosphoric acid) at 37°C. DOX-loaded CSOAA-based nanoparticles (150 μl) were placed in a mini GeBA-flex tube (molecular weight cut-off = 12–14 kDa). That tube was then transferred to 10 ml release medium and kept in the horizontal shaker at 37°C and 50 rpm of rotation speed. An aliquot (0.2 ml) of the release medium was periodically collected (at 1, 2, 3, 4, 6, 9, 12, 24, 48, 72, 96, 120, and 144 h) and the same volume of fresh medium was replaced. The released DOX was quantitatively analyzed by HPLC system.

2.5. In vitro cytotoxicity of CSOAA

FaDu cells were purchased from the Korean Cell Line Bank (Seoul, Korea). These cells were cultured in MEM containing 10% FBS, 100 U/ml penicillin, and 100 μg/ml streptomycin at 37°C under 5% CO_2 atmosphere and 95% relative humidity. The cytotoxicity of CSOAA was determined by a 3-(4,5-dimethylthiazol-2-yl)-5(3-carboxymethonyphenol)-2-(4-sulfophenyl)-2H- tetrazolium (MTS)-based assay. Cells were seeded in 96-well plates at a density of 1.0×10^4 cells per well. After 24 h of incubation, the cell culture medium was replaced with 200 μl medium containing various concentrations (5–500 μg/ml) of CSOAA and incubated for 12 and 24 h. After discarding the culture medium, cells were treated with the MTS-based Cell Titer 96 AQ_{ueous} One Solution Cell Proliferation Assay Reagent (Promega Corp., Madison, WI, USA) at 37°C for 4 h, according to the manufacturer's protocol. The spectrophotometric absorbance of samples were measured at a wavelength of 490 nm using an EMax Precision Microplate Reader (Molecular Devices, Sunnyvale, CA, USA).

2.6. In vitro cellular uptake

Cellular uptake efficiency was evaluated by flow cytometry analysis. FaDu cells were seeded in 6-well plates at a density of 6×10^5 cells per well and grown overnight

at 37°C. The culture medium was then removed, and the cells were incubated with free DOX or the DOX-loaded CSOAA-based nanoparticles at an equivalent DOX concentration (50 μg/ml) for 1 h. After washing with PBS (pH 7.4) at least three times, the cells were detached and centrifuged. The supernatant was then removed and the cell pellets were resuspended with PBS containing 2% (v/v) FBS. DOX uptake was analyzed using a Calibur fluorescence-activated cell sorter equipped with CELLQuest software (Becton Dickinson Biosciences, San Jose, CA, USA).

2.7. In vivo anti-tumor efficacy

Female BALB/c nude mice (5 weeks old; Charles River) were used to prepare a tumor-bearing mouse model for evaluating anti-cancer efficacy. Mice were maintained in a light-controlled room kept at a temperature of 22 ± 2°C and a relative humidity of 55 ± 5% (Animal Center for Pharmaceutical Research, College of Pharmacy, Seoul National University, Seoul, Korea). Experimental protocols used were approved by the Animal Care and Use Committee of the College of Pharmacy, Seoul National University. BALB/c nude mice bearing FaDu tumors were prepared by subcutaneous injection of 3×10^6 cells at the right back of mice. Tumor size was measured with Verniercalipers and tumor volume (mm^3) was calculated according to the following formula: volume = 0.5 × longest diameter × shortest diameter^2. Measuring tumor volume and weighing body weight started 10 days post-inoculation,

when the tumor volume reached about 50–100 mm^3. The mice were divided into three groups: control, DOX solution, and DOX-loaded CSOAA-based nanoparticles. Both DOX solution and DOX-loaded nanoparticles were injected intravenously at a dose of 2.5 mg/kg on days 6, 8, 11, and 13. The tumor volume and body weight were monitored for 18 days.

2.8. Statistical analysis

Statistical analyses were performed using analysis of variance. All experiments were performed at least three times and the data are presented as mean ± standard deviation (SD).

3. Results

3.1. Synthesis and characterization of CSOAA

The CSOAA conjugate was synthesized by EDC- and NHS-mediated amide bond formation between the carboxylic group of AA and the amine group of CSO. The synthesis scheme is shown in Fig. 1. EDC can react with the carboxylic group of AA to form an EDC active ester, and the NHS ester intermediate forms rapidly. The intermediate can then react with the primary amine of CSO to form an amide

bond.

The structural characterization of CSOAA was performed using FTIR and ^{1}H-NMR. The FTIR spectrum (Fig. 2) confirmed the synthesis of the CSOAA conjugate. Absorption bands of CSO at 1591 and 1643 cm^{-1} were assigned to N-H bending of the deacetylated amine (-NH_2) and carbonyl stretching of a non-deacetylated amide (NHC=OCH_3; amide I band), respectively. After the reaction, the amine peak at 1591 cm^{-1} of CSO disappeared and a new absorption band at 1558 cm^{-1} in the spectrum of CSOAA was observed, which was associated with the formation of a new amide bond (amide II band). Additionally, absorption bands at 2918 and 2851 cm^{-1} of CSOAA represented stretching vibrations of the acyl chain, -CH_2- and –CH_3 of AA, respectively. The conjugation of AA to CSO was also confirmed by ^{1}H-NMR analysis (Fig.3). The ^{1}H-NMR spectrum of CSOAA exhibited proton signals for both CSO and AA. Although the proton peaks of the glucosamine ring of CSO at 3–4 ppm overlapped with the DMSO-d_6 solvent, the proton peaks at 0.86 and 1.23 ppm indicated a terminal methyl group (-CH_3) and an alkyl chain (-CH_2-) of AA, respectively. Furthermore, the proton peak of –CH_2-, which links with carbonyl group of unconjugated AA, was present at 2.21 ppm. This proton peak shifted to 2.07 ppm after the carboxylic group of AA was conjugated to the amine group of CSO. In addition, the new proton peak was absent in the spectrum of a physical mixture of CSO and AA (Fig. 4). This result indicated that AA was successfully conjugated to the CSO backbone *via* amide bond formation.

To calculate the MS of CSOAA, the homogeneous physical mixtures of CSO

and AA (at different molar ratios) were prepared as standard samples and analyzed by ^{1}H-NMR. As shown in Fig. 5, the linear regression line was generated by plotting the ratio of integration area between peak of the alkyl chain protons of AA (δ = 1.23 ppm; -CH_2-) and the N-acetyl protons of CSO (δ=1.81 ppm; NH-CO-CH_3) according to the molar ratio of AA/CSO. The MS of CSOAA was 1.00 (mole of AA/mole of CSO), calculated from the equation of regression line with its ^{1}H-NMR integration ratio (1.23/1.81ppm), when the initial molar ratio (AA/CSO) was 3 in the conjugation reaction. The chemical yield of CSOAA was 61.2%.

The self-assembly behavior of CSOAA in the aqueous phase was investigated by fluorescence measurements, using pyrene as a fluorescence probe (Fig. 6). CMC can be determined by measuring the intensity ratio (I_1/I_3) between the first (373 nm) and third (384 nm) emission peaks of pyrene according to the CSOAA concentration. As shown in Fig. 6, the CMC of CSOAA was 1.42 μg/ml.

3.2. Preparation and characterization of CSOAA-based self-assembled nanoparticles

Blank self-assembled nanoparticles were prepared by dissolving CSOAA in the aqueous solution. The formation of nanoparticles was confirmed by measuring particle size and zeta potential values. To load DOX into the CSOAA-based nanoparticles (Fig. 7), a solvent evaporation method was used. The mean diameter

and zeta potential values were measured by DLS and are shown in Table 1. The mean diameter of blank nanoparticles was smaller than that of DOX-loaded nanoparticles (73.67 ± 3.91 nm *vs*. 130.00 ± 5.76 nm). The polydispersity index of the DOX-loaded nanoparticles was 0.23 ± 0.02, indicating a narrow size distribution of nanoparticles (Fig. 8a). The zeta potential value was also increased slightly after loading DOX into the nanoparticles (from 7.58 ± 0.62 mV to 12.98 ± 0.55 mV). The spherical shape of the DOX-loaded CSOAA-based nanoparticles was observed by TEM (Fig. 8b). No aggregation of CSOAA-based nanoparticles was observed in that image. The loading amount of DOX in the nanoparticles was measured by HPLC analysis and the EE was 53.12 ± 2.60%.

3.3. In vitro DOX release

DOX release patterns from nanoparticles were investigated under different pH conditions (pH 5.5, 6.8 and 7.4) at 37°C (Fig. 9). DOX release from the CSOAA-based nanoparticles was monitored for 6 days. Sustained drug release was observed and it was dependent on the pH of the release medium. About 30% of DOX was released in the first 12 h under all pH conditions. After that, the amounts of DOX released from CSOAA-based nanoparticles increased as the pH value of the releasing medium decreased. After 6 days, DOX was completely released at pH 5.5; in contrast, 78% and 64% of DOX was released at pH 6.8 and 7.4, respectively.

3.4. In vitro cytotoxicity test

To examine the cytotoxicity of CSOAA, cell viability was measured in FaDu cells, a head and neck cancer cell line. The cells were treated with various concentrations of CSOAA for 12 and 24 h. As shown in Fig. 10, FaDu cell viability (%) was over 90% for all CSOAA concentrations tested. Thus, it can be concluded that CSOAA had no severe toxicity for FaDu cells.

3.5. In vitro cellular uptake study

The cellular uptake efficiency of DOX in FaDu cells was investigated by flow cytometry. Fluorescence intensity was assumed to be proportional to the amount of DOX internalized into the cells. Fig. 11 shows that higher amount of DOX from CSOAA-based nanoparticles was taken up into the cells than from the DOX solution group.

3.6. In vivo anti-tumor efficacy

In vivo anti-tumor efficacy of DOX-loaded nanoparticles was assessed in a FaDu tumor- bearing mouse model. DOX solution and DOX-loaded CSOAA-based nanoparticles were injected intravenously on days 6, 8, 11, and 13. Tumor volume

(mm^3) and body weight (g) were monitored for 18 days. As shown in Fig. 12a, tumor growth inhibition in the DOX-loaded nanoparticle-treated group was significantly higher than in either the DOX solution–treated group or the control group ($p < 0.05$). After 18 days of treatment with DOX solution or DOX-loaded nanoparticles, tumor volumes were 44.63 ± 9.02% and 25.24 ± 5.61% of that for control group. No significant difference in body weight change was observed among the three groups; control, DOX solution–, and DOX-loaded nanoparticle-treated groups (Fig. 12b).

4. Discussion

In this study, CSOAA was successfully synthesized as a hydrophobically modified CSO for the preparation of self-assembled nanoparticles. The synthesis of CSOAA conjugate was confirmed by ^{1}H-NMR analysis, but accurate substitution ratio (AA to CSO) might not be obtained from ^{1}H-NMR spectrum of CSOAA. From ^{1}H-NMR analysis of CSOAA, the proton peak of the glucosamine ring of CSO could be overlapped with the solvent peak and deacetylation degree of CSO was not obviously determined. Because of these limitations, the correlation between the integration ratio (1.23/1.81 ppm) and molar ratio of AA/CSO, based on physical mixture, was evaluated in this investigation (Fig. 5). With the input of the integration ratio (1.23/1.81 ppm) for CSOAA conjugate into this regression line, the stoichiometry of CSOAA can be determined more accurately. It is assumed that

established assay (Fig. 5) could help identify the synthesis of CSOAA and calculate substitution ratio. The CMC value is also an important characteristic of micellar structured nanoparticle. The CMC value of CSOAA was significantly lower than those of low-molecular-weight surfactants in water (Lee et al., 1998). It can be concluded that CSOAA can form stable nanoparticulate structures at its low concentration after dilution with a large volume of body fluids.

The CSOAA synthesized could readily produce self-assembled nanoparticles in aqueous solution because of its amphiphilic property. The AA part could constitute an internal hydrophobic core, while CSO could provide a hydrophilic outer shell of the nanoparticles. The DOX-loaded CSOAA-based self-assembled nanoparticles were prepared by a solvent evaporation method. This method can provide several advantages over dialysis methods, such as the short preparation period and high drug loading efficiency (Park et al., 2004). DOX-loaded CSOAA-based nanoparticles exhibited <200 nm of mean diameter and narrow size distribution, high drug encapsulation efficiency, and negligible cytotoxicity. Because of these properties, it is assumed that DOX-loaded CSOAA-based nanoparticles can effectively accumulate in the tumor region *via* the EPR effect and exhibit reduced uptake by RES (Maeda et al., 2000; Yuan et al., 1995).

The sustained and pH-dependent drug release patterns from the CSOAA-based nanoparticles developed were observed (Fig. 8). Sustained drug release can lead to reduce *in vivo* drug clearance and maintenance of effective drug concentrations for tumor growth inhibition. Additionally, larger amount of DOX was released at acidic

pH, simulating the endocytic compartment of cancer cells, compared with normal pH condition (pH 7.4). This difference may have been due to the slack structure of the nanoparticle, following protonation of amino groups in CSO and the higher solubility of DOX at an acidic pH. These results indicate that DOX-loaded CSOAA-based nanoparticles can be highly accumulated and release a large amount of drug in tumor tissues, with less DOX delivery to non-tumor regions. Moreover, enhanced drug release at pH 5.5 can imply endosomal escape of the drug and its improved transport to the cell nucleus.

As shown in Fig. 11, larger amount of DOX from nanoparticle-treated group was taken up to the cells compared to that from DOX solution group. This result may be explained by the interaction between the positively charged surface of the CSOAA-based nanoparticle and the negatively charged cellular membrane, and subsequent endocytosis of nanoparticles (Chavanpatil et al., 2006; Lee et al., 2011; Zauner et al., 1998). Furthermore, fatty acid–modified CS nanoparticles have been reported to form self-assembled nanoparticles with a multi-hydrophobic core (You et al., 2007). A hydrophobic minor core may help the internalization of nanoparticles into the cells by inserting fatty acids into the cell membrane.

FaDu cells were selected as a head and neck cancer cell line for this investigation. As shown in Fig. 12a, DOX-loaded CSOAA-based nanoparticles exhibited significant inhibitory effects on FaDu tumor growth, compared with both the control and DOX solution–treated groups. The physiochemical properties of drug-loaded nanoparticles, sustained drug release, and passive targeting, *via* mainly

an EPR effect, may explain the efficient tumor growth inhibition by DOX-loaded CSOAA-based nanoparticles. In conclusion, the self-assembled CSOAA-based nanoparticle developed can be used as an anti-cancer drug delivery system, especially for head and neck cancer therapy.

5. Conclusions

CSOAA was synthesized for the preparation of self-assembled nanoparticles for DOX delivery. Its CMC value was relatively low and it could form self-assembled nanoparticles in an aqueous environment with a narrow size distribution. DOX-loaded CSOAA-based nanoparticles showed a sustained and pH-dependent drug release profile. It seemed that the nanoparticulate structure and drug release profile of the nanoparticles influenced on the cellular uptake and anti-tumor activity. DOX-loaded CSOAA-based nanoparticles significantly inhibited FaDu tumor growth *in vivo*. Considering all of experimental results in this study, CSOAA-based self-assembled nanoparticles may be a promising carrier for anti-cancer drug delivery.

6. References

Airoldi, M, Cattel, L, Milla, P, Pedani, F, Garzaro, M, Dosio, F, 2008. Paclitaxel and pegylated liposomal doxorubicin in recurrent head and neck cancer: clinical and unexpected pharmacokinetic interactions. Anticancer Res. 28, 2519–2527.

Aliabadi, H.M., Brocks, D.R., Lavasanifar, A., 2005. Polymeric micelles for the solubilization and delivery of cyclosporine A: pharmacokinetics and biodistribution. Biomaterials 26, 7251–7259.

Chae, S.Y., Son, S., Lee, M., Jang, M.K., Nah, J.W., 2005. Deoxycholic acid-conjugated chitosan oligosaccharide nanoparticles for efficient gene carrier. J. Control. Release 109, 330–344.

Chavanpatil, M.D., Khdair, A., Panyam, J., 2006. Nanoparticles for cellular drug delivery: mechanisms and factors influencing delivery. J. Nanosci. Nanotechnol. 6, 2651–2663.

Cho, H.J., Chong, S., Chung, S.J., Shim, C.K., Kim, D.D., 2012a. Poly-L-arginine and dextran sulfate-based nanocomplex for epidermal growth factor receptor (EGFR) siRNA delivery: its application for head and neck cancer treatment. Pharm. Res. 29, 1007–1019.

Cho, H.J., Yoon, H.Y., Koo, H., Ko, S.H., Shim, J.S., Lee, J.H., Kim, K., Kwon, I.C., Kim, D.D., 2011. Self-assembled nanoparticles based on hyaluronic acid-ceramide (HA-CE) and Pluronic® for tumor-targeted delivery of docetaxel.

Biomaterials 32, 7181–7190.

Cho, H.J., Yoon, I.S., Yoon, H.Y., Koo, H., Jin, Y.J., Ko, S.H., Shim, J.S., Kim, K., Kwon, I.C., Kim, D.D., 2012b. Polyethylene glycol-conjugated hyaluronic acid-ceramide self-assembled nanoparticles for targeted delivery of doxorubicin. Biomaterials 33, 1190–1200.

Choi, J.S., Seo, K., Yoo, J.W., 2012. Recent advances in PLGA particulate systems for drug delivery. J. Pharm. Invest. 42, 155–163.

Kaida, S., Cabral, H., Kumagai, M., Kishimura, A., Terada, Y., Sekino, M., Aoki, I., Nishiyama, N., Tani, T., Kataoka, K., 2010. Visible drug delivery by supramolecular nanocarriers directing to single-platformed diagnosis and therapy of pancreatic tumor model. Cancer Res. 70, 7031–7041.

Kolishetti, N., Dhar, S., Valencia, P.M., Lin, L.Q., Karnik, R., Lippard, S.J., Langer, R., Farokhzad, O.C., 2010. Engineering of self-assembled nanoparticle platform for precisely controlled combination drug therapy. Proc. Natl. Acad. Sci. U. S. A. 107, 17939–17944.

Kratz, F., Ehling, G., Kauffmann, H., Unger, C., 2007. Acute and repeat-dose toxicity studies of the (6-maleimidocaproyl) hydrazone derivative of doxorubicin (DOXO-EMCH), an albumin-binding prodrug of the anticancer agent doxorubicin. Hum. Exp. Toxicol. 26, 19–35.

Kumar, M., Muzzarelli, R.A.A., Muzzarelli, C., Sashiwa, H., Domb, A., 2004. Chitosan chemistry and pharmaceutical perspectives. Chem. Rev. 1014, 6017–6084.

Kwon, G.S., 2003. Polymeric micelles for delivery of poorly water-soluble compounds. Crit. Rev. Ther. Drug Carrier Syst. 20, 357–403.

Lee, J.Y., Choi, Y.S., Suh, J.S., Kwon, Y.M., Yang, V.C., Lee, S.J., Chung, C.P., Park, Y.J., 2011. Cell-penetrating chitosan/doxorubicin/TAT conjugates for efficient cancer therapy. Int. J. Cancer 128, 2470–2480.

Lee, K., Kwon, I., Kim, Y.H., Jo, W., Jeong, S., 1998. Preparation of chitosan self-aggregates as a gene delivery system. J. Control. Release 51, 213–220.

Li, L., Tan, Y.B., 2008. Preparation and properties of mixed micelles made of Pluronic polymer and PEG-PE. J. Colloid Interface Sci. 317, 326–331.

Maeda, H., Wu, J., Sawa, T., Matsumura, Y., Hori, K., 2000. Tumor vascular permeability and the EPR effect in macromolecular therapeutics: a review. J. Control. Release 65, 271–284.

Muzzarelli, R., Muzzarelli, C., 2005. Chitosan chemistry: Relevance to the biomedical sciences. Adv. Polym. Sci. 186, 151–209.

Park, J.H., Kwon, S., Nam, J.O., Park, R.W., Chung, H., Seo, S.B., Kim, I.S., Kwon, I.C., Jeong, S.Y., 2004. Self-assembled nanoparticles based on glycol chitosan bearing 5 beta-cholanic acid for RGD peptide delivery. J. Control. Release 95, 579–588.

Reuter, C.W., Morgan, M.A., Eckardt, A., 2007. Targeting EGF-receptor-signalling in squamous cell carcinomas of the head and neck. Br. J. Cancer 96, 408−416.

Vishu Kumar, A.B., Varadaraj, M.C., Lalitha, R.G., Tharanathan, R.N., 2004. Low molecular weight chitosans: preparation with the aid of papain and

characterization. Biochim. Biophys. Acta. 1670, 137–146.

Wildiers, H., Jurcut, R., Ganame, J., Herbots, L., Neven, P., De Backer, J., Denys, H., Cocquyt, V., Rademakers, F., Voigt, J.U., 2008. A pilot study to investigate the feasibility and cardiac effects of pegylated liposomal doxorubicin (PL-DOX) as adjuvant therapy in medically fit elderly breast cancer patients. Crit. Rev. Oncol. Hematol. 67, 133–138.

Yoon, H.Y., Koo H, Choi, K.Y., Lee, S.J., Kim, K., Kwon, I.C., Leary, J.F., Park, K., Yuk, S.H., Park, J.H., Choi, K., 2012. Tumor-targeting hyaluronic acid nanoparticles for photodynamic imaging and therapy. Biomaterials 33, 3980–3989.

You, J., Hu, F.Q., Du, Y.Z., Yuan, H., Ye, B.F., 2007. High cytotoxicity and resistant-cell reversal of novel paclitaxel loaded micelles by enhancing the molecular-target delivery of the drug. Nanotechnology 18, 495101.

Yuan, F., Dellian, M., Fukumura, D., Leunig, M., Berk, D.A., Torchilin, V.P., Jain, R.K., 1995. Vascular permeability in a human tumor xenograft: molecular size dependence and cutoff size. Cancer Res. 55, 3752–3756.

Zauner, W., Ogris, M., Wagner, E., 1998. Polylysine-based transfection systems utilizing receptor-mediated delivery. Adv. Drug Deliv. Rev. 30, 97–113.

Table 1. Characteristics of CSOAA-based nanoparticles.

Formulations	Mean diameter (nm)	Polydispersity Index	Zeta potential (mV)	Encapsulation efficiency (%)
Blank nanoparticles	73.67± 3.91	0.32± 0.01	7.58± 0.62	-
CSOAA:DOX (7.5:1)	130.0± 5.76	0.23± 0.02	12.98± 0.55	53.12± 2.60

Data represent as mean± SD ($n \geq 3$).

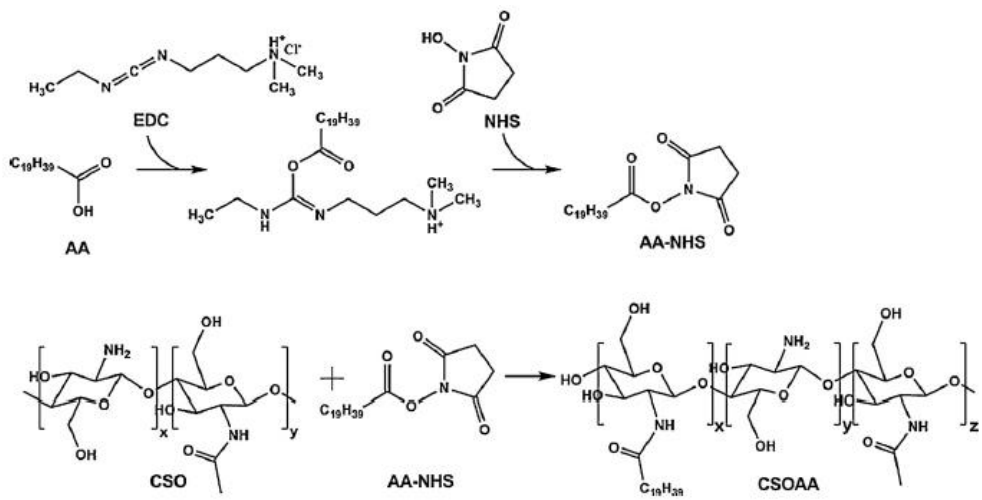

Figure 1 The synthetic scheme of CSOAA.

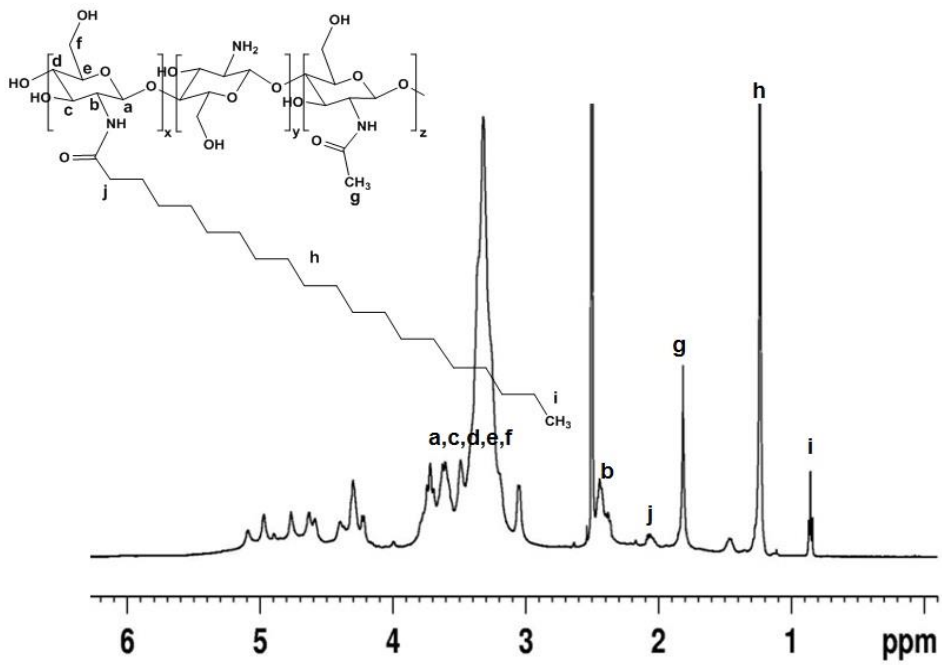

Figure 2 ^{1}H-NMR spectrum of CSOAA. CSOAA was dissolved in DMSO-d_6 for ^{1}H-NMR analysis.

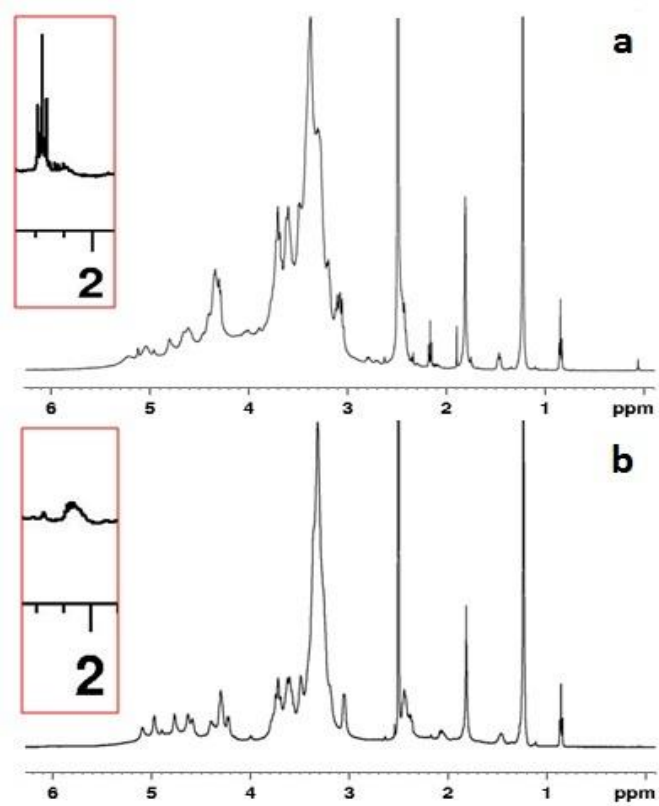

Figure 3 ^{1}H-NMR spectra of (a) physical mixture of CSO and AA and (b) chemically conjugated CSOAA.

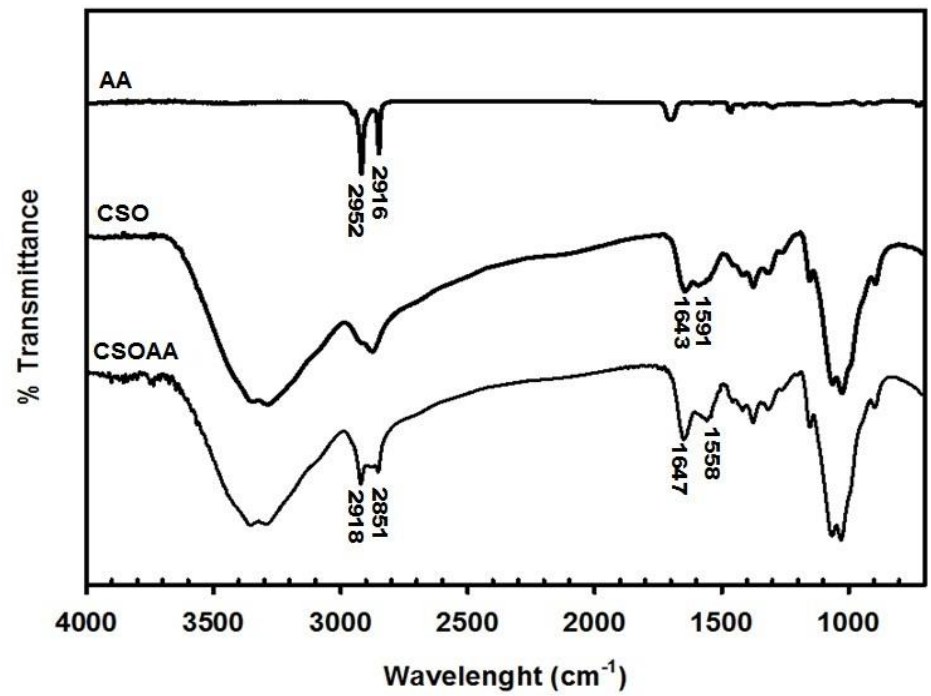

Figure 4 FT-IR spectra of AA, CSO and CSOAA.

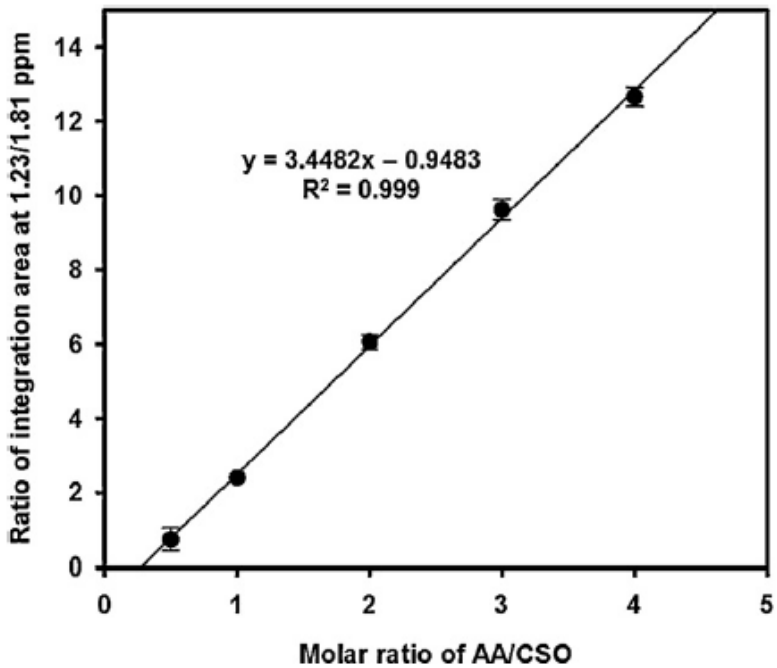

Figure 5 The correlationship between the ratio of integration area (1.23/1.81 ppm) and molar ratio of AA/CSO based on their physical mixture. Each point represents the means ± SD (n = 3).

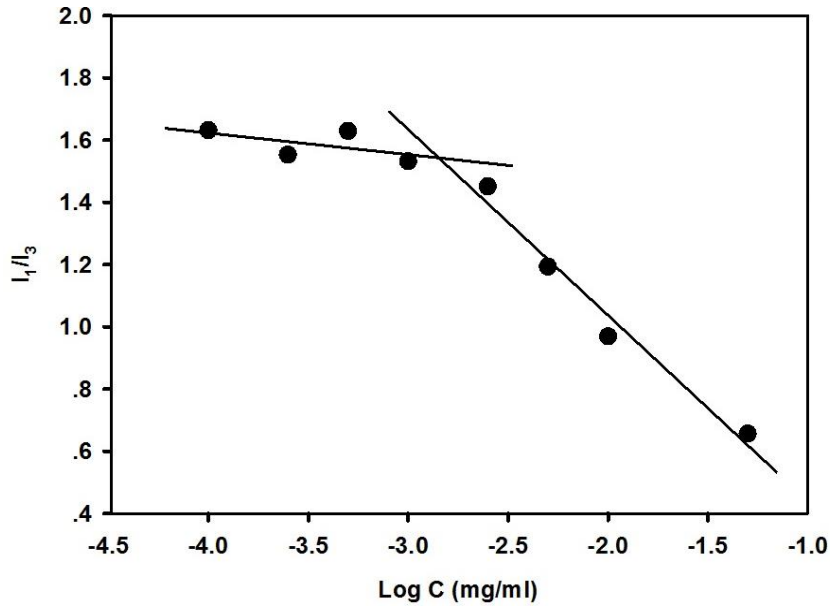

Figure 6 CMC determination of CSOAA. Fluorescence intensity ratio (I_{373}/I_{384}) was plotted against CSOAA concentration.

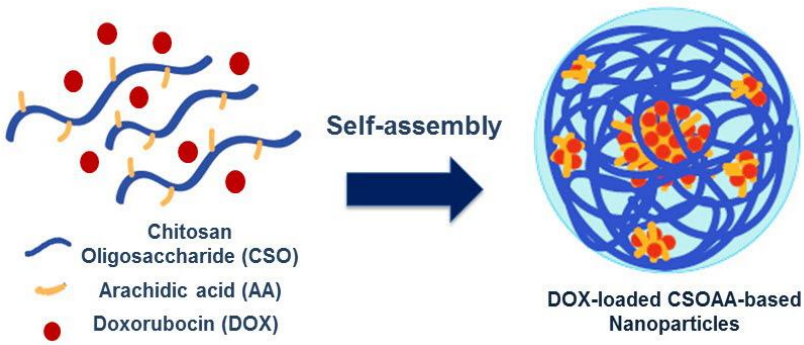

Figure 7 Schematic illustration of DOX-loaded CSOAA nanoparticles.

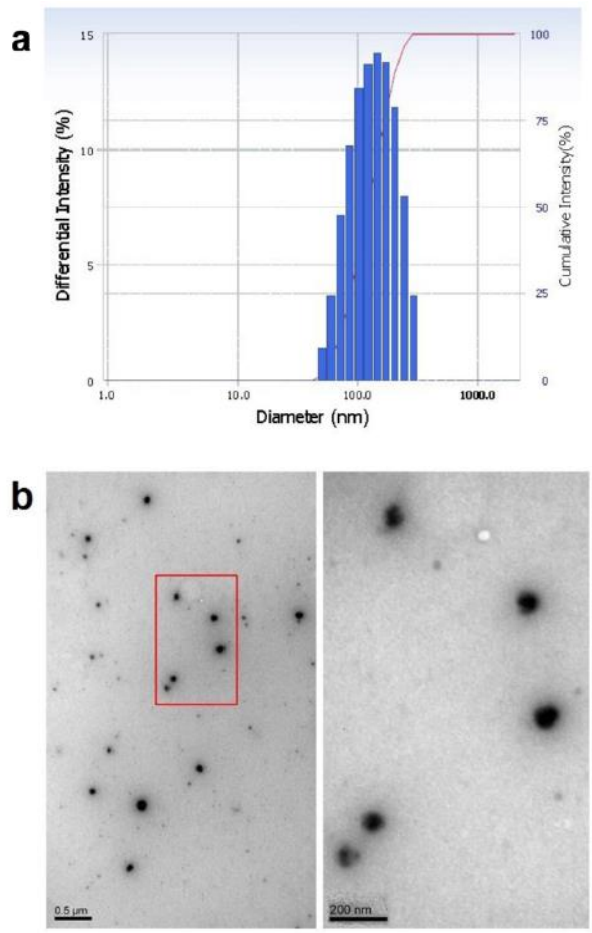

Figure 8 Size distribution and morphology of DOX-loaded CSOAA-based nanoparticles. (a) Size distribution of DOX-loaded CSOAA-based nanoparticles is determined by dynamic light scattering (DLS). The weight ratio between CSOAA and DOX was 7.5 to 1. (b) TEM images of DOX-loaded CSOAA-based nanoparticles were shown. The length of bar is 500 (left) and 200 (right) nm, respectively.

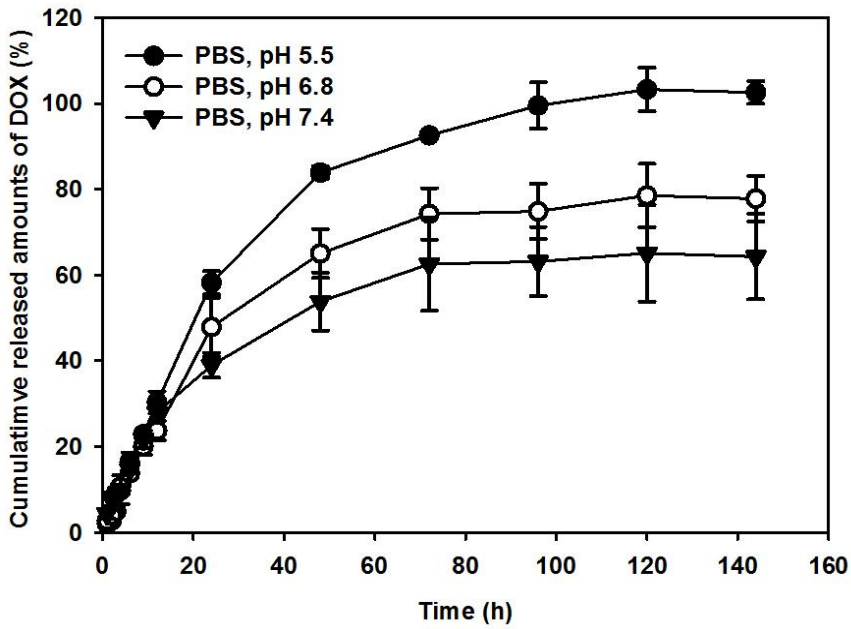

Figure 9 *In vitro* DOX release profiles of CSOAA-based self-assembled nanoparticles. Drug release profiles from CSOAA: DOX = 7.5:1 formulation at different pH conditions (pH 5.5, 6.8 and 7.4) were shown. Each point represents mean ± SD (n = 3).

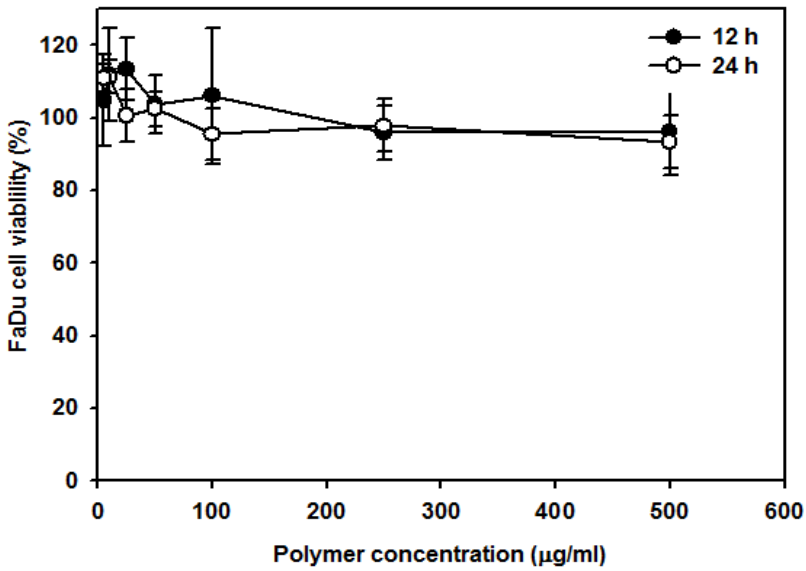

Figure 10 *In vitro* cytotoxicity tests of CSOAA in FaDu cells. Various concentrations of CSOAA were incubated for 12 and 24 h. Cell viability was determined by MTS-based assay. Each point represents mean ± SD (n = 4).

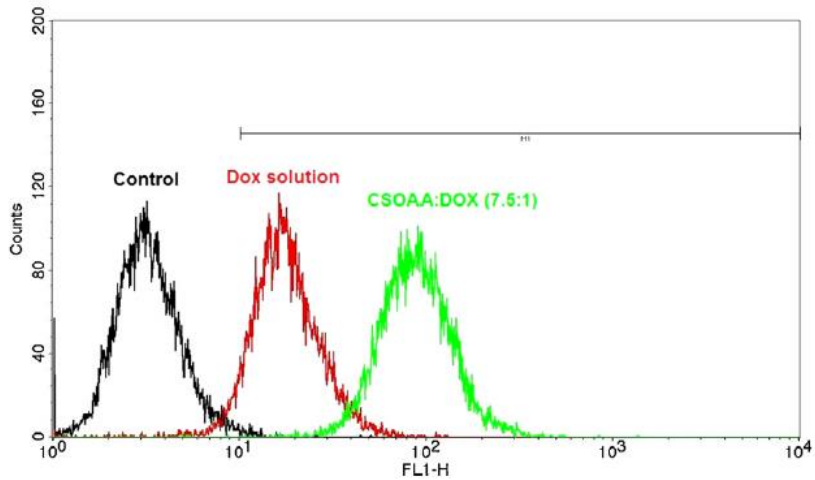

Figure 11 Cellular uptake efficiency of DOX was analyzed by flow cytometer. DOX solution and DOX-loaded nanoparticles were incubated for 1 h. Various colors indicate each experimental group (black: control, red: DOX solution, green: DOX-loaded nanoparticle-treated group).

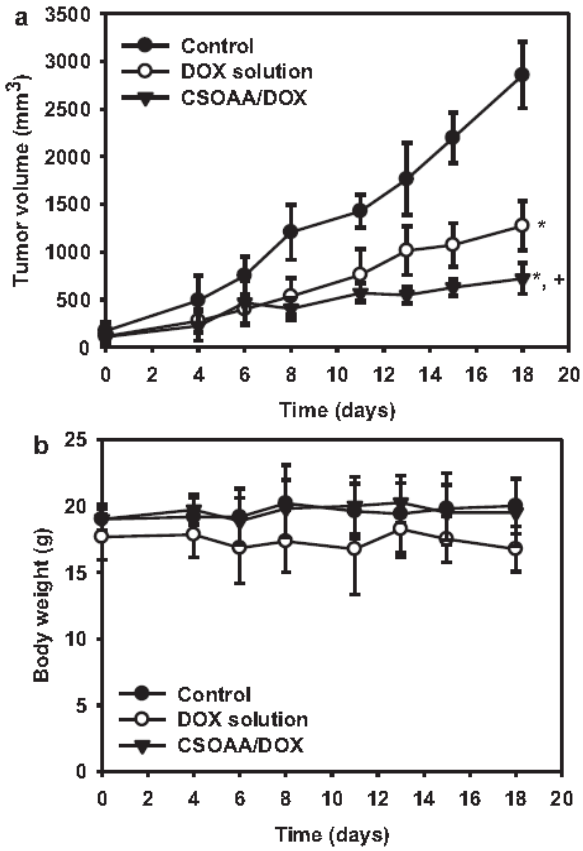

Figure 12 Anti-tumor efficacy test of DOX-loaded CSOAA-based nanoparticles in a FaDu tumor bearing BALB/c nude mouse model. (a) Tumor volume (mm^3) profiles according to the time (days) for 18 days are shown. DOX solution and DOX-loaded nanoparticles were injected intravenously on days 6, 8, 11, and 13. (b) Body weight (g) was monitored. Each point indicates mean ± S.D ($n \geq 4$). $^{*}P < 0.05$ *vs.* control group; $^{+}P < 0.05$ *vs.* DOX solution group.

PART II. Self-assembled magnetic resonance imaging nanoprobes based on arachidyl chitosan for cancer diagnosis

1. Introduction

Alongside innovations in drug delivery for cancer therapy, imaging techniques for cancer diagnosis have also evolved. Progress in imaging agents and apparatus used for magnetic resonance imaging (MRI), computed tomography (CT), positron emission tomography (PET), single-photon emission computed tomography (SPECT) and ultrasound have contributed to more accurate diagnosis of cancer. MRI is one of the most powerful imaging techniques for diagnosis and has several advantages, such as high resolution of specific tissues and organs and deep penetration into the soft tissues (Janib et al., 2010; Liu et al., 2012; Villaraza et al., 2010). MRI can provide abundant information on the anatomical and physiological state of the body (Cho et al., 2012b). Additionally, contrast agents are used to improve sensitivity resulting from the interaction with surrounding water protons and shortening of the proton relaxation time to enhance contrast (Johnson et al., 2011). Contrast agents can be classified into the T_1-weighted type (paramagnetic gadolinium chelates) and the T_2-weighted type (superparamagnetic iron oxide nanoparticles; SPION), which could enhance the contrast of regions of interest positively or negatively, respectively (Liu et al., 2012; Villaraza et al., 2010). In particular, the T_1 contrast agents (paramagnetic Gd^{3+} chelates) have several advantages: high magnetic moment, suitable electron relaxation time, and a positive contrast enhancing effect (Liu et al., 2012; Caravan et al., 1999). Clinically relevant

Gd^{3+} chelates are as follows (Caravan et al., 1999) Gd-diethylenetriaminepentaacetic acid (Gd-DTPA), Gd-1,4,7,10-tetra- azacyclododecane-1,4,7,10-tetraacetic acid (Gd-DOTA), and Gd-10- (2-hydroxypropyl)-1,4,7,10-tetraazacyclododecane-1,4,7-triacetic acid (Gd-HP- DO_3A). Although these Gd^{3+} chelates have been used successfully clinically, they have some problems; reduction of relaxivity (r_1) by chelation (mainly due to the decreased number of coordination sites for water proton exchange), lack of specificity for certain tissues or organs, and rapid clearance from the blood due to renal excretion (Ananta et al., 2010; Kobayashi et al., 2001). Therefore, acquisition of enough spatial information on long-term application and disease targeting is difficult. It is expected that development of polymeric nanoparticles-based imaging agents will solve these problems. Recently, polysaccharide-based nanoprobes for MR imaging have been investigated (Cho et al., 2012b; Ernsting et al., 2012; Lim et al. 2011; Yim et al., 2011). Various MR imaging probes based on chitosan or its derivatives have been developed (Cheng et al., 2012; Key et al., 2012; Yuk et al., 2011). Pure chitosan does not include any tumor-targeting ligand for cancer diagnosis, but chitosan nanoparticles can accumulate in the tumor region after intravenous injection, mainly due to the enhanced permeability and retention (EPR) effect. In our previous study (Termsarasab et al., 2013), chitosan oligosaccharide–arachidic acid (CSOAA), as an amphiphilic CSO derivative, was synthesized and used to prepare self-assembled nanoparticles. A hydrophobic anti-cancer drug was incorporated into the hydrophobic internal cavity of nanoparticles and injected intravenously into a head

and neck cancer xenografted mouse model to evaluate in vivo anti-tumor efficacy. Herein, we report the development and in vitro evaluation of CSOAA-DTPA-Gd nanoprobes for MR imaging of cancer. DTPA was conjugated to CSO, after which Gd^{3+} was chelated to the DTPA ligand. It is expected that self-assembled CSOAA can form a nano-sized MRI probe (mean diameter, ~150 nm) in an aqueous environment, and thus can act as a useful MR imaging probe for cancer diagnosis.

2. Materials and methods

2.1. Materials

Chitosan oligosaccharide (average molecular weight = 5 kDa, degree of deacetylation >90%) was purchased from Kitto Life Co., Ltd. (Seoul, Korea). Arachidic acid (AA), 1-ethyl-3-(3-dimethylaminopropyl) carbodiimide (EDC), N-hydroxysuccinimide (NHS), pyrene, diethylenetriaminepentaacetic dianhydride (DTPA), and gadolinium (III) chloride hexahydrate ($GdCl_3 \cdot 6H_2O$) were purchased from Sigma Chemical Co. (St. Louis, MO, USA). Cy5.5 NHS ester was purchased from Amersham Biosciences (Piscataway, NJ, USA). Dulbecco's modified Eagle's medium (DMEM), minimum essential medium (MEM), penicillin, streptomycin, and heat-inactivated fetal bovine serum (FBS) were obtained from

Gibco Life Technologies, Inc. (Grand Island, NY, USA). All other chemicals were of reagent grade and used without further purification.

2.2. Synthesis of CSOAA-DTPA-Gd

CSOAA was synthesized according to our previous method (Termsarasab et al., 2013). In brief, CSO (0.2 mmol) and AA (0.6 mmol) were dissolved separately in 20 ml dimethyl sulfoxide (DMSO) at 50 ◦C for 15 min. The carboxyl groups of AA were activated by adding EDC and NHS (molar ratio for AA = 1.5:1) and stirring for 30 min at room temperature. The activated AA solutions were added to the CSO solution for 5 min, then allowed to react for a further 12 h, after which double distilled water (DDW) at a volume ratio of 10% was added. The pH of mixed solutions was adjusted to 3.5 with 1 N HCl and stirred for 30 min. The solution was precipitated with acetone (ten times the volume of the mixture, v/v) and centrifuged at 7500 rpm for 30 min to eliminate unreacted AA. The precipitation step was repeated three times. After precipitation, the precipitates were dispersed with DDW and dialyzed against DDW with a dialysis membrane (molecular weight cut-off: 1 kDa, Spectrum Laboratories, Laguna Hills, CA, USA) for 1 day. Dialysis products were obtained by freeze drying. DTPA was conjugated to CSO by amide bond formation between the carboxylic group of DTPA and the amine group of CSO. DTPA (0.1 mmol) was dissolved in DDW (15 ml), and EDC (0.2 mmol) and NHS (0.2 mmol) were added. After stirring for 30 min, the solution was slowly added to

CSOAA (0.02 mmol) solution in DDW (20 ml). It was further stirred for 12 h at room temperature and dialyzed with a dialysis membrane (molecular weight cut-off: 3.5 kDa) against DDW for 3 days. CSOAA-DTPA was obtained by lyophilization. For Gd^{3+} chelation, $GdCl_3 \cdot 6H_2O$ (0.05 mmol) dissolved in 5 ml of DDW was slowly added to CSOAA-DTPA (0.01 mmol) dissolved in 30 ml DDW and the pH was adjusted to 7 by 1 N NaOH. It was stirred for 24 h and dialyzed for 3 days against DDW to remove free Gd^{3+}. CSOAA-DTPA-Gd was obtained by freeze-drying. DTPA conjugation to CSOAA was identified by ^1H NMR analysis (500 MHz). CSOAA-DTPA was solubilized in deuterium oxide (D2O) for ^1H NMR analysis. DTPA conjugation and Gd^{3+} chelation were also confirmed by FT-IR analysis with a JASCO FT-IR 4200 spectrometer (JASCO Company Ltd., Hachioji, Japan). Gd content in the CSOAA-based nanoprobe was determined by an inductive coupled plasma-atomic emission spectrometer (ICP-AES, Optima 4300 DV, Perkin Elmer Inc., Wellesley, MA, USA).

2.3. Characteristics of the CSOAA-based nanoprobe

To produce CSOAA-based nanoprobes, CSOAA-DTPA-Gd was solubilized in DDW, phosphate buffered saline (PBS, pH 7.4) or 50% (v/v) FBS solution (in PBS pH 7.4). After dissolving at a predetermined concentration, the sample was sonicated using a probe-type sonicator (Vibra-Cell VC 750 ultrasonic processor, Sonics & Materials, CT, USA) for 1 min. Mean diameter, polydispersity index, and zeta

potential values of the nano-sized probe were measured using a light scattering spectrophotometer (ELS-Z; Otsuka Electronics, Tokyo, Japan) according to the manufacturer's protocol. The morphology of the CSOAA-based nanoprobe was observed by transmission electron microscopy (TEM). The nanoprobes were placed on copper grids with films. After air-drying for 10 min, they were observed by TEM (JEM 1010; JEOL, Tokyo, Japan). The scale bar in the images represents 1 μm. Critical aggregation concentration (CAC) of the CSOAA-based nanoprobe was determined using a fluorescence spectrophotometer with pyrene as a hydrophobic substance. Pyrene dissolved in acetone (2×10^{-6} M) was prepared and 0.3 ml of that solution was transferred to each 1.5 ml tube. Acetone was evaporated under a gentle nitrogen (N2) gas stream for 1 h at 60°C. The nanoprobe solution in DDW (1 ml), the concentration of which ranged from 0.1–1000 μg/ml, was added to each tube to make a 6×10^{-7} M pyrene concentration. The emission spectrum (310–550 nm) was obtained at a fixed 334 nm excitation wavelength with a fluorescence spectrometer FP-6500 (JASCO Co., Tokyo, Japan).

2.4. In vitro cytotoxicity of the nanoprobe

Hep-2 and FaDu cells were purchased from Korean Cell Line Bank (KCLB, Seoul, Korea). Hep-2 cells were cultured with DMEM supplemented with 10% FBS, 100 U/ml penicillin, and 100 μg/ml streptomycin, and FaDu cells were cultured with MEM containing 10% FBS, 100 U/ml penicillin, and 100 μg/ml streptomycin, in a

5% CO_2 atmosphere with 95% relative humidity at 37°C. After Hep-2 and FaDu cells reached 70–80% confluency, they were trypsinized and seeded in a 96-well plate at a density of 1.0×10^4 per well. After incubation for 24 h, the culture medium was removed. After 12 and 24 h incubation of CSOAA-DTPA and CSOAA-DTPA-Gd (15–300 μg/ml) with both cell types at 37 °C, 5% CO_2 and 95% relative humidity, the cell viability (%) was determined using the MTS-based CellTiter 96 AQueous One Solution Cell Proliferation Assay Reagent (Promega Corp., WI, USA) at 37 °C for 4 h, according to the manufacturer's protocol. The absorbance at 490 nm was measured using an Emax Precision Microplate Reader (Molecular Devices, Sunnyvale, CA, USA).

2.5. In vitro cellular uptake

To monitor the intracellular uptake of nanoprobes, Cy5.5, a near-infrared fluorescence (NIRF) dye for observation by confocal laser scanning microscopy (CLSM), was conjugated to a CSO backbone by amide bond formation. The CSOAA-DTPA conjugate (100 mg) was dissolved in 50 ml carbonate/bicarbonate buffer (50 mM, pH 9.6). Cy5.5 NHS ester (0.2 mg) dissolved in 0.02 ml DMSO was slowly added to a CSOAA-DTPA-containing buffer and stirred for 3 h at room temperature. Free Cy5.5 was removed by dialysis against DDW for 3 days. The final product was obtained by lyophilization. For Gd^{3+} chelation, the previously described synthesis method was used. In brief, $GdCl_3\bullet6H_2O$ (0.05 mmol) dissolved in 5 ml

DDW was slowly added to Cy5.5-CSOAA-DTPA (0.01 mmol) dissolved in 30 ml DDW and the pH was adjusted to 7 using 1 N NaOH. The solution was stirred for 24 h and dialyzed for 3 days against DDW to remove free Gd^{3+}. Cy5.5-CSOAA-DTPA-Gd was obtained by freeze-drying. The Cy5.5 content in the Cy5.5-labeled CSOAA-based nanoprobe was determined by measuring absorbance at 650 nm with a UV/vis spectrophotometer (Emax Precision Microplate Reader, Molecular Devices, Sunnyvale, CA, USA). Linearity was established in the range 1–25 μg/ml Cy5.5. After Hep-2 and FaDu cells acquired 70–80% confluency, the cells were trypsinized and seeded onto culture slides (BD Falcon, Bedford, MA) at a density of 1.0×10^5 per well (surface area of 1.7 cm^2 per well, four-chamber slides) and incubated for 24 h at 37 °C. The Cy5.5-labeled nanoprobe (1 mg/ml) was incubated for 0.5, 8 and 12 h at 37 °C. The cells were then washed with phosphate buffered saline (PBS, pH 7.4) at least three times and fixed with a 4% formaldehyde solution for 5 min. VECTASHIELD mounting medium with 4',6-diamidino-2-phenylindole (DAPI) (H-1200; Vector Laboratories, Inc., Burlingame, CA, USA) was added to stain nuclei and prevent the fading of fluorescence. The preparations were observed by CLSM (LSM 710; Carl-Zeiss, Thornwood, NY, USA).

2.6. In vitro MRI study

All MRI studies were performed with a 4.7-T MRI apparatus (Bruker BioSpec 47/40, Karlsruhe, Germany). T_1 contrast intensities of Gd-DTPA (Magnevist®, Bayer Schering Pharma AG, Berlin, Germany) and the CSOAA-based nanoprobe were scanned at 5–100 μM Gd concentrations. Specific parameters were as follows: echo time (TE) = 6.5 ms, repetition time (TR) = 1000 ms, field of view (FOV) = 5 × 4 cm, matrix = 128 × 128, slice thickness = 2 mm. The proton relaxation enhancement can be expressed using the following formula:

$$\left(\frac{1}{T_1}\right)_{obs} = \left(\frac{1}{T_1}\right)_{d} + R_1[M] \qquad (1)$$

where $(1/T_1)_{obs}$ and $(1/T_1)_{d}$ are the relaxation rates of the protons in the presence and absence of paramagnetic species (Gd), respectively, and [M] is the concentration of the paramagnetic species (Gd).

2.7. Data analysis

All experiments were performed at least three times and the data were represented as mean ± standard deviation (SD).

3. Results and discussions

3.1. Synthesis of the CSOAA-based nanoprobe

CSOAA was synthesized, as an amphiphilic CSO derivative, to prepare self-assembled nanoparticles according to the reported method (Termsarasab et al., 2013). CSOAA was synthesized by amide bond formation between the carboxylic group of AA and the amine bond of CSO by an EDC-coupled reaction (Fig. 1). Synthesis was identified by ^{1}H-NMR analysis. Though the proton peaks for the glucosamine ring of CSO overlapped those of the solvent, the proton peaks at 0.86 and 1.23 ppm indicated that the terminal methyl group (-CH_3) and alkyl chain (-CH_2-) of AA were present (Termsarasab et al., 2013). In particular, the proton peak of CH_2 of AA linked with the carbonyl group without conjugation (2.21 ppm) was shifted after amide bond formation (2.16 ppm). According to our previous report (Termsarasab et al., 2013), conjugation of AA to the CSO backbone was also confirmed by FT-IR analysis. In particular, the amide II band was shifted from 1591 cm^{-1} in the CSO spectrum to 1558 cm^{-1} in the CSOAA spectrum. Prior to Gd chelation, DTPA was conjugated to CSOAA, as confirmed by ^{1}H-NMR and FT-IR analysis. An amide bond was formed between the amine group of CSO and the carboxylic group of DTPA by an EDC coupled reaction (Fig. 1). As shown in Fig. 2, peaks indicating DTPA (3.3 ppm) and CSO (2.0 ppm) were presented in the ^{1}H-NMR spectrum of

CSOAA-DTPA. The FT-IR spectra also revealed the conjugation of DTPA to CSOAA (Fig. 1B). The FT-IR spectrum of CSOAA was reported in our previous study (Termsarasab et al., 2013). Considering the FT-IR spectrum of CSOAA, the amide I band was shifted from 1648 cm^{-1} in the CSOAA spectrum to 1632 cm^{-1} in the CSOAA-DTPA spectrum (Fig. 3). In particular, the amide II band at 1558 cm^{-1} in the spectrum of CSOAA was altered in the spectrum of CSOAA-DTPA. Absorption intensity of the C-O stretching band in CSOAA-DTPA at 1075 cm^{-1} was attenuated in the spectrum of CSOAA-DTPA-Gd by coordination of Gd^{3+} to DTPA. Furthermore, the Gd content in the CSOAA-based nanoprobe measured by ICP-AES was 5.43% (w/w). Synthesis of CSOAA-DTPA-Gd was also evaluated by measurement of zeta potential, as reported previously (Cho et al., 2012b; Yim et al., 2011). As shown in Table 1, the zeta potential was decreased by DTPA conjugation from 12.50 ± 0.81 mV (CSOAA) to 9.21 ± 0.85 mV (CSOAA-DTPA). It may be induced by ionization of the carboxylic group of DTPA. After chelation of Gd^{3+} to CSOAA-DTPA, its zeta potential was slightly increased to 11.19 ± 0.39 mV. The zeta potential can be altered by several factors, such as nanoprobe concentration, DTPA conjugation degree, and Gd content.

3.2. Characteristics of the nanoprobe

A nano-sized CSOAA-based probe was prepared using the self-assembled property of CSOAA (Fig. 4). The mean diameter, polydispersity index, and zeta

potentials of the nanoprobe were measured. As shown in Table 1, the mean diameter of the CSOAA-DTPA-Gd nanoprobe was 146.30 ± 5.51 nm (at 1 mg/ml concentration of the nanoprobe) and was around 150 nm within 5 mg/ml concentration in DDW (Fig. 5A). Mean diameter of CSOAA-based nanoprobe (at 5 mg/ml concentration) was 248.97 ± 6.70 and 167.70 ± 0.92 nm in 50% (v/v) FBS solution (in PBS pH 7.4) and PBS (pH 7.4), respectively (Fig. 5B). The mean diameters of nanoprobe in both media were maintained constantly for 4 h. Although the particle size of nanoprobe in 50% FBS solution slightly increased compared to that in DDW or PBS, it is still considered to be suitable for the cellular uptake and passive tumor targeting. The morphology was observed by TEM to be spherical (Fig. 6A). The CSOAA-based nanoprobe also exhibited a narrow size distribution (Fig. 2B). The CAC value of CSOAA was 1.42 μg/ml (Termsarasab et al., 2013) and that of CSOAA-DTPA-Gd was 3.86 μg/ml (Fig. 7); the lower value implies that the CSOAA-based nanoprobe may be more stable after dilution in body fluids. Gd-DTPA (Magnevist) has a terminal elimination half-life of about 20 min (Weinmann et al., 1984). Considering the higher molecular weight and larger particle size of the developed polymeric nanoprobe, a polymeric nanoprobe including Gd-DTPA likely exhibits reduced *in vivo* clearance, thereby increasing its blood circulation time compared to the commercial contrast agent (Magnevist). Moreover, the EPR effect can improve accumulation of nanoprobes in the tumor region. In our previous report, the nano-sized polymeric probe exhibited MR signal-enhancing effects in the tumor region compared to the commercial formulation (Cho et al., 2012b). The particle size

(~150 nm) of the experimental nanoprobe in this study may yield improved tumor targetibility and cancer diagnosis.

3.3. In vitro cytotoxicity

The cytotoxicity of the CSOAA-based nanoprobe (CSOAA-DTPA and CSOAA-DTPA-Gd) was evaluated in cancer cells according to nanoprobe concentration and incubation time. In this investigation, Human laryngeal and pharyngeal cancer (Hep-2 and FaDu) cells were used. These two cell types have previously been used for head and neck cancer research (Cho et al., 2012a; Termsarasab et al., 2013). CSOAA showed no severe cytotoxicity in FaDu cells in a previous report (Termsarasab et al., 2013); therefore, its cytotoxicity was not evaluated in this study. Viability (%) in both cell types was assessed by MTS-based assay. As shown in Fig. 8, the cytotoxicity of CSOAA-DTPA and CSOAA-DTPA-Gd seemed to be inconsequential in both cell lines at the probe concentrations and incubation times (12 and 24 h) used. Although Gd has been used as a representative T_1-weighted contrast agent, the aqueous Gd^{3+} ion exhibited severe cytotoxicity (Ananta et al., 2010). Therefore, organic linear and macrocyclic ligands (e.g. DTPA) are required to chelate Gd^{3+} to reduce toxicity (Ananta et al., 2010; Bartolini et al., 2003). CSOAA-DTPA-Gd exhibited no severe cytotoxicity in head and neck cancer cells (Fig. 8), implying that this nanoprobe is safe for MR imaging.

3.4. In vitro cellular uptake

The cellular uptake efficiency of the experimental nanoprobe was determined by CLSM. The nanoprobe was labeled with Cy5.5 and its intracellular uptake and distribution were observed. Cy5.5 was used as a NIRF imaging dye for *in vivo* tumor imaging in our previous studies (Cho et al., 2012b; Cho et al., 2011; Cho et al., 2012c). The Cy5.5 NHS ester was conjugated to the amine group of CSO by amide bond formation; the Cy5.5 content of the Cy5.5-labeled CSOAA-based nanoprobe was 0.13% (w/w). Cellular uptake and distribution patterns of Cy5.5-labeled nanoprobe were monitored up to 12 h in both Hep-2 and FaDu cells. The Cy5.5 fluorescence intensity, indicating the amount of nanoprobe taken up by cells, increased according to incubation time in both cell types (Fig. 9).

The physicochemical properties of nanoparticles, such as mean diameter, surface charge, morphology and composition, can influence their cellular uptake and distribution (Chavanpatil et al., 2006). Though smaller nanoparticles with a uniform size distribution exhibit increased uptake, other factors can play important roles in cellular uptake of chitosan-based nanoparticles (Desai et al., 1996; Kim et al., 2001; Nam et al., 2009). The surface charge of a nanoparticle can affect its cellular uptake and subsequent cellular distribution. Electrostatic interaction between positively charged chitosan-based nanoparticles and the negatively charged cellular membrane can facilitate cellular binding and uptake of nanoparticles. The positive charge of a chitosan-based nanoparticle promoted its internalization rate and level in eight cell

lines (Yue et al., 2011). In addition, some positively charged nanoparticles escaped the lysosome and localized perinuclearly. Endocytosis of the nanoprobe is thought to be governed by its particle size (~150 nm) and positive zeta potential (Table 1).

3.5. Phantom study

In vitro paramagnetism of Gd-DTPA (Magnevist) and CSOAA-DTPA-Gd were evaluated by 4.7-T MRI. In Fig. 10A, T_1-weighted MR images of both formulations according to the Gd concentration (5–100 μM) are shown. As Gd concentration increased, MR signals were also enhanced, as indicated by the brightness in both groups. The MR signals were analyzed quantitatively and a linear relationship between the proton longitudinal relaxation rate ($1/T_1$) and Gd concentration was identified. T_1 relaxivity (r_1) was calculated using Eq. (1). T_1 relaxivity of the CSOAA-based nanoprobe was 15.28 $mM^{-1}s^{-1}$, 2.43-fold higher than that of Gd-DTPA (Magnevist) in this investigation (Fig. 10B). In our previous report (Cho et al., 2012b), a contrast enhancing effect of a hyaluronic acid derivative-based nanoprobe compared to the commercial formulation (Magnevist) was found. CSOAA also has several hydroxyl groups in its glucose ring unit that can attract adjacent water molecules, thereby improving the local density of water molecules (Cho et al., 2012b). This may increase the water exchange rate in Gd molecules and lead to enhanced T_1 relaxivity (Yim et al., 2011; Caraban, 2006).

Although therapeutic drugs were not incorporated in this study, the formation of an internal hydrophobic core due to the AA segment is expected to facilitate loading of hydrophobic drugs. Anti-cancer drug delivery using an unmodified CSOAA nanoparticle and its anti-tumor efficacy in a head and neck cancer model have been reported previously (Termsarasab et al., 2013). Therefore, although it is expected that the theranostic nanoparticle based on CSOAA is feasible for cancer therapy and diagnosis, further studies of its usefulness are required.

4. Conclusions

Self-assembled CSOAA-based nanoprobes including a T_1 contrast agent was developed for MR imaging. DTPA was conjugated to CSOAA via an amide bond and Gd^{3+} was chelated to the DTPA ligand. This created a spherical nanoprobe of ~150 nm mean diameter with a positive zeta potential. The CSOAA-based nanoprobe exhibited negligible cytotoxicity in head and neck cancer cell lines. Cellular uptake and distribution of the Cy5.5-labeled nanoprobe were also observed by CLSM and the amount of nanoprobe taken up in head and neck cancer cells increased according to incubation time. The T_1 contrast-enhancing effect of the CSOAA-based nanoprobe, compared to the commercial formulation (Magnevist), was demonstrated in a phantom study. These results suggest that the CSOAA-based nanoprobe is a promising MR imaging probe for cancer diagnosis.

5. References

Ananta, J.S., Godin, B., Sethi, R., Moriggi, L., Liu, X., Serda, R.E., Krishnamurthy, R., Muthupillai, R., Bolskar, R.D., Helm, L., 2010. Geometrical confinement of gadolinium-based contrast agents in nanoporous particles enhances T1 contrast. Nat. Nanotechnol. 5, 815-821.

Bartolini, M., Pekar, J., Chettle, D., McNeill, F., Scott, A., Sykes, J., Prato, F., Moran, G., 2003. An investigation of the toxicity of gadolinium based MRI contrast agents using neutron activation analysis. Magn. Reson. Imaging 21, 541-544.

Caravan, P., 2006. Strategies for increasing the sensitivity of gadolinium based MRI contrast agents. Chem. Soc. Rev. 35, 512-523.

Caravan, P., Ellison, J.J., McMurry, T.J., Lauffer, R.B., 1999. Gadolinium (III) chelates as MRI contrast agents: structure, dynamics, and applications. Chem. Rev. 99, 2293-2352.

Chavanpatil, M.D., Khdair, A., Panyam, J., 2006. Nanoparticles for cellular drug delivery: mechanisms and factors influencing delivery. J. Nanosci. Nanotechnol. 6, 2651-2663.

Cheng, J.-J., Zhu, J., Liu, X.-S., He, D.-N., Xu, J.-R., Wu, L.-M., Zhou, J., Feng, Q., 2012. Gadolinium-chitosan nanoparticles as a novel contrast agent for potential use in clinical bowel-targeted MRI: a feasibility study in healthy rats. Acta Radiol. 53, 900-907.

Cho, H.-J., Chong, S., Chung, S.-J., Shim, C.-K., Kim, D.-D., 2012a. Poly-L-arginine and dextran sulfate-based nanocomplex for epidermal growth factor receptor (EGFR) siRNA delivery: its application for head and neck cancer treatment. Pharm. Res. 29, 1007-1019.

Cho, H.-J., Yoon, H.Y., Koo, H., Ko, S.-H., Shim, J.-S., Cho, J.-H., Park, J.H., Kim, K., Kwon, I.C., Kim, D.-D., 2012b. Hyaluronic acid-ceramide-based optical/MR dual imaging nanoprobe for cancer diagnosis. J. Control. Release 162, 111-118.

Cho, H.-J., Yoon, H.Y., Koo, H., Ko, S.-H., Shim, J.-S., Lee, J.-H., Kim, K., Kwon, I.C., Kim, D.-D., 2011. Self-assembled nanoparticles based on hyaluronic acid-ceramide (HA-CE) and Pluronic® for tumor-targeted delivery of docetaxel. Biomaterials 32, 7181-7190.

Cho, H.-J., Yoon, I.-S., Yoon, H.Y., Koo, H., Jin, Y.-J., Ko, S.-H., Shim, J.-S., Kim, K., Kwon, I.C., Kim, D.-D., 2012c. Polyethylene glycol-conjugated hyaluronic acid-ceramide self-assembled nanoparticles for targeted delivery of doxorubicin. Biomaterials 33, 1190-1200.

Desai, M.P., Labhasetwar, V., Amidon, G.L., Levy, R.J., 1996. Gastrointestinal uptake of biodegradable microparticles: effect of particle size. Pharm. Res. 13, 1838-1845.

Ernsting, M.J., Foltz, W.D., Undzys, E., Tagami, T., Li, S.-D., 2012. Tumor-targeted drug delivery using MR-contrasted docetaxel–carboxymethylcellulose nanoparticles. Biomaterials 33, 3931-3941.

Janib, S.M., Moses, A.S., MacKay, J.A., 2010. Imaging and drug delivery using theranostic nanoparticles. Adv. Drug Deliv. Rev. 62, 1052-1063.

Johnson, N.J., Oakden, W., Stanisz, G.J., Scott Prosser, R., van Veggel, F.C., 2011. Size-tunable, ultrasmall NaGdF4 nanoparticles: insights into their T1 MRI contrast enhancement. Chem. Mater. 23, 3714-3722.

Key, J., Cooper, C., Kim, A.Y., Dhawan, D., Knapp, D.W., Kim, K., Park, J.H., Choi, K., Kwon, I.C., Park, K., 2012. In vivo NIRF and MR dual-modality imaging using glycol chitosan nanoparticles. J. Control. Release 163, 249-255.

Kim, Y.H., Gihm, S.H., Park, C.R., Lee, K.Y., Kim, T.W., Kwon, I.C., Chung, H., Jeong, S.Y., 2001. Structural characteristics of size-controlled self-aggregates of deoxycholic acid-modified chitosan and their application as a DNA delivery carrier. Bioconjug. Chem. 12, 932-938.

Kobayashi, H., Sato, N., Hiraga, A., Saga, T., Nakamoto, Y., Ueda, H., Konishi, J., Togashi, K., Brechbiel, M.W., 2001. 3D-micro-MR angiography of mice using macromolecular MR contrast agents with polyamidoamine dendrimer core with reference to their pharmacokinetic properties. Magn. Reson. Med. 45, 454-460.

L. Villaraza, A.J., Bumb, A., Brechbiel, M.W., 2010. Macromolecules, dendrimers, and nanomaterials in magnetic resonance imaging: the interplay between size, function, and pharmacokinetics. Chem. Rev. 110, 2921-2959.

Lim, E.-K., Kim, H.-O., Jang, E., Park, J., Lee, K., Suh, J.-S., Huh, Y.-M., Haam, S., 2011. Hyaluronan-modified magnetic nanoclusters for detection of CD44-overexpressing breast cancer by MR imaging. Biomaterials 32, 7941-7950.

Liu, T., Li, X., Qian, Y., Hu, X., Liu, S., 2012. Multifunctional pH-disintegrable micellar nanoparticles of asymmetrically functionalized β-cyclodextrin-based star copolymer covalently conjugated with doxorubicin and DOTA-Gd moieties. Biomaterials 33, 2521-2531.

Nam, H.Y., Kwon, S.M., Chung, H., Lee, S.-Y., Kwon, S.-H., Jeon, H., Kim, Y., Park, J.H., Kim, J., Her, S., 2009. Cellular uptake mechanism and intracellular fate of hydrophobically modified glycol chitosan nanoparticles. J. Control. Release 135, 259-267.

Termsarasab, U., Cho, H.-J., Kim, D.H., Chong, S., Chung, S.-J., Shim, C.-K., Moon, H.T., Kim, D.-D., 2013. Chitosan oligosaccharide–arachidic acid-based nanoparticles for anti-cancer drug delivery. Int. J. Pharm. 441, 373-380.

Weinmann, H.-J., Brasch, R., Press, W., Wesbey, G., 2005. 6.4 Characteristics of gadolinium-DTPA complex: a potential NMR contrast agent. Classic Papers in Modern Diagnostic Radiology, 416.

Yim, H., Yang, S.-G., Jeon, Y.S., Park, I.S., Kim, M., Lee, D.H., Bae, Y.H., Na, K., 2011. The performance of gadolinium diethylene triamine pentaacetate-pullulan hepatocyte-specific T1 contrast agent for MRI. Biomaterials 32, 5187-5194.

Yue, Z.-G., Wei, W., Lv, P.-P., Yue, H., Wang, L.-Y., Su, Z.-G., Ma, G.-H., 2011. Surface charge affects cellular uptake and intracellular trafficking of chitosan-based nanoparticles. Biomacromolecules 12, 2440-2446.

Yuk, S.H., Oh, K.S., Cho, S.H., Lee, B.S., Kim, S.Y., Kwak, B.-K., Kim, K., Kwon, I.C., 2011. Glycol chitosan/heparin immobilized iron oxide nanoparticles with a tumor-targeting characteristic for magnetic resonance imaging. Biomacromolecules 12, 2335-2343.

Table 1 Characteristics of CSOAA-DTPA and CSOAA-DTPA-Gd nanoprobes.

Nanoprobe	Mean diameter (nm)	Polydispersity index	Zeta potential (mV)
CSOAA	177.03 ± 2.75	0.20 ± 0.02	12.50 ± 0.81
CSOAA-DTPA	177.90 ± 18.79	0.09 ± 0.01	9.21 ± 0.85
CSOAA-DTPA-Gd	146.30 ± 5.51	0.20 ± 0.05	11.19 ± 0.39

Value are presented as means ± standard deviation (SD) (*n*=3).

Concentration of all samples was 1 mg/ml.

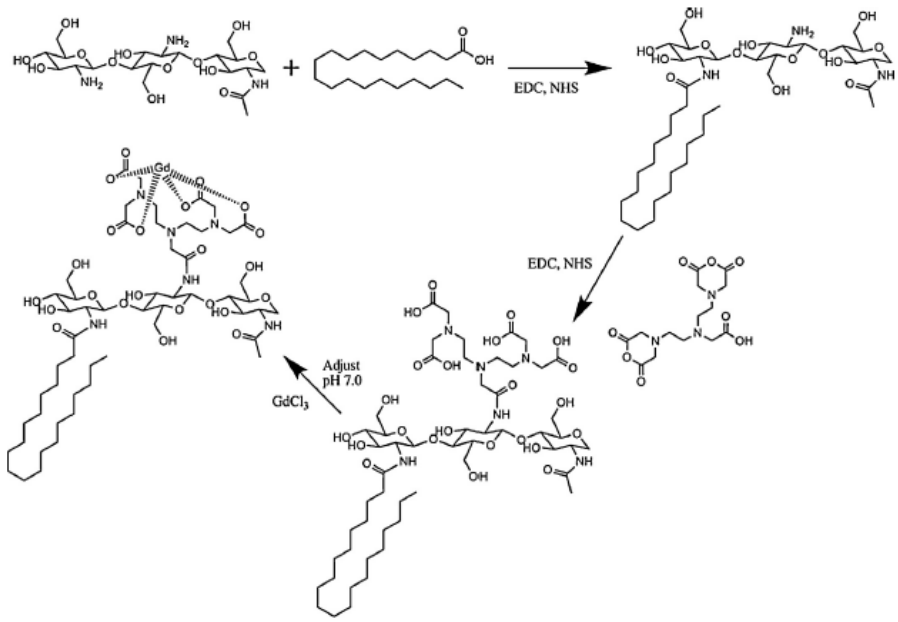

Figure 1. Synthetic scheme of CSOAA-DTPA-Gd.

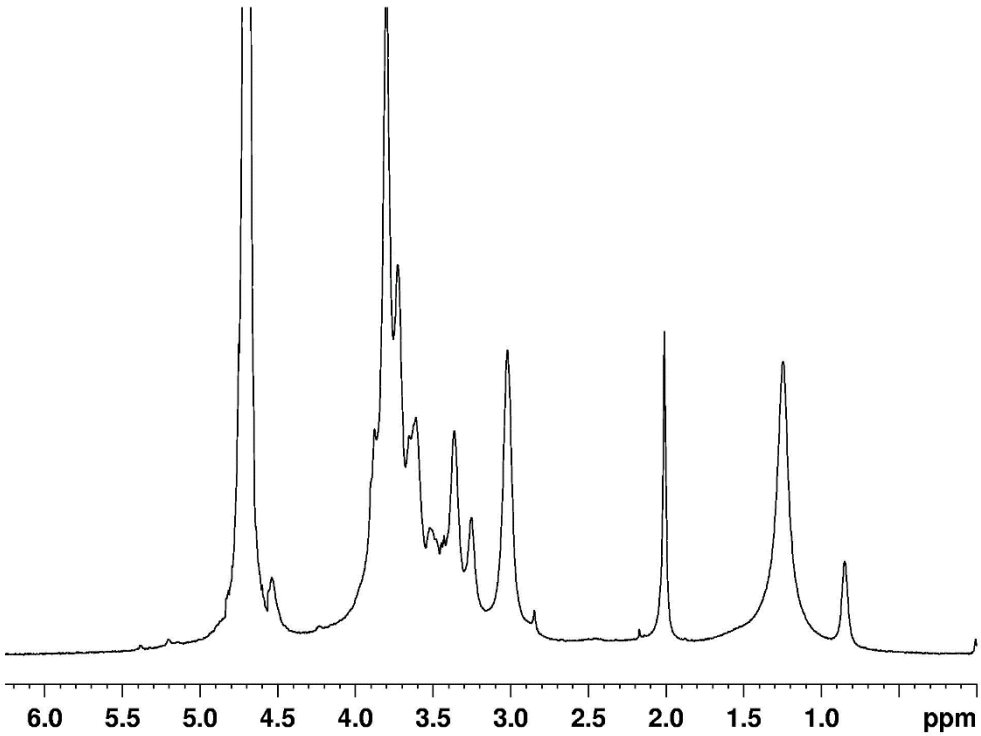

Figure 2 ^{1}H-NMR spectrum of CSOAA-DTPA. It was solubilized in D_2O for ^{1}H-NMR analysis (500 MHz).

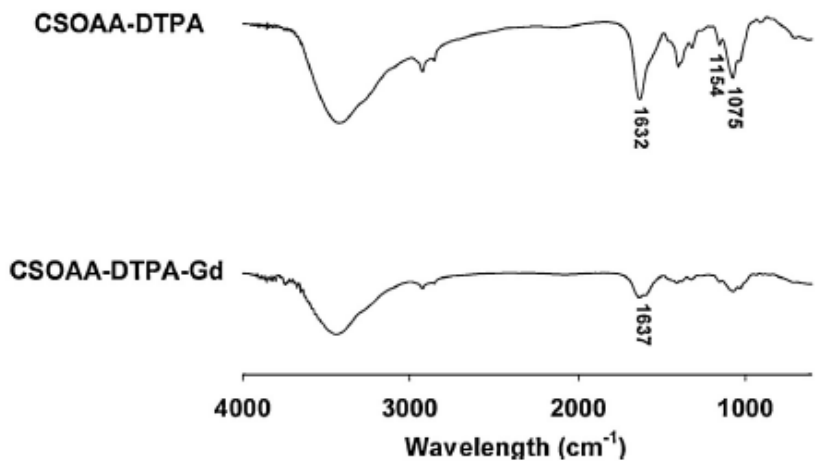

Figure 3 FT-IR spectra of CSOAA-DTPA and CSOAA-DTPA-Gd.

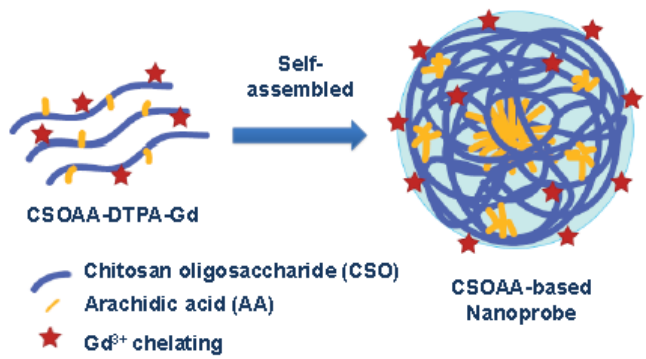

Figure 4 Schematic illustration of CSOAA-DTPA-Gd nanoprobe.

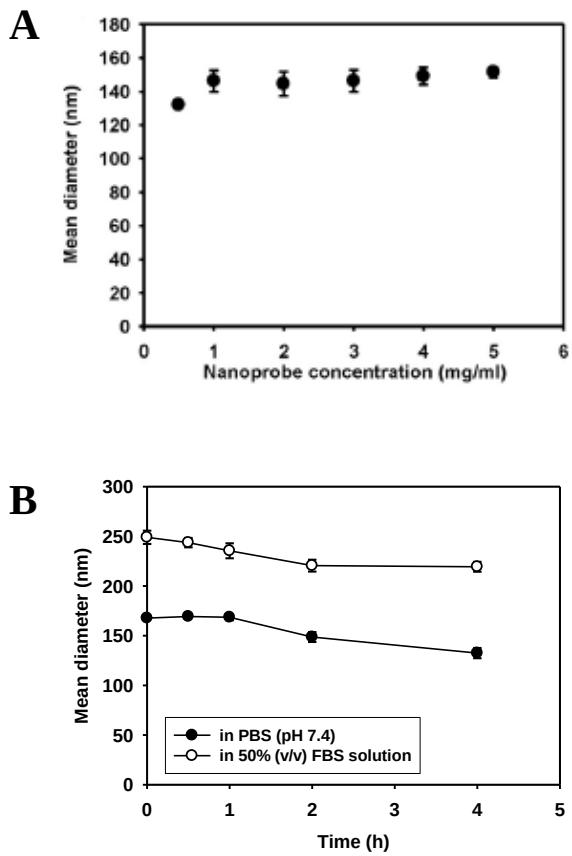

Figure 5 Characteristics of the CSOAA-based nanoprobe. (A) The mean diameter of the nanoprobe was plotted according to its concentration (0.5-5 mg/ml). (B) Monitoring particle size according to incubation time. CSOAA-based nanoprobe (at 5 mg/ml concentration) was dissolved in PBS (pH 7.4) or 50% (v/v) FBS solution (in PBS pH 7.4). Data are expressed as mean ± SD (n = 3).

A

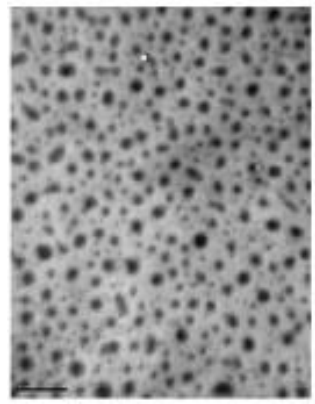

B

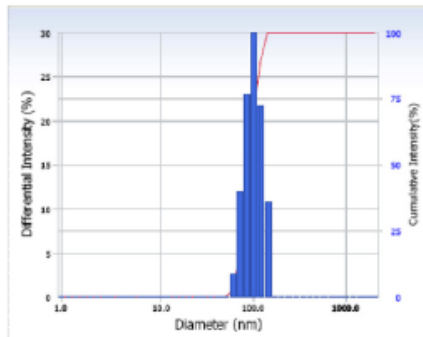

Figure 6 TEM image (A) and size distribution (B) of CSOAA-DTPA-Gd nanoprobes (2.5 mg/ml). The scale bar in TEM image represents 1 μm.

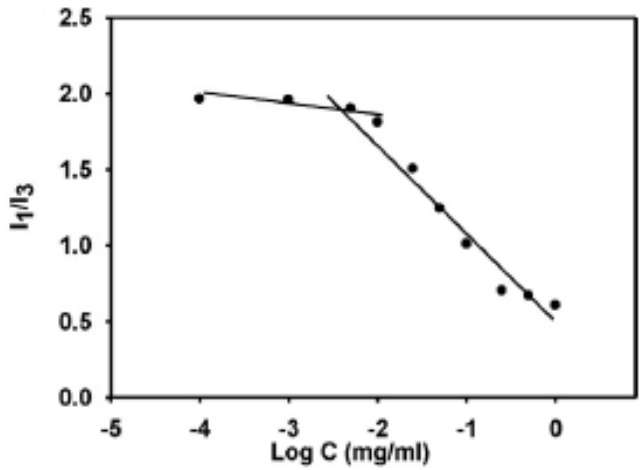

Figure 7 CAC determination of the CSOAA-based nanoprobe. The fluorescence intensity ratio (I_{373}/I_{383}, I_1/I_3) was plotted according to nanoprobe concentration and the CAC was estimated from the threshold concentration of the nanoprobe.

A

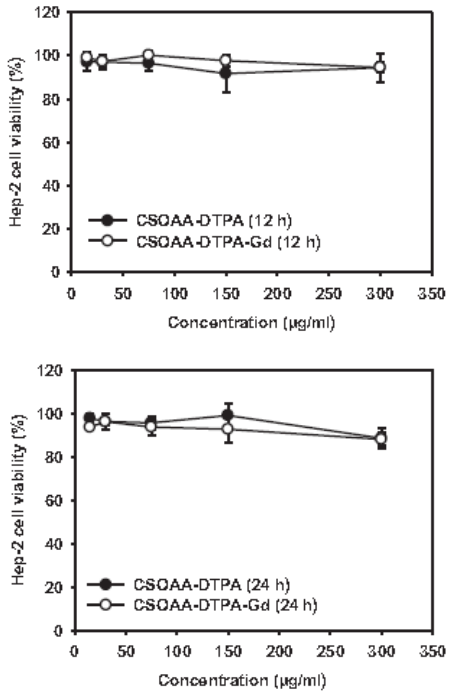
Hep-2 cell viability (%)
120
100
80
60
40
20
0
0
50
100
150
200
250
300
350
Concentration (μg/ml)
CSOAA-DTPA (12 h)
CSOAA-DTPA-Gd (12 h)
Hep-2 cell viability (%)
120
100
80
60
40
20
0
0
50
100
150
200
250
300
350
Concentration (μg/ml)
CSOAA-DTPA (24 h)
CSOAA-DTPA-Gd (24 h)

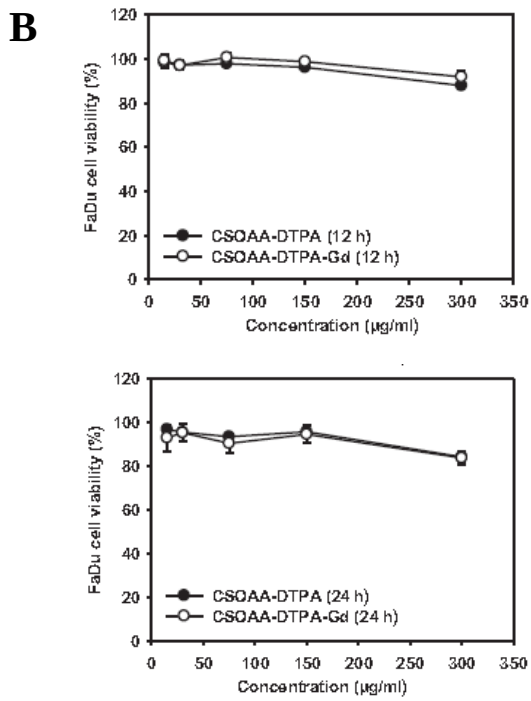

Figure 8 *In vitro* cytotoxicity tests of the CSOAA-based nanoprobe in (A) Hep-2 and (B) FaDu cells after 12 and 24 h of incubation. Cell viability (%) was measured by MTS-based assay according to nanoprobe concentration. Data are expressed as means ± SD (n = 4).

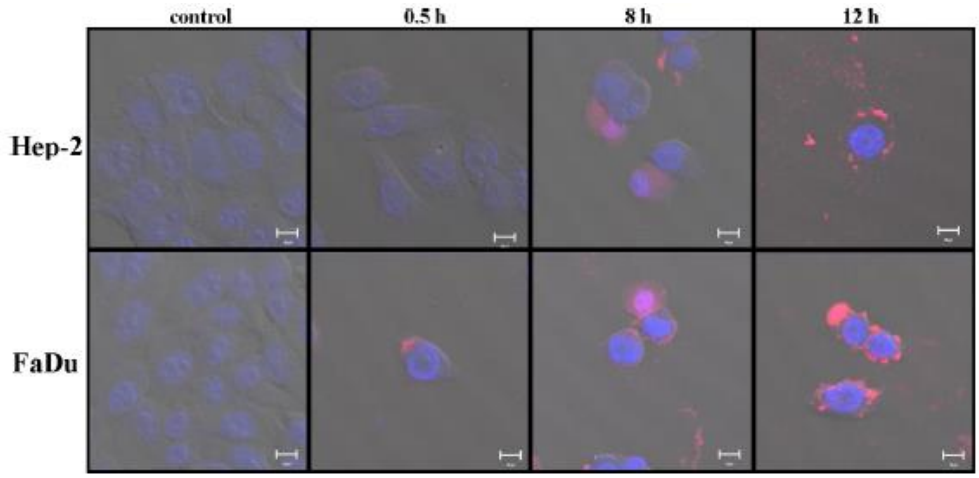

Figure 9 Cellular uptake studies of the nanoprobe in Hep-2 and FaDu cells. Intracellular uptake and distribution of the Cy5.5-labeled nanoprobe were visualized by CLSM. Merged images of the control (no treatment), and 0.5 h, 8 h and 12 h incubation groups are shown. Red and blue indicate Cy5.5 and DAPI, respectively. The bar in the picture represents 10 μm.

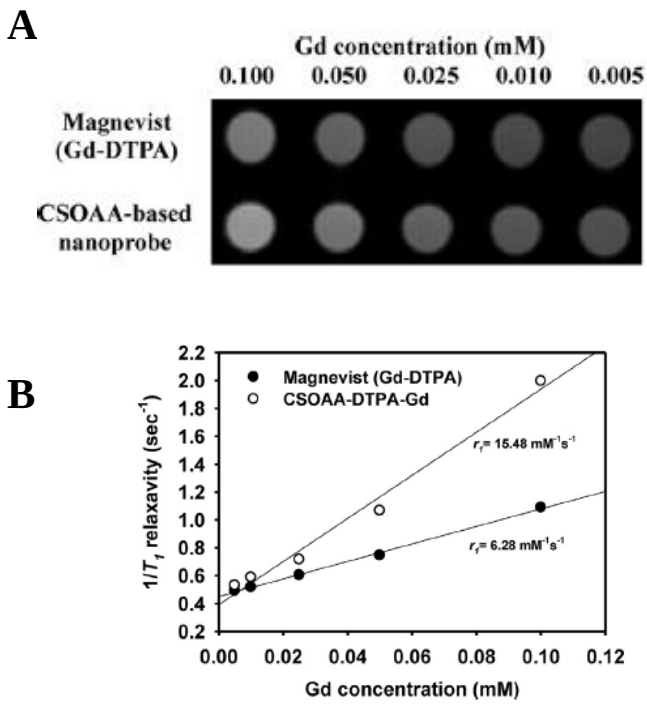

Figure 10 *In vitro* MRI test of Magnevist (Gd-DTPA) and CSOAA-DTPA-Gd at 4.7-T. (A) T_1-weighted phantom image with 5–100 μM Gd concentrations was shown. (B) Longitudinal relaxation (1/ T_1) according to the Gd concentration was plotted.

PART III. Polyethylene glycol-modified arachidyl chitosan-based nanoparticles for prolonged blood circulation of doxorubicin

1. Introduction

Nano-sized carriers have been developed for anti-cancer drug delivery to tumor regions to overcome the intrinsic drawbacks of using the pure drug, which include a short half-life and undesired distribution to normal tissues and organs (Bae et al., 2007; Cho et al., 2011; ElBayoumi and Torchilin, 2009; Jin et al., 2012; Mu et al., 2010; Xiao et al., 2012; Yang et al., 2007). Several approaches for modifying the surfaces of nanovehicles to modulate the pharmacokinetic and pharmacodynamic properties of drugs have been investigated. Shielding groups, adsorbed or conjugated to the surface of nanoparticles, can disturb the electrostatic and hydrophobic interactions between opsonins and nanoparticles (Owens and Peppas, 2006). Among them, PEG has been grafted or adsorbed onto the drug itself or polymers (Cho et al., 2012b; Kaminskas et al., 2013; Veronese et al., 2005). It is known that an outer PEG shell can prevent the opsonization of nanoparticles in the blood and maintain their camouflage for phagocytosis (Owens and Peppas, 2006). Thus, this "stealth effect" can enhance systemic drug exposure and prolong circulation of nanocarriers in the blood stream. It has also been reported that the density of the PEG chain on the surface of nanoparticles may affect their interaction with blood components and macrophages (Owens and Peppas, 2006). Studies of the influence of PEG conjugation to various polymeric nanoparticles, for anti-cancer drug delivery, on the blood circulation time and anti-tumor efficacy have been reported (Cho et al., 2012b;

Lv et al., 2012; Qu et al., 2009; Yadav et al., 2011). Moreover, a PEG shell on nanoparticles containing anti-cancer agents reduced their hematological toxicity after intravenous administration (Jain et al., 2012); thus, it can be used to mask the toxicity of polymeric matrix in the blood stream.

Natural polymers and their derivatives have been widely used for the development of self-assembled nanoparticles for cancer therapy and diagnosis (Cho et al., 2012a; Chung et al., 2013; Lee et al., 2011; Nogueira et al., 2013). In our previous reports (Termsarasab et al., 2013a,b), chitosan oligosaccharide-arachidic acid (CSOAA), as an amphiphilic chitosan oligosaccharide derivative, was synthesized, and self-assembled nanoparticles based on CSOAA were prepared. CSOAA-based nanoparticles were developed for delivery of anti-cancer drugs to the tumor region and cancer diagnosis. Although anti-tumor efficacy after intravenous injection based on passive targeting strategy, mainly due to the enhanced permeability and retention (EPR) effect, has been achieved in a head and neck cancer xenograft mouse model, the nanoparticles developed may exhibit greater in vivo anti-tumor efficacy as a result of the surface modification. Here, PEGylated CSOAA-based nanoparticles were prepared in an effort to prolong their circulation in the blood stream after intravenous administration. CSOAA-PEG conjugate was synthesized, and the physicochemical properties of CSOAA-PEG nanoparticles were investigated. Their application for leukemia therapy was tried and the alterations in the pharmacokinetic properties of the drug were assessed in an animal model.

2. Materials and methods

2.1. Materials

Chitosan oligosaccharide (CSO; average molecular weight = 5 kDa, deacetylation degree > 90%) was obtained from Kitto Life Co., Ltd. (Seoul, Korea). Arachidic acid (AA), 1-ethyl-3-(3-dimethylaminopropyl) carbodiimide (EDC), N-hydroxysuccinimide (NHS), deuterochloroform ($CDCl_3$) and deuterium oxide (D_2O) were purchased from Sigma–Aldrich Co. (St. Louis, MO, USA). Methoxypolyethylene glycol succinimidyl succinate (mPEG-SS; molecular weight = 2 kDa) was provided by Sunbio Co. (Anyang, Korea). Doxorubicin hydrochloride (DOX HCl) was purchased from Boryung Pharmaceutical Co., Ltd. (Seoul, Korea). RPMI 1640 medium, penicillin, streptomycin, and heat-inactivated fetal bovine serum (FBS) were purchased from Gibco Life Technologies Inc. (Grand Island, NY, USA). All other reagents were of analytical grade and were obtained from commercial sources.

2.2. Synthesis and characterization of CSOAA-PEG

CSOAA was synthesized as described in our previous report, with slight modifications (Termsarasab et al., 2013a). Briefly, CSO (0.2 mmol) and AA (1 mmol)

were solubilized in 25 ml dimethyl sulfoxide (DMSO) separately at 50 °C for 15 min and cooled to room temperature. EDC (1.5 mmol) and NHS (1.5 mmol) were added to the AA solution and stirred for 30 min. Then, the AA solution was added to the CSO solution; the reaction was conducted for 12 h with stirring. That solution was then adjusted to pH 3.5 with 1 N HCl, prior to precipitating with 450 ml acetone three times to remove unreacted AA. The precipitate was collected by centrifugation (8608×g, 30 min), and resuspended in 50-ml double-distilled water (DDW). This solution was dialyzed (dialysis membrane molecular weight cut-off = 1 kDa; Spectrum Laboratories, Laguna Hills, CA, USA) against DDW for 2 days. CSOAA was obtained after freeze-drying.

To synthesize CSOAA-PEG, CSOAA (0.125 mmol) was solubilized in 30-ml DMSO, followed by addition of mPEG-SS (0.25 mmol). After stirring for 12 h, the solution was dialyzed (dialysis membrane molecular weight cut-off = 3.5 kDa) against DDW for 1 day and then freeze-dried. The freeze-dried product was precipitated by adding excess acetone to remove unreacted mPEG-SS. The precipitate was collected by filtering and dried at 60 °C. The conjugations of CSOAA and CSOAA-PEG were confirmed by ^{1}H-NMR analysis (Varian FT 500-MHz, Varian Inc., Palo Alto, CA, USA). To prepare the ^{1}H-NMR samples (15 mg/ml concentration), CSOAA and CSOAA-PEG were dissolved in D_2O and mPEG-SS was solubilized in $CDCl_3$, respectively. Standard samples were prepared by mixing mPEG-SS and CSOAA at various molar ratios (0.5:1, 1:1, 1:2, 1:3, and 1:4) and freeze-drying for the determination of molar substitution (MS) of CSOAA-PEG. The

MS of CSOAA-PEG was calculated based on the ratio of the integration values of the CSOAA and mPEG-SS 1H NMR spectra. Those substances were dissolved in DMSO-d_6.

2.3. Preparation and characterization of DOX-loaded nanoparticles

DOX-loaded CSOAA and CSOAA-PEG nanoparticles were prepared by a solvent evaporation method as reported previously (Termsarasab et al., 2013a). DOX base was prepared by the reaction between DOX HCl and triethylamine in DMSO for 12 h and lyophilization. CSOAA or CSOAA-PEG and DOX base (7.5:1.5, w/w) were dissolved in DMSO and DDW mixture (1:1, v/v). The solvent was removed under a nitrogen gas stream at 70 °C for 4 h. The drug and polymer film coated-tube was hydrated with DDW, followed by sonication using a probe sonicator (Vibra-Cell, Sonics & Materials Inc., CT, USA) for 5 min. The nanoparticle suspension was then filtered through a syringe filter with 0.45-μm pore size (Minisart RC15; Satorius Stedim Biotech GmbH, Gottingen, Germany) to remove unloaded DOX. The average mean diameter, polydispersity index, and zeta potential values of DOX-loaded CSOAA and CSOAA-PEG nanoparticles in DDW were measured using a dynamic light scattering (DLS) spectrophotometer (ELS-Z; Otsuka Electronics Co. Ltd., Osaka, Japan). Change of particle size (nm) in DDW and 50% (v/v) FBS was

also measured according to the incubation time (0.5, 1, 1.5, 2, 4, 6, 24, 48, and 72 h). The morphology of nanoparticles was observed by transmission electron microscopy (TEM; LIBRA 120; Carl Zeiss, Oberkochen, Germany). Samples were stained with 2% (w/v) phosphotungstic acid, loaded on a copper grid coated with carbon film, and dried at 20 °C. To determine the encapsulation efficiency (EE) of the drug, aliquots of samples (0.1 ml of each nanoparticle suspension) were diluted with a 100×volume of DMSO to disrupt the nanoparticles. DOX content was analyzed by a high-performance liquid chromatography (HPLC) method using a Waters HPLC system (Waters Co., Milford, MA, USA) equipped with a reversed-phase (RP) C-18 column (Xbridge, RP-18, 250 mm×4.6 mm, 5 μm; Waters Co.), a separation module (Waters e2695), and a fluorescence detector (Waters 2475). The mobile phase consisted of 10 mM K_2HPO_4 (pH 2.5) and 0.01% (v/v) triethylamine in acetonitrile (71:29, v/v) with a flow rate of 1 ml/min. The excitation and emission wavelengths were 470 and 565 nm, respectively. The injection volume was 20 μl. The inter-day and intra-day variances were within the acceptable range. The EE value of DOX in nanoparticles was determined by the following equation:

$$EE\ (\%) = \frac{actual\ amount\ of\ DOX\ in\ nanoparticle}{theoretical\ amount\ of\ DOX\ in\ nanoparticle} \times 100 \qquad (1)$$

2.4. In vitro DOX release test

DOX-loaded CSOAA or CSOAA-PEG nanoparticles (150 μl) were loaded in a mini GeBA-flex tube (molecular weight cut-off: 12–14 kDa, Gene Bio-Application Ltd., Kfar Hanagide, Israel) and placed in 15 ml of phosphate-buffered saline (PBS: pH 5.5, 6.8, and 7.4, adjusted with phosphoric acid). The drug release test was conducted in a shaking bath at 37 °C and 50 rpm rotation speed. Aliquots of release medium (200 μl) were collected at set times (1, 2, 3, 4, 6, 9, 12, 24, 48, 72, 96, and 120 h), and an equivalent volume of fresh medium was replaced. The amount (%) of DOX released was determined by the HPLC method described above. 2.5. *In vitro* cytotoxicity of CSOAA and CSOAA-PEG Human leukemia K562 cells were purchased from the Korean Cell Line Bank (Seoul, Korea). The cells were cultured in RPMI 1640 medium containing 10% FBS, 100 U/ml penicillin, and 100 μg/ml streptomycin at 37 °C in a 5% CO_2 atmosphere and 95% relative humidity. The cytotoxicities of CSOAA and CSOAA-PEG to K562 cells were determined using a 3-(4,5-dimethylthiazol-2-yl)-5(3-carboxymethonyphenol)-2-(4-sulfophenyl)-2H tetrazolium (MTS)-based assay. Various concentrations (~100 μg/ml) of CSOAA and CSOAA-PEG were added to 1×10^4 cells suspended in 100 μl culture media and incubated for 24, 48, and 72 h. Then, the cells were treated with the MTS-based CellTiter 96 AQ_{ueous} One Solution Cell Proliferation Assay Reagent (Promega Corp., Madison, WI, USA) at 37 °C for 4 h, according to the manufacturer's protocol. The

absorbance at 490 nm was measured using a microplate reader (EMax, Molecular Devices, Sunnyvale, CA).

2.5. In vitro cytotoxicity of CSOAA and CSOAA-PEG

Human leukemia K562 cells were purchased from the Korean Cell Line Bank (Seoul, Korea). The cells were cultured in RPMI 1640 medium containing 10% FBS, 100 U/ml penicillin, and 100 μg/ml streptomycin at 37 °C in a 5% CO_2 atmosphere and 95% relative humidity. The cytotoxicities of CSOAA and CSOAA-PEG to K562 cells were determined using a 3-(4,5-dimethylthiazol-2-yl)-5(3-carboxymethonyphenol)-2-(4-sulfophenyl)-2H-tetrazolium (MTS)-based assay. Various concentrations (~100 μg/ml) of CSOAA and CSOAA-PEG were added to 1×10^4 cells suspended in 100-μl culture media and incubated for 24, 48, and 72 h. Then, the cells were treated with the MTS-based CellTiter 96 AQueous One Solution Cell Proliferation Assay Reagent (Promega Corp., Madison, WI, USA) at 37 °C for 4 h, according to the manufacturer's protocol. The absorbance at 490 nm was measured using a microplate reader (EMax, Molecular Devices, Sunnyvale, CA).

2.6. In vitro cellular uptake study

K562 cells at a density of 6×10^5 per well were treated with free DOX, DOX-loaded CSOAA nanoparticles, or CSOAA-PEG nanoparticles at an equivalent DOX concentration (15 μg/ml). After the cells were incubated for 1 h, they were washed with PBS (pH 7.4) and resuspended in medium with 2% (v/v) FBS. DOX uptake efficiency was evaluated by flow cytometry using a FACSCalibur equipped with the CELLQuest software (Becton Dickinson Biosciences, San Jose, CA, USA).

2.7. In vivo pharmacokinetics in rats

Animal study protocol was approved by the Institutional Animal Care and Use Committee of Seoul National University (Seoul, Korea). Male Sprague-Dawley (SD) rats, weighing 250 – 300 g (Orient Bio, Inc., Seongnam, Korea), were used. The rats were housed under standard room (Animal Center for Pharmaceutical Research, College of Pharmacy, Seoul National University) at a temperature of 20 – 23 °C and a relative humidity of 50 ± 5%. A polyethylene tube (PE-50; Clay Adams, Parsippany, NJ, USA) was cannulated into the femoral veins and arteries of rats under ketamine anesthesia (50 mg/kg, intramuscular injection). Each group was administered at a single dose of 4 mg/kg DOX intravenously via the femoral vein. Blood samples (300 μl) were then collected via the femoral artery at 0, 2, 5, 15, 30,

60, 90, 120, 180, 240, 360, and 480 min and centrifuged (16,000×g, 5 min). Aliquots (150 µl) of plasma were stored at −20 °C until the quantitative analysis of DOX. The DOX concentration in plasma was analyzed by a reported HPLC method (Cho et al., 2012b) with slight modifications. An aliquot of plasma sample (150 µl) with propranolol solution (internal standard, 50 µl, 1 µg/ml) was mixed with acetonitrile (400 µl). After vortexing and centrifuging (16,000×g, 10 min), supernatant (300 µl) was transferred to a clean tube and evaporated under a gentle stream of nitrogen at 40 °C. The residue was reconstituted with 60-µl mobile phase (a mixture of 10 mM K_2HPO_4 (pH 2.5) and 0.01% (v/v) triethylamine in acetonitrile, 73:27, v/v). After vortexing and centrifuging, a 10-µl aliquot was subjected to HPLC analysis. The samples were injected into the RP-HPLC column as described above. The fluorescence intensity was monitored at excitation/emission wavelengths of 470/565 nm for DOX, and 230/540 nm for propranolol. The lower limit of quantification (LLOQ) value of DOX in rat plasma was 0.01 µg/ml. The intra-day and inter-day coefficients of variation were within the acceptable range. The total area under the plasma concentration–time curve from time zero to infinity (AUC), terminal half-life ($t_{1/2}$), time-averaged total body clearance (CL), apparent volume of distribution at steady state (Vss), and mean residence time (MRT) were calculated using the WinNonlin software (Pharsight, Mountain View, CA, USA).

2.8. Statistical analysis

Statistical analysis was conducted using t-test and analysis of variance (ANOVA). All experiments were performed at least three times. The data are shown as means ± standard deviation (SD).

3. Results and discussion

3.1. Synthesis of CSOAA-PEG

PEGylated CSOAA was synthesized to develop nanoparticles for DOX delivery. The synthetic method for CSOAA was reported in our previous study (Termsarasab et al., 2013a). Briefly, CSOAA was synthesized by a coupling reaction between the amine groups of CSO and carboxyl groups of AA using EDC and NHS as coupling reagents. EDC was introduced into the carboxyl groups of AA, and an AA-NHS intermediate was formed by adding NHS to EDC active ester. This intermediate was reacted with the amine group of CSO to generate CSOAA. Then, mPEG-SS was introduced to the remaining amine groups of CSOAA. To characterize the structure of CSOAA and CSOAA-PEG, ^{1}H NMR analyses of mPEG-SS, CSOAA, and CSOAAPEG were performed; their spectra are shown in Fig. 1. The proton peaks of the alkyl chain and methyl group of AA appeared at 1.2 and 0.8 ppm, respectively.

The specific proton peaks for the oxyethylene group (-CH_2CH_2O-) and methoxy group (CH_3O-) of mPEG appeared at 3.5–3.7 ppm and 3.3 ppm, respectively. The proton peaks between 2.5 and 3.0 ppm were corresponded to the succinimidyl succinate group of mPEG-SS. Compared with CSOAA and mPEG-SS, the ^{1}H NMR spectrum of CSOAA-PEG exhibited the specific proton peaks of CSOAA and mPEG, while the proton peak of the succinimidyl succinate group shifted to 2.2 ppm. These results confirmed PEG conjugation to CSOAA. A homogeneous physical mixture of CSOAA and PEG was prepared and each component was analyzed by ^{1}H NMR to calculate the molar substitution (MS) of PEG to CSOAA, according to a modified method reported previously (Termsarasab et al., 2013a). The molar substitution of PEG to CSOAA was calculated using the linear regression line, which was plotted between the integration ratio of the methoxy group of PEG (δ = 3.3; CH_3O-) to the N-acetyl proton group of CSO (δ = 1.8; CH_3CONH-), and the molar ratio of mPEG-SS to CSOAA prepared from standard samples (Fig. 2). The molar substitution (mole of mPEG-SS/mole of CSOAA) of PEG to CSOAA was 1.8 in this investigation.

3.2. Preparation and characterization of DOX-loaded nanoparticles

Based on the CSOAA-PEG synthesized, nanoparticles loaded with DOX were prepared using a solvent evaporation method (Termsarasab et al., 2013a). In this

study, CSOAA/DOX and CSOAAPEG/DOX, at a weight ratio of 7.5–1.5 (polymer to drug), nanoparticles were prepared (Fig. 3). The mean diameters of the CSOAA/DOX and CSOAA-PEG/DOX nanoparticles were 124.17 ± 2.58 and 165.75 ± 6.75 nm, respectively (Table 1). As shown in Fig. 4b, TEM image of the CSOAA-PEG/DOX nanoparticles showed a spherical shape and similar particle size to that measured by ELS. The hydrophilic PEG, conjugated to CSOAA, constituted the outer shell of the nanoparticles (Fig. 3). Because of this PEG shell, the mean diameter of drug-loaded CSOAA/PEG nanoparticles was increased versus drug-loaded CSOAA nanoparticles. This phenomenon was also reported by us previously (Cho et al., 2012b) for amphiphilic hyaluronic acid oligomer-based nanoparticles. Despite the outer hydrophilic PEG shell on the CSOAA-based nanoparticles, the mean diameter was less than 200 nm, indicating a low probability of reticuloendothelial system (RES) clearance (Gaucher et al., 2005). The polydispersity index of PEGylated CSOAA-based nanoparticles containing DOX was 0.19 ± 0.03, indicating a narrow size distribution (Fig. 4a). The zeta potential value of the CSOAA-PEG/DOX nanoparticles was lower than that of the CSOAA/DOX nanoparticles ($p < 0.05$), possibly due to the presence of the outer PEG shell.

The mean diameters of drug-loaded CSOAA and CSOAA-PEG nanoparticles were measured in DDW and those values of both nanoparticle groups were constantly maintained for 72 h (Fig. 5a). However, they are not enough to reflect the actual particle size in the blood stream. Additionally, *in vivo* pharmacokinetic and

pharmacodynamics performances cannot be predicted precisely from particle size measurements in DDW. Nanoparticles administered by the intravenous route can interact with blood components and form large aggregates or complexes (Liu et al., 2012; Rausch et al., 2010). These unwanted aggregates can inhibit normal blood circulation and are readily eliminated by RES organs (liver and spleen). Thus, changes in particle size in the presence of serum (50%, v/v) were monitored according to the incubation time. As shown in Fig. 5b, the mean diameter of CSOAA-PEG/DOX nanoparticles increased by 20.92% over 72 h, while CSOAA/DOX nanoparticles showed a 223.16% increase in mean diameter during the same period. The hydrophilic PEG shell of CSOAA-PEG/DOX nanoparticles hampered the interaction between blood constituents and the chitosan-based surface, and thus reduced the aggregation of nanoparticles in the presence of serum. Maintaining the initial mean diameter of PEGylated nanoparticles under serum conditions can lead to the improved stability by "stealth effect" (Qu et al., 2009; Zhang et al., 2013), and thereby prolonging circulation of the nanoparticles in the blood stream.

3.3. In vitro drug release

DOX release in vitro from the nanoparticle formulations was monitored at pH 5.5, 6.8, and 7.4 (Fig. 6). DOX release profiles from CSOAA-based nanoparticles under several pH conditions have been reported previously (Termsarasab et al.,

2013a). Despite different weight ratios between CSOAA and DOX compared with the current study, DOX release was improved in acidic pH condition. In this investigation, the proportions (%) of DOX released from CSOAA and CSOAA-PEG nanoparticles after 24 h were 56.69 ± 4.04% and 31.19 ± 0.95%, respectively. After a steady increase in DOX release from the CSOAA-PEG nanoparticles, the two values reached 56.02 ± 2.07% and 50.77 ± 5.88%, respectively, at day 5. Although the proportions of DOX released from both nanoparticle formulations were similar at steady state (around day 5), a sustained pattern of DOX release from the CSOAA-PEG nanoparticles was observed. Thus the PEG shell may delay drug diffusion and dissolution from the reservoir. Sustained drug release from PEGylated nanoparticle formulations has been reported previously (Cho et al., 2012b; Jain et al., 2012). Additionally, pH-dependent DOX release from CSOAA-PEG nanoparticles was observed. The proportions of DOX released from CSOAA-PEG nanoparticles at pH 7.4 and 5.5 on day 5 were 50.77 ± 5.88% and 83.57 ± 0.24%, respectively. This can be explained by the higher solubility of DOX under acidic pH conditions and changes in the binding strength between the drug and nanoparticle structure (Jin et al., 2012; Nukolova et al., 2011; Termsarasab et al., 2013a). Enhanced DOX release at pH 5.5 and 6.8, which reflects the conditions in endocytic compartments (endosomes and lysosomes, pH 5.5) and the tumor microenvironment (pH 6.8), may facilitate DOX uptake into cancer cells and so enhance its anti-tumor effect.

3.4. In vitro cytotoxicity

The cytotoxicity of CSOAA and CSOAA-PEG was assessed against K562 cells, human erythromyeloblastoid leukemia cells (Laroche-Clary et al., 2000), using an MTS-based assay. Cell viability (%) is presented after 24, 48, and 72 h of incubation with various concentrations of both conjugates (Fig. 7). One of the indications for DOX is leukemia; thus, K562 cells were used for determination of the cytotoxicity of the conjugates synthesized. Neither CSOAA nor CSOAA-PEG induced serious toxic effects in K562 cells at the concentrations tested after incubation for 24–72 h. In our previous study (Termsarasab et al., 2013a), CSOAA also showed no significant cytotoxicity in head and neck cancer cell line (FaDu cell). Our results here suggest that CSOAA-PEG can be used safely for the preparation of drug delivery vehicle.

3.5. In vitro cellular uptake

The cellular uptake efficiency of DOX from the nanoparticles developed was assessed using flow cytometry. In this investigation, the K562 cell was selected as a model cell line of human leukemia. DOX has been used in leukemia therapy in the clinic; thus, its uptake into K562 cells could be related to its anti-tumor efficacy. As shown in Fig. 8, DOX uptake was higher in the nanoparticle-treated groups than the

DOX solution-treated group. This might be due to the electrostatic interaction between the positive charge of the chitosan molecules and the negative charge of the cell membrane (Chavanpatil et al., 2006; Termsarasab et al., 2013a; Zauner et al., 1998). As reported in other cell line (Termsarasab et al., 2013a), DOX uptake from CSOAA-based nanoparticle was enhanced compared with DOX solution in K562 cells. However, the cellular uptake of DOX from the PEGylated CSOAA-based nanoparticles was lower than from CSOAA-based nanoparticles. This may be explained by the outer PEG shell reducing the electrostatic force between chitosan and the cell membrane, blocking interactions between the fatty acids in the minor hydrophobic core of the nanoparticles and the cell membrane, thus delaying drug release. Notwithstanding the lower cellular uptake efficiency of PEGylated CSOAA nanoparticles, they may exert a stealth effect, due to the prolonged circulation time in the blood stream after intravenous injection.

3.6. In vivo pharmacokinetics in rats

DOX-loaded nanoparticles were administered intravenously at a dose of 4 mg/kg to rats to investigate their effects on the pharmacokinetic properties of DOX. The DOX concentration in plasma according to time is shown in Fig. 9, and the pharmacokinetic parameters are listed in Table 2. The pharmacokinetic parameters of a DOX solution (4 mg/kg dose)-treated group reported in our previous study (Cho et al., 2012b) were used as the control. CL values of CSOAA and CSOAA-PEG

nanoparticle groups were decreased, to 11.17% and 2.09% of the value of DOX solution. AUC values of CSOAA and CSOAA-PEG nanoparticle groups exhibited 8.64- and 48.00-fold increases compared with that of the DOX solution group, respectively. Half-life ($t_{1/2}$) values in both groups were increased to 173.50% and 899.82%, respectively, compared with that of the DOX solution group. Additionally, MRT values showed 10.52- and 47.58-fold increases compared to the DOX solution group. These data indicated that the nanoparticles developed here exhibited lower *in vivo* clearance of DOX and prolonged circulation of nanoparticles in the blood stream. The PEGylated nanoparticles also showed decreased in vivo clearance, and increased AUC, half-life, and MRT values, compared with CSOAA-based nanoparticles ($p < 0.05$). It has been reported that nanoparticles modified with PEG exhibited enhanced systemic exposure of the drug after intravenous injection (Qu et al., 2009; Zhang et al., 2013). The decreased *in vivo* clearance of DOX in the PEGylated CSOAA nanoparticles seems to be based on their greater stability in the presence of serum (Fig. 5) and sustained drug release (Fig. 6). The stealth effect of the PEG shell likely contributes to the longer dosing interval and improved anti-tumor efficacy. In particular, prolonged circulation of the CSOAA-PEG nanoparticles developed may be appropriate for the therapy of hematological malignancies, such as leukemia and lymphoma.

4. Conclusions

PEGylated CSOAA-based nanoparticles containing DOX were developed to achieve a prolonged circulation time of the drug in the blood stream. Synthesis of the CSOAA-PEG conjugate was confirmed by ^{1}H NMR analysis. DOX-loaded CSOAA-PEG nanoparticles with a ~166-nm mean diameter and positive zeta potential were prepared and a sustained pattern of drug release from the CSOAA-PEG nanoparticles was observed. The cytotoxicity of CSOAA-PEG in K562 cells seemed negligible in the concentration range tested, and the cellular uptake efficiency of the drug from nanoparticles was improved compared with DOX in solution. Decreased *in vivo* clearance and a longer DOX half-life in the blood stream in the CSOAA-PEG nanoparticles group was demonstrated in a pharmacokinetic study. The CSOAA-PEG nanoparticle developed may be a useful candidate of anti-cancer drug delivery system, especially for the treatment of blood cancers.

5. References

Bae, Y., Diezi, T.A., Zhao, A., Kwon, G.S., 2007. Mixed polymeric micelles for combination cancer chemotherapy through the concurrent delivery of multiple chemotherapeutic agents. J. Control. Release 122, 324–330.

Chavanpatil, M.D., Khdair, A., Panyam, J., 2006. Nanoparticles for cellular drug delivery: mechanisms and factors influencing delivery. J. Nanosci. Nanotechnol. 6, 2651–2663.

Cho, H.J., Yoon, H.Y., Koo, H., Ko, S.H., Shim, J.S., Lee, J.H., Kim, K., Kwon, I.C., Kim, D.D., 2011. Self-assembled nanoparticles based on hyaluronic acid-ceramide (HA-CE) and Pluronic® for tumor-targeted delivery of docetaxel. Biomaterials 32, 7181–7190.

Cho, H.J., Yoon, H.Y., Koo, H., Ko, S.H., Shim, J.S., Cho, J.H., Park, J.H., Kim, K., Kwon, I.C., Kim, D.D., 2012a. Hyaluronic acid-ceramide-based optical/MR dual imaging nanoprobe for cancer diagnosis. J. Control. Release 162, 111–118.

Cho, H.J., Yoon, I.S., Yoon, H.Y., Koo, H., Jin, Y.J., Ko, S.H., Shim, J.S., Kim, K., Kwon, I.C., Kim, D.D., 2012b. Polyethylene glycol-conjugated hyaluronic acid-ceramide self-assembled nanoparticles for targeted delivery of doxorubicin. Biomaterials 33, 1190–1200.

Chung, C.W., Chung, K.D., Jeong, Y.I., Kang, D.H., 2013. 5-Aminolevulinic acid-incorporated nanoparticles of methoxy poly(ethylene glycol)–chitosan copolymer for photodynamic therapy. Int. J. Nanomedicine 8, 809–819.

ElBayoumi, T.A., Torchilin, V.P., 2009. Tumor-targeted nanomedicines: enhanced antitumor efficacy in vivo of doxorubicin-loaded, long-circulating liposomes modified with cancer-specific monoclonal antibody. Clin. Cancer Res. 15, 1973–1980.

Gaucher, G., Dufresne, M.H., Sant, V.P., Kang, N., Maysinger, D., Leroux, J.C., 2005. Block copolymer micelles: preparation, characterization and application in drug delivery. J. Control. Release 109, 169–188.

Jain, V., Swarnakar, N.K., Mishra, P.R., Verma, A., Kaul, A., Mishra, A.K., Jain, N.K., 2012. Paclitaxel loaded PEGylated gleceryl monooleate based nanoparticulate carriers in chemotherapy. Biomaterials 33, 7206–7220.

Jin, Y.J., Termsarasab, U., Ko, S.H., Shim, J.S., Chong, S., Chung, S.J., Shim, C.K., Cho, H.J., Kim, D.D., 2012. Hyaluronic acid derivative-based self-assembled nanoparticles for the treatment of melanoma. Pharm. Res. 29, 3443–3454.

Kaminskas, L.M., Ascher, D.B., McLeod, V.M., Herold, M.J., Le, C.P., Sloan, E.K., Porter, C.J., 2013. PEGylation of interferon α2 improves lymphatic exposure after subcutaneous and intravenous administration and improves antitumour efficacy against lymphatic breast cancer metastases. J. Control. Release 168, 200–208.

Laroche-Clary, A., Larrue, A., Robert, J., 2000. Down-regulation of bcr-alb an bclxL expression in a leukemia cell line and its doxorubicin-resistant variant by topoisomerase II inhibitors. Biochem. Pharmacol. 60, 1823–1828.

Lee, S.J., Koo, H., Jeong, H., Huh, M.S., Choi, Y., Jeong, S.Y., Byun, Y., Choi, K., Kim, K., Kwon, I.C., 2011. Comparative study of photosensitizer loaded and conjugated glycol chitosan nanoparticles for cancer therapy. J. Control. Release 152, 21–29.

Liu, Z., Jiao, Y., Wang, T., Zhang, Y., Xue, W., 2012. Interactions between solubilized polymer molecules and blood components. J. Control. Release 160, 14–24.

Lv, P.P., Ma, Y.F., Yu, R., Yue, H., Ni, D.Z., Wei, W., Ma, G.H., 2012. Targeted delivery of insoluble cargo (paclitaxel) by PEGylated chitosan nanoparticles grafted with Arg-Gly-Asp (RGD). Mol. Pharm. 9, 1736–1747.

Mu, C.F., Balakrishnan, P., Cui, F.D., Yin, Y.M., Lee, Y.B., Choi, H.G., Yong, C.S., Chung, S.J., Shim, C.K., Kim, D.D., 2010. The effects of mixed MPEG-PLA/Pluronic copolymer micelles on the bioavailability and multidrug resistance of docetaxel. Biomaterials 31, 2371–2379.

Nogueira, D.R., Tavano, L., Mitjans, M., Pérez, L., Infante, M.R., Vinardell, M.P., 2013. In vitro antitumor activity of methotrexate via pH-sensitive chitosan nanoparticles. Biomaterials 34, 2758–2772.

Nukolova, N.V., Oberoi, H.S., Cohen, S.M., Kabanov, A.V., Bronich, T.K., 2011. Folatedecorated nanogels for targeted therapy of ovarian cancer. Biomaterials 32, 5417–5426.

Owens 3rd, D.E., Peppas, N.A., 2006. Opsonization, biodistribution, and pharmacokinetics of polymeric nanoparticles. Int. J. Pharm. 307, 93–102.

Qu, G., Yao, Z., Zhang, C., Wu, X., Ping, Q., 2009. PEG conjugated N-octyl-O-sulfate chitosan micelles for delivery of paclitaxel: in vitro characterization and in vivo evaluation. Eur. J. Pharm. Sci. 37, 98–105.

Rausch, K., Reuter, A., Fischer, K., Schmidt, M., 2010. Evaluation of nanoparticle aggregation in human blood serum. Biomacromolecules 11, 2836–2839.

Termsarasab, U., Cho, H.J., Kim, D.H., Chong, S., Chung, S.J., Shim, C.K., Moon, H.T., Kim, D.D., 2013a. Chitosan oligosaccharide-arachidic acid-based nanoparticles for anti-cancer drug delivery. Int. J. Pharm. 441, 373–380.

Termsarasab, U., Cho, H.J., Moon, H.T., Park, J.H., Yoon, I.S., Kim, D.D., 2013b. Self-assembled magnetic resonance imaging nanoprobes based on arachidyl chitosan for cancer diagnosis. Colloids Surf. B: Biointerfaces 109, 280–286.

Veronese, F.M., Schiavon, O., Pasut, G., Mendichi, R., Andersson, L., Tsirk, A., Ford, J., Wu, G., Kneller, S., Davies, J., Duncan, R., 2005. PEG–doxorubicin conjugates: influence of polymer structure on drug release, in vitro cytotoxicity, biodistribution, and antitumor activity. Bioconjug. Chem. 16, 775–784.

Xiao, Z., Levy-Nissenbaum, E., Alexis, F., Lupták, A., Teply, B.A., Chan, J.M., Shi, J., Digga, E., Cheng, J., Langer, R., Farokhzad, O.C., 2012. Engineering of targeted nanoparticles for cancer therapy using internalizing aptamers isolated by celluptake selection. ACS Nano 6, 696–704.

Yadav, K.S., Jacob, S., Sachdeva, G., Chuttani, K., Mishra, A.K., Sawant, K.K., 2011. Long circulating PEGylated PLGA nanoparticles of cytarabine for targeting leukemia. J. Microencapsul. 28, 729–742.

Yang, T., Choi, M.K., Cui, F.D., Kim, J.S., Chung, S.J., Shim, C.K., Kim, D.D., 2007. Preparation and evaluation of paclitaxel-loaded PEGylated immunoliposome. J. Control. Release 120, 169–177.

Zauner, W., Ogris, M., Wagner, E., 1998. Polylysine-based transfection systems utilizing receptor-mediated delivery. Adv. Drug Deliv. Rev. 30, 97–113.

Zhang, L., Zhao, Z.L., Wei, X.H., Liu, J.H., 2013. Preparation and in vitro and in vivo characterization of cyclosporin A-loaded, PEGylated chitosan-modified, lipidbased nanoparticles. Int. J. Nanomedicine 8, 601–610.

Table 1 Characteristics of DOX-loaded CSOAA and CSOAA-PEG nanoparticles.

Formulations	Mean diameter (nm)	Polydispersity Index	Zeta potential (mV)	Encapsulation efficiency (%)
CSOAA/DOX (7.5/1.5)	124.17± 2.58	0.20± 0.04	27.28± 1.50	60.03± 2.14
CSOAA-PEG/DOX (7.5:1.5)	165.75± 56.75	0.19± 0.03	21.47± 2.05	63.80± 3.19

Values are present as mean ± SD ($n \geq 3$).

Table 2. Pharmacokinetic parameters of DOX in rats after intravenous administration at a dose of 4 mg/kg.

Parameter	DOX solution[a]	CSOAA/DOX	CSOAA-PEG/DOX
AUC (μg·min/ml)	65.18 ± 16.47	563.24 ± 33.34[#]	3128.65 ± 621.52[#,*]
Terminal $t_{1/2}$ (min)	76.37 ± 8.83	132.50 ± 32.80[#]	687.19 ± 221.97[#,*]
CL (ml/min/kg)	63.76 ± 14.18	7.12 ± 0.41[#]	1.33 ± 0.31[#,*]
V_{ss} (ml/kg)	1189.49 ± 204.99	1195.81 ± 192.67	1117.43 ± 207.24
MRT (min)	18.82 ± 1.14	197.94 ± 64.87[#]	895.41 ± 319.77[#,*]

[#] $p < 0.05$ compared to DOX solution group.

[*] $p < 0.05$ compared to CSOAA/DOX nanoparticle group.

Data present as mean ± SD ($n \geq 3$).

[a]Data were cited from our previous report (Cho et al., 2012b).

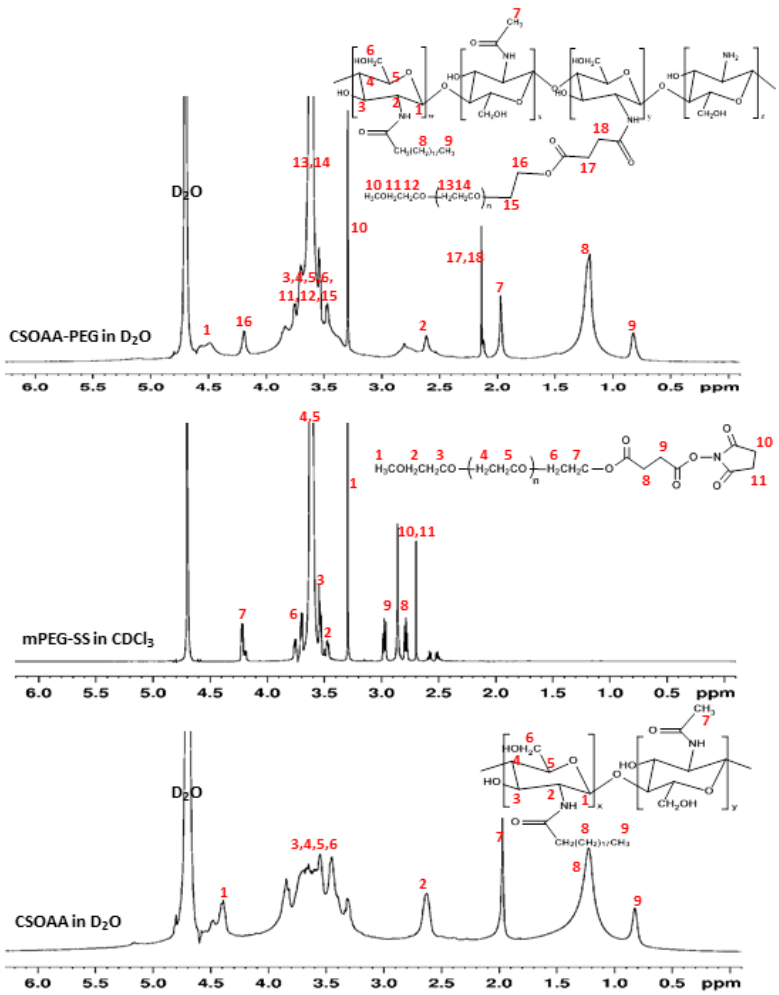

Figure 1 ^{1}H-NMR spectra of CSOAA, mPEG-SS, and CSOAA-PEG. CSOAA and CSOAA-PEG were solubilized in D_2O, and mPEG-SS was dissolved in $CDCl_3$.

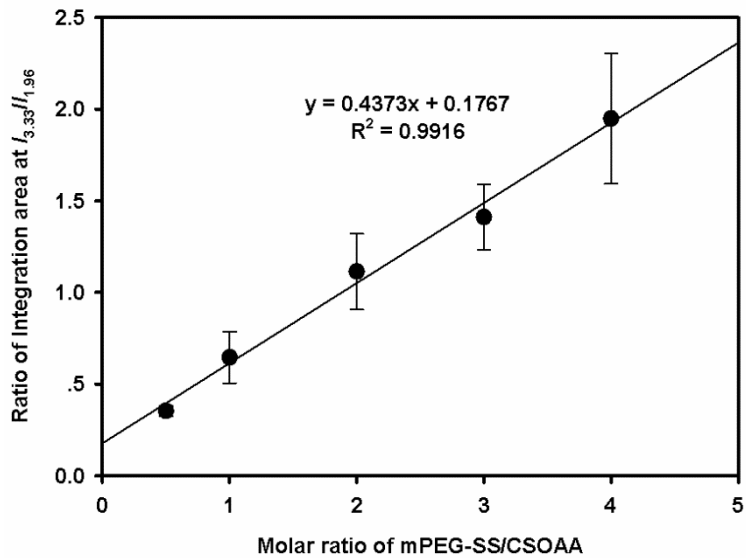

Figure 2 The correlationship between the ratio of integration area (3.33/1.98 ppm) and molar ratio of mPEG-SS/CSOAA based on their physical mixture. Each point represents the mean ± SD (*n*=3).

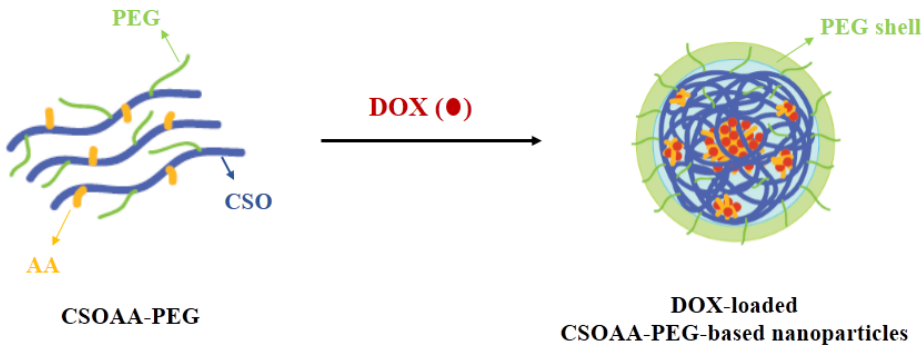

Figure 3 Schematic illustration of DOX-loaded CSOAA-PEG nanoparticles.

a

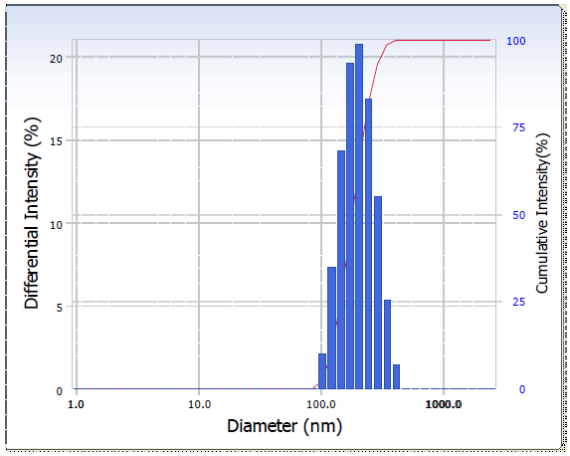

b

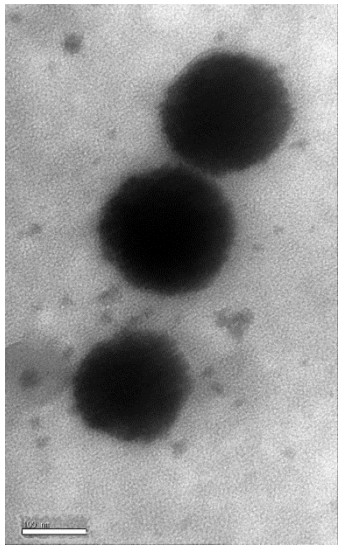

Figure 4 Characterization and illustration of CSOAA-PEG/DOX nanoparticles. (a) Size distribution and (b) TEM image of CSOAA-PEG/DOX nanoparticles.

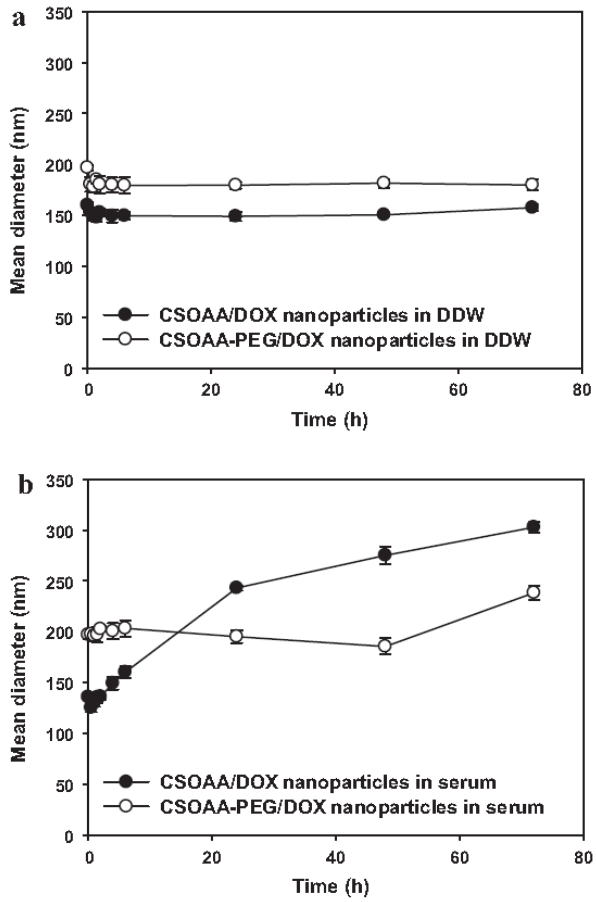

Figure 5 The change in mean diameter (nm) of the nanoparticles in the presence of 50% serum according to incubation time. CSOAA/DOX and CSOAA-PEG/DOX nanoparticles were incubated at 37°C for various periods. Each point represents the mean ± SD (n = 3).

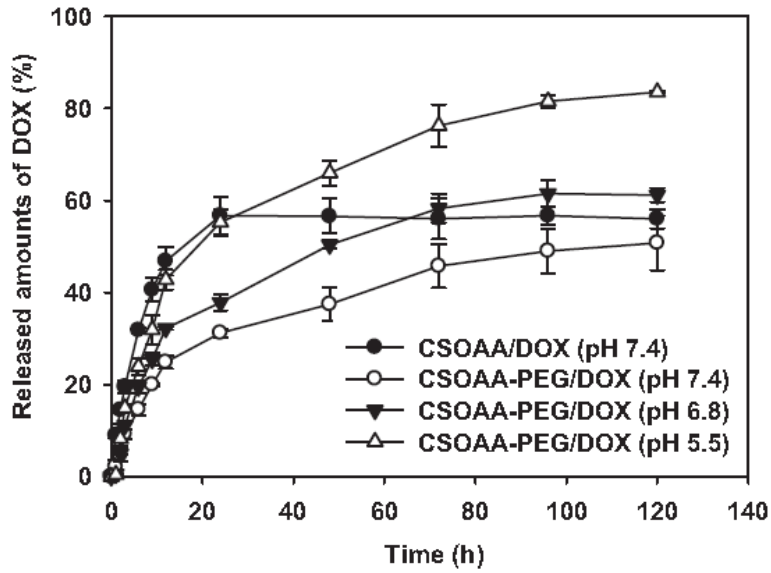

Figure 6 *In vitro* DOX release profiles of CSOAA and CSOAA-PEG-based nanoparticles. Drug release profiles of DOX-loaded CSOAA nanoparticles (pH 7.4) and CSOAA-PEG nanoparticles at pH 5.5, 6.8, and 7.4 are shown. Each point represents the mean ± SD (n = 3).

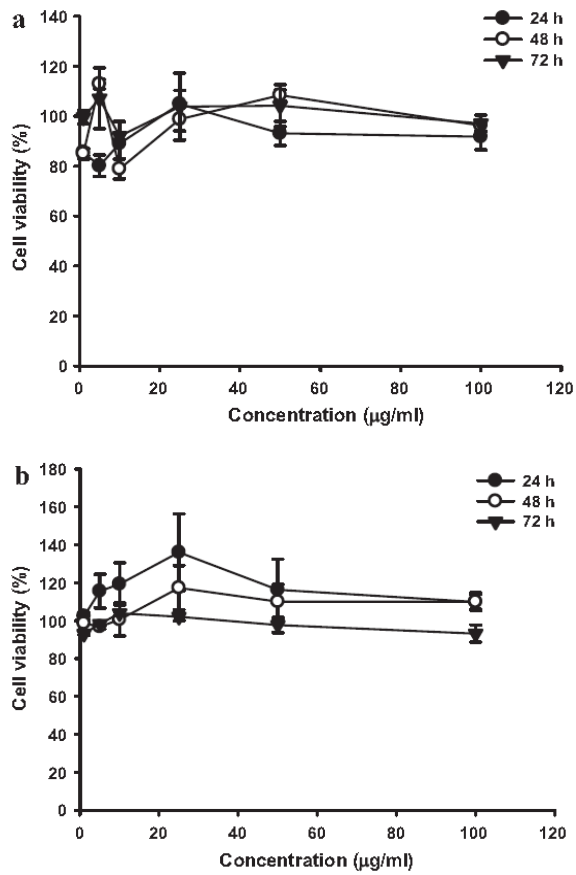

Figure 7 *In vitro* cytotoxicity test of CSOAA (a) and CSOAA-PEG (b) in K562 cells. Each conjugate at various concentrations was incubated for 24, 48, and 72 h in the presence of K562 cells. Each point represents the mean ± SD (n = 4).

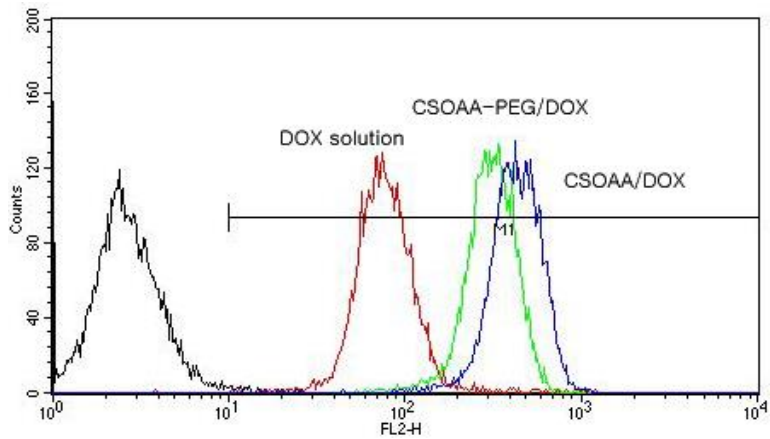

Figure 8 Flow cytometry analysis of DOX uptake by K562 cells. DOX solution (red), DOX-loaded CSOAA nanoparticles (blue), and DOX-loaded CSOAA-PEG nanoparticles (green) were incubated for 1 h.

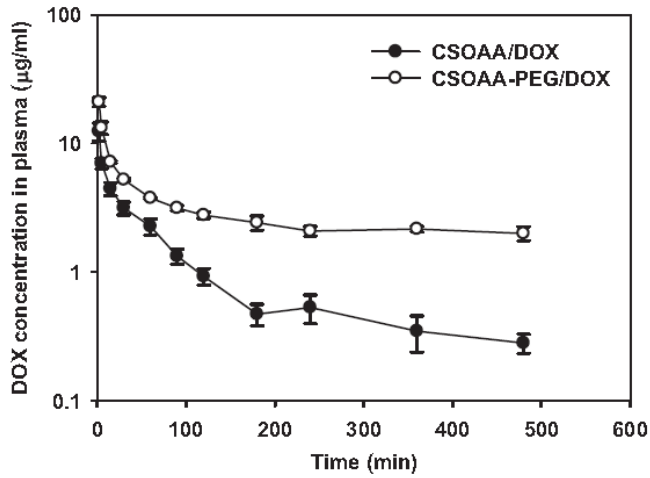

Figure 9 *In vivo* pharmacokinetic profiles of DOX in rats. Nanoparticles were administered intravenously at a dose of 4 mg/kg. Each point represents the mean ± SD ($n \geq 3$).

국문초록

본 연구에서는 항암제인 독소루비신의 표적화 전달을 위해 키토산 올리고당 유도체를 합성하여 자가조립 나노입자를 제조하였다. 양친매성을 가진 고분자인 키토산-아라키드산(CSOAA)을 우선적으로 합성하였다. 이 고분자를 기본골격으로 하여 약물의 혈중 순환을 연장시키기 위해 폴리에틸렌글리콜(PEG)을 결합시켰고, 한편으로 암조직에 대한 자기공명영상 조영제로서의 기능을 부여하기 위해 DTPA-Gd를 결합시켰다. CSOAA로 입자 제조시 200nm 이하의 균일한 입도분포를 가진 나노입자가 형성되었고, 고분자의 낮은 임계 미셀 농도를 통해 입자로서의 안정성을 가지는 것을 확인하였다. 용출실험 결과 CSOAA 나노입자에서 약물의 서방출이 나타났고, 산성 조건일수록 방출 속도가 더 증가하였다. FaDu 세포를 이용한 in vitro 세포 유입 실험에서는 용액 상태보다 나노입자 형태로 적용할 때 세포내 약물 유입이 증가하였다. FaDu 세포를 이식한 누드마우스를 이용한 In vivo 항암 실험에서도 나노입자를 이용했을 때 더 우수한 항암효과가 나타났다. CSOAA-DTPA-Gd 관련 실험에서, FaDu 세포와 Hep2 세포에 Cy5.5를 결합시킨 나노탐침을 반응시킨 후 공초점레이저주사현미경으로 관찰한 결과 시간에 따라 세포내 유입이 증가하는 것으로 나타났다. 이 함성 고분자를 이용한 팬텀 실

험에서도 상용조영제인 마그네비스트보다 조영 효과가 높은 것으로 확인됐다. CSOAA-PEG 관련 실험에서 혈청에서의 입자 안정성 시험을 진행한 결과, 일반 CSOAA 입자의 경우 입자 크기가 크게 증가한 반면 CSOAA-PEG 입자의 경우 72시간 이상 일정한 입자크기를 유지했다. 인간 백혈병 세포인 K562 세포에 대한 약물 전달시험에서는 독소루비신 자체보다 나노입자에 봉입된 상태로 적용된 경우 약물 유입이 높게 발생했다. in vivo 약물동태학 실험에서 CSOAA-PEG 그룹의 경우 일반 CSOAA, 독소루비신 용액과 비교시 약물의 소실 속도가 낮고 혈중 순환이 연장되는 것으로 나타났다. 위와 같은 결과를 통해 키토산 유도체를 이용한 자가조립 나노입자는 표적화 치료 및 암진단에 이용될 수 있음을 보여준다. 또한 이 시스템을 다른 약물에 응용하여 암조직으로의 선택적 약물 전달을 향상시키고, 약물동태학적 특성, 항암활성, 부작용 등을 최적화하는데 이용할 수 있을 것이다.

주요어: 키토산-아라키드산, 가돌리늄, 폴리에틸렌글리콜, 독소루비신, 나노입자, 항암효능

학번: 2012-30774

Appendix

Self-assembled nanoparticles of chitosan oligosaccharide derivatives for targeted delivery of anticancer drugs

Ubonvan Termsarasab
Ph.D. candidate
College of Pharmacy
Seoul National University
2015.06.16

Nanoparticles for cancer therapy

- Particles, usually comprising lipid or polymer
- <200 nm in diameter

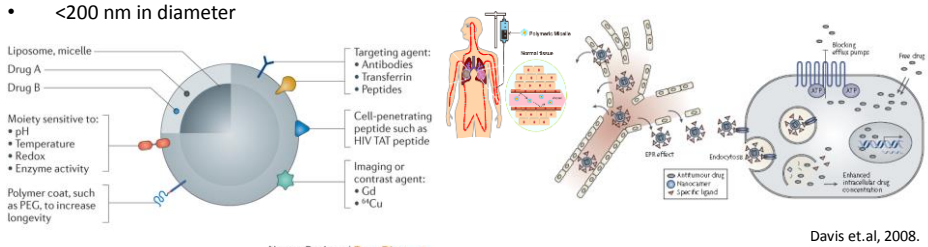

Davis et.al, 2008.

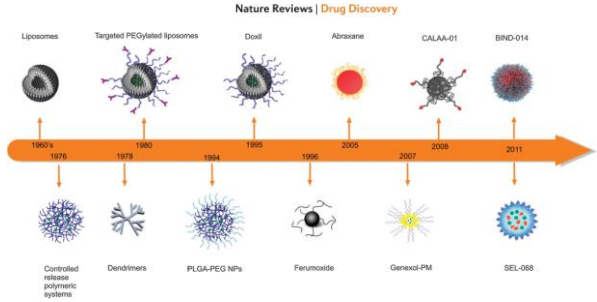

Kamaly et al., 2012

Passive targeting
- EPR effect
- Reducing P-gp efflux pump

Active targeting
- Specific receptor site on cell surface of tumor cell

Polymer-based Nanoparticles

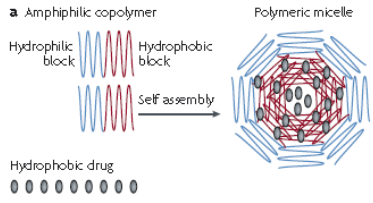

Schluep, T. *et al.*, 2006.

- The self-assembly of amphiphilic block of copolymer in aqueous environment
- Spherical, core/shell structure consist of hydrophobic core and hydrophilic shell

Chitosan oligosaccharide (CSO)

- Soluble in water and various organic solvents
- Cationic polymer and low viscosity
- Biocompatibility, biodegradability and low toxicity
- Hydrophilic polymer contains with free amino groups

(Kumar et al., 2004)

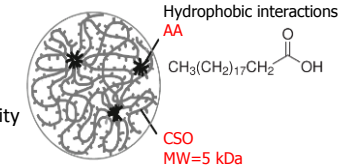

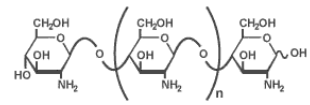

Arachidic acid (AA)

- Saturated fatty acid with a 20-carbon chain
- Using as cell or skin permeation enhancer

(Mittal et al., *2009)*

Polymer-based Nanoparticles (cont.)

Table Various synthetic polymers of hydrophobically modified chitosan for drug and gene delivery

Polymer	Hydrophobic part	Drug	References
chitosan oligosaccharide	stearic acid	DNA	Du et al., 2010
	stearic acid/PEG	mitomycin	Hu et al., 2008
	linoleic acid	Doxorubicin	Du et al., 2009

Table 3
Characteristics of different DOX-loaded CSO-LA micelles with 20% charged ratio of DOX.

Type of CSO-LA	Micelle size (nm)	PI (–)
CSO(8000)-LA(5%)	218.1 ± 0.3[a]	0.477
CSO(8000)-LA(10%)	219.5 ± 5.6[a]	0.550
CSO(8000)-LA(20%)	204.0 ± 3.3[ab]	0.530
CSO(14,000)-LA(20%)	199.2 ± 6.2[b]	0.450
CSO(20,000)-LA(20%)	205.7 ± 2.8[b]	0.528

[a,b] $p > 0.05$.
[c] $p < 0.05$

Wide size distribution??

- MW of chitosan
- Substitution degree of fatty acid

High CMC value??

Table 1
Physicochemical properties of CSO-SA with different graft ratio of stearic acid and molecular weight of CSO.

Samples	M_w (g/mol)	Theoretical SD (%)	Actual SD (%)	Z-average diameter (nm)	pKa value	Critical micelle concentration (μg/mL)
18000, CSO-25%SA	18,000	25.00	9.79	158.7 ± 15.8	8.432	89.6
11000, CSO-50%SA	11,000	50.00	49.46	309.4 ± 13.8	7.640	6.59
8000, CSO-50%SA	8000	50.00	47.58	202.7 ± 2.0	7.801	7.44
3000, CSO-25%SA	3000	25.00	13.88	139.0 ± 11.1	8.157	69.2
3000, CSO-50%SA	3000	50.00	45.00	143.0 ± 2.8	7.478	4.38
3000, CSO-80%SA	3000	80.00	63.41	188.1 ± 6.9	6.026	6.13
3000, CSO	3000	–	–	–	6.515	–

M_w represents in term of weight-average molecular weight of CSO. SD refers to the substitution degree of amino groups of CSO in CSO-SA.

Polymer-based Nanoparticles (cont.)

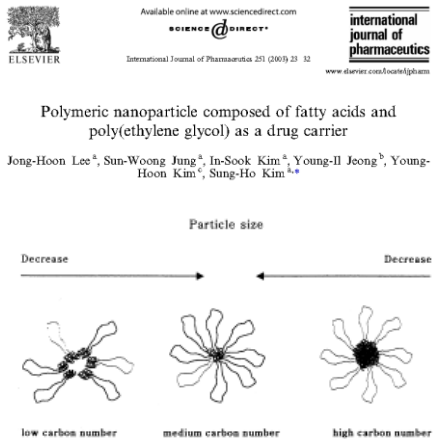

Optimized chain length and hydrophobic interaction force

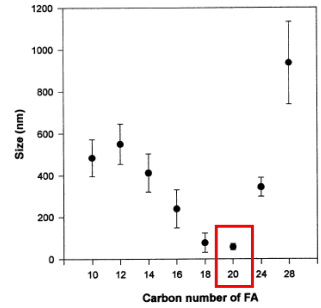

Fig. 8. Particle size distributions of FA–PEG–FA polymeric nanoparticles.

Carbon number of fatty acid
→ particle size
→ stability of nanoparticles

Lee et al., 2003

Rationale of CSOAA nanoparticles

- Novel type of fatty acid (arachidic acid) conjugated on chitosan oligosaccharide
- Forming nanoparticle with nano-sized (<200 nm) and uniform size distribution
- Low CAC value

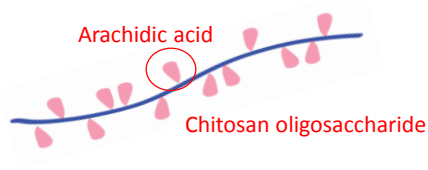

Challenging!! → The difficulty to synthesize CSOAA because of solubility problem of arachidic acid (very low solubility in organic solvents and insoluble in water of arachidic acid)

Doxorubicin

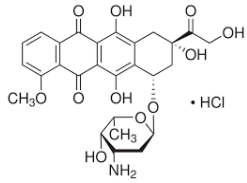

Anthracycline antibiotic

Formular:	$C_{27}H_{29}NO_{11}$
MW:	543.53 g/mol
Fluorescence:	Ex470/Em590
BA:	5% (oral)
Protein binding:	75%
Metabolism:	hepatic
Half-life:	1-3 h
Excretion	Urine (5-12%)
	faeces (40-50%)

Side effects
- Myelosupression
- Extravasation
- Cardiotoxicity

Limitation of using!!

Mechanism of action

- Interacts with DNA by intercalation and inhibition of macromolecular biosynthesis (topoisomerase II inhibitor)

Indications

- Acute lymphocytic leukemia
- Acute myeloblastic leukemia
- Bladder cancer (intravenous and intravesical)
- Breast cancer/sarcoma
- Gastric cancer
- Head and neck cancer, squamous cell
- Hodgkin's lymphoma
- Small cell lung cancer
- Non-small cell lung cancer
- Neuroblastoma
- Non-Hodgkin's lymphoma
- Osteogenic sarcoma
- Gynecologic cancer/sarcoma
- Sarcoma, soft tissue
- Testicular cancer
- Thyroid cancer
- Wilms' tumour

Adraimycin (DOX HCl)

Doxil (PEGylated liposomal DOX)

Combination therapy

- ABVD - doxorubicin, bleomycin, vinblastin, dacarbazine (Hodgkin's lymphoma)
- AC - doxorubicin, cyclophosphamide (breast cancer)
- CAV - cyclophosphamide, doxorubivin, vincristine (lung cancer)
- CHOP - cyclophosphamide, doxorubicin, vincristine, prednisone (non-Hodgkin lyphoma)
- TAC - docetaxel/paclitaxel, doxorubicin, cyclophosphamide (breast cancer)
- VAD - vincristine, doxorubicin, dexamethasone (multiple myeloma)

7

Schematic of studies

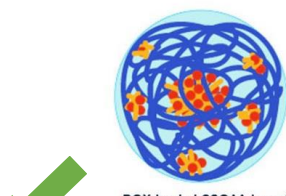

DOX-loaded CSOAA-based Nanoparticles

Part I. Chitosan oligosaccharide-arachidic acid- based nanoparticles for anticancer drug delivery

CSOAA-based Nanoprobe

Part II. Self-assembled magnetic resonance imaging nanoprobes based on arachidyl chitosan for cancer diagnosis

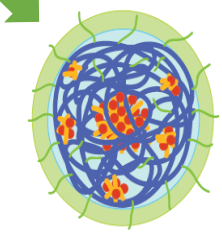

PEGylated CSOAA

Part III. Polyethylene glycol-modified chitosan-based nanoparticles for prolonged blood circulation of doxorubicin

8

Part I

- Chitosan oligosaccharide-arachidic acid- based nanoparticles for anticancer drug delivery

Objectives

To develop a novel self-assembled nanoparticle using chitosan oligosaccharide-archidic acid (CSOAA) for anticancer drug delivery

- Improve cellular uptake and anti-tumor efficacy of DOX

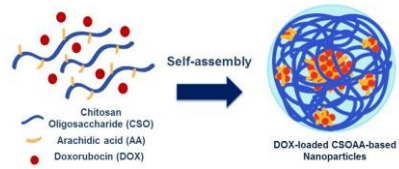

9

Synthesis of chitosan oligosaccharide-conjugated arachidic acid

Figure The synthesis schemes of CSO-AA by EDC coupling reaction

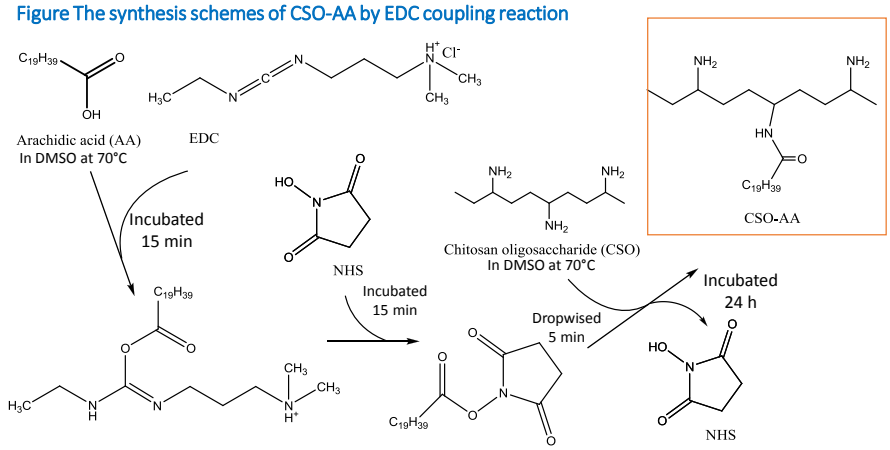

- CSO:AA:EDC:NHS = 1:3:4.5:4.5
- Controlled temperature about 30°C
- Decomposing CSO/AA physical complex→ pH titration at 3.5
- Removing unreacted AA → Acetone (9:1) washing 3 times
- Removing unreacted EDC/NHS and by-product → Dialysis for 1 day
- lyophilization

10

Characterization of CSOAA nanoparticles

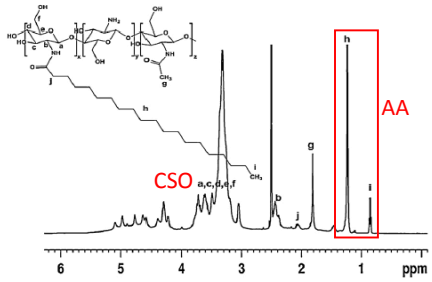

Figure. ^{1}H-NMR spectrum of CSOAA.

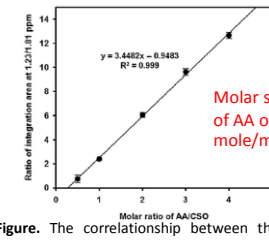

Molar substitution ratio of AA on CSO = 1.00 mole/mole

Figure. The correlationship between the ratio of integration are (1.23/1.81 ppm) and molar ration of AA/CSO based on their physiochemical mixture.

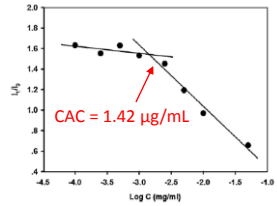

Low CAC→ form stable nanoparticulate structure after dilution with a large volume of body fluids.

Figure. Determination of the CAC of CSOAA.

Preparation and characterization of CSOAA nanoparticles

Solvent evaporation method

Table 1
Characteristics of CSOAA-based nanoparticles.

Formulation	Mean diameter (nm, mean ± SD)	Polydispersity index	Zeta potential (mV)	Encapsulation efficiency (%)
Blank nanoparticles	73.67 ± 3.91	0.32 ± 0.01	7.58 ± 0.62	–
CSOAA: DOX (7.5:1)	130.00 ± 5.76	0.23 ± 0.02	12.98 ± 0.55	53.12 ± 2.60

Values are presented as mean ± SD ($n \geq 3$).

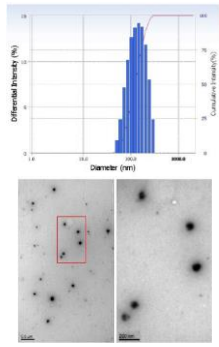

Figure. Size distribution and TEM images of DOX-loaded CSOAA-based nanoparticles.

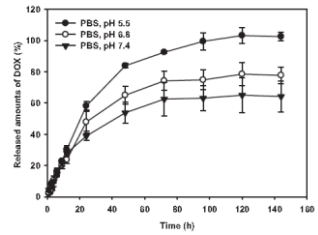

Figure. *In vitro* DOX release profiles from CSOAA-based nanoparticles.

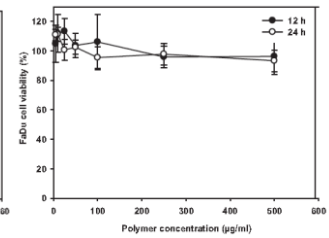

Figure. *In vitro* cytotoxicity test of CSOAA in FaDu cells. Cell viability (%) was determined by an MTS-based assays. Each point represents the mean±SD (n = 3).

- narrow size distribution and spherical shape
- Sustained release profiles and high drug released rate and amount at acidic pH
- No toxicity for FaDu cells

In vitro cellular uptake study

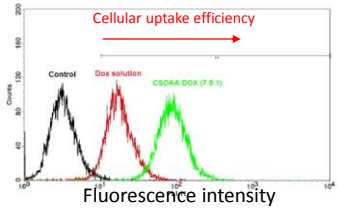

Figure. Cellular uptake efficiency of DOX in FaDu cells analyzed by flow cytometry. DOX solution and DOX-loaded nanoparticles were incubated for 1 h.

CSOAA nanoparticles > DOX solution

*electrostatic interaction between chitosan and cell membrane
*hydrophobic core of nanoparticles may help the internalization of DOX into the cells

In vivo antitumor efficacy

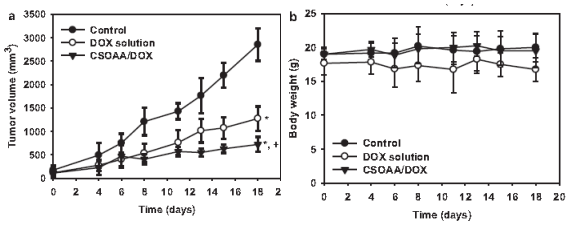

Figure. Anti-tumor efficacy test of DOX-loaded CSOAA NPs in FaDu tumor-bearing BALB/c nude mouse model. (a) Tumor volume (mm^3) profiles according to the time (days) for 18 days are shown. DOX solution and DOX-loaded CSOAA NPs were injected intravenously at a dose of 2.5 mg/kg on day 6, 8, and 13. (b) Body weight (g) was monitored. Each point indicates the mean±SD (n≥4). *P < 0.05 vs. control group; +P < 0.05 vs. DOX solution group.

CSOAA nanoparticles > DOX solution > control

*passive targeting of nanoparticles: nano-sized, sustained and pH dependent release profile, high cellular uptake

Part II

- Self-assembled magnetic resonance imaging nanoprobes based on arachidyl chitosan for cancer diagnosis

Objective

To develop arachidyl chitosan nanoprobe for magnetic resonance imaging (MRI) of cancer diagnosis

- Enhance the contrast efficiency of contrast agent

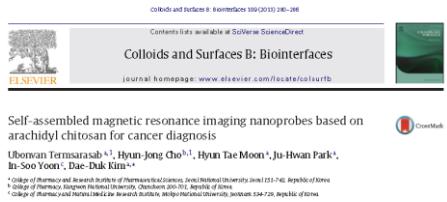

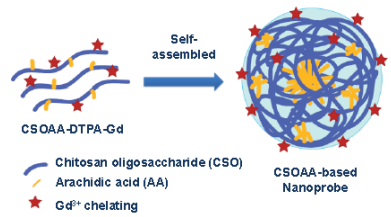

Part II

Synthesis and Characterization of CSOAA-DTPA-Gd

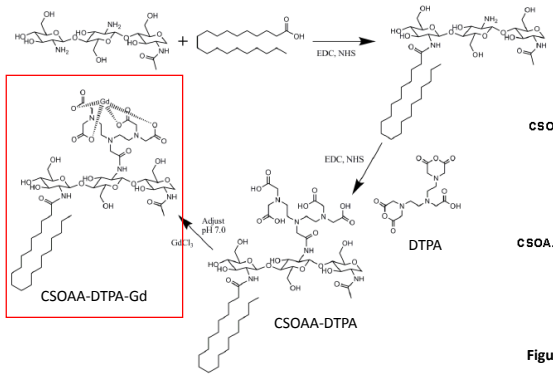

Figure. Synthesis scheme of CSOAA-DTPA-Gd

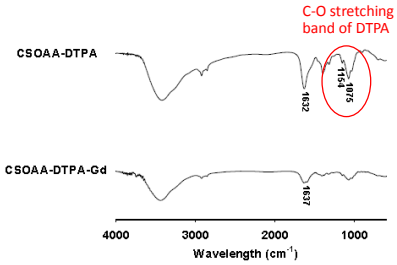

Figure. FT-IR spectra of CSOAA-DTPA and CSOAA-DTPA-Gd

- EDC and NHS coupling reaction
- CSO:AA:EDC:NHS = 1:3:4.5:4.5
- CSOAA:DTPA:EDC:NHS = 1:5:10:10
- CSOAA-DTPA:Gd = 1:5

Gd content in CSOAA-based nanoprobe = 5.43 % (w/w)

*Inductive coupled plasma-atomic emission spectrometer (ICP-AES)

DTPA; diethylenetriamine pentaacetic dianhydride
$GdCl_3$; gadolinium (III) chloride hexahydrate

15

Part II

Preparation and characterization of CSOAA-based nanoprobes

Solvent evaporation method

Table. Characteristics of CSOAA, CSOAA-DTPA and CSOAA-DTPA-Gd nanoprobes (1 mg/mL).

Nanoprobe	Mean diameter (nm)	Polydispersity index	Zeta potential (mV)
CSOAA	177.03 ± 2.75	0.20 ± 0.02	12.50 ± 0.81
CSOAA-DTPA	177.90 ± 18.79	0.09 ± 0.01	9.21 ± 0.85
CSOAA-DTPA-Gd	146.30 ± 5.51	0.20 ± 0.05	11.19 ± 0.39

Values are presented as means ± standard deviation (SD) ($n = 3$).

A

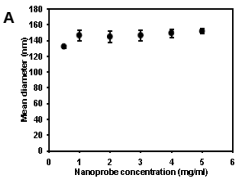

The mean diameter of the nanoprobes according to its concentration.

B

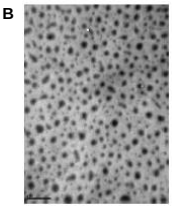

TEM image of the nanoprobes (2.5 mg/ml).

C

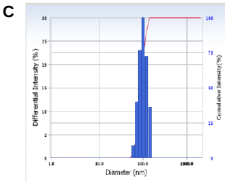

The size distribution of the nanoprobes (2.5 mg/ml).

D

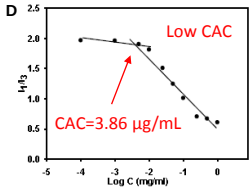

CAC determination of the CSOAA-based nanoprobe.

Figure. Characteristics of the CSOAA-based nanoprobe.

16

In vitro cytotoxicity tests

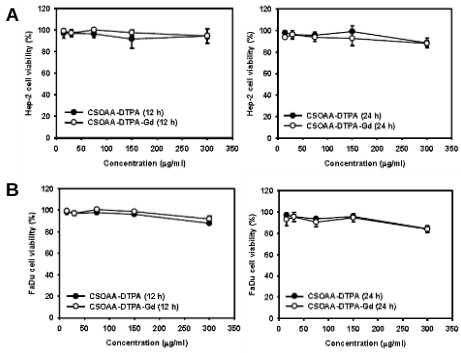

Figure. *In vitro* cytotoxicity tests of CSOAA-based nanoprobes in (A) Hep-2 and (B) FaDu cells after 12 and 24 h of incubation. Cell viability was measured by MTS-based assay according to nanoparobe concentration. Data are express as means ± SD (n=4).

No severe toxicity to Hep-2 and FaDu cells

In vitro cellular uptake of nanoprobes

Cy 5.5-labled CSOAA-based nanoprobes
Cy5.5 content of Cy5.5-CSOAA-DTPA-Gd = 0.13 %w/w
(absorbance at 650 nm using UV/vis spectrophotometer)

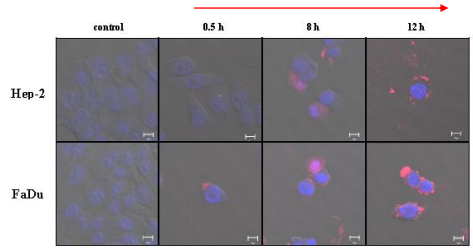

Figure. Cellular uptake studies of the nanoprobe in Hep-2 and FaDu cells. Intracellular uptake and distribution of the Cy5.5-labled nanoprobe were visualized by CLSM. Red and blue indicate Cy5.5 and DAPI, respectively.

increasing cellular uptake according to incubation time in Hep-2 and FaDu cells

In vitro MRI study (Phantom study)

T1 contrast intensity of Magnevist® and CSOAA-based nanoparobe were scanned using a 4.7-T MRI apparatus.

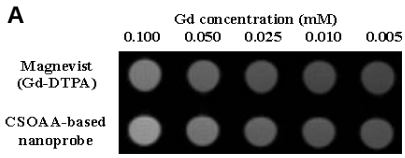

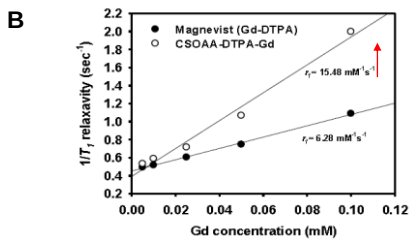

Figure. *In vitro* MRI test of Magnevist (Gd-DTPA) and CSOAA-DTPA-Gd at 4.7T. (A) T_1-weighted phantom image with 5-100 μM Gd concentrations was shown. (B) Longitudinal relaxation ($1/T_1$) according to the Gd cencentration was plotted.

$$\left(\frac{1}{T_1}\right)_{obs} = \left(\frac{1}{T_1}\right) d + R_1[M]$$

- R_1 is relaxivity.
- $(1/T_1)_{obs}$ and $(1/T_1)_d$ are the relaxation rates of the protons in the presence and absence of paramagnetic species (Gd), respectively
- [M] is the concentration of the parameagnetic species (Gd).

Increasing of T_1 relaxivity (R_1)

CSOAA-base nanoprobe > Manevist®
(2.43 fold)

*Several hydroxyl groups of CSOAA can attract adjacent water molecules

↓

Increase the water exchange rate in Gd molecules

Part III

- Polyethylene glycol-modified chitosan-based nanoparticles for prolonged blood circulation of doxorubicin

Objective

To develop PEGylated arachidyl chitosan-based nanoparticles for prolong blood circulation of anticancer drugs

- Improve pharmacokinetics of DOX

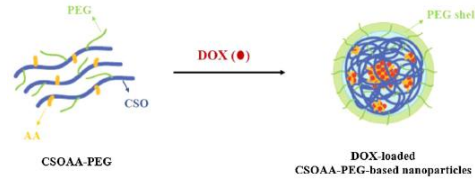

Synthesis and characterization of CSOAA-PEG

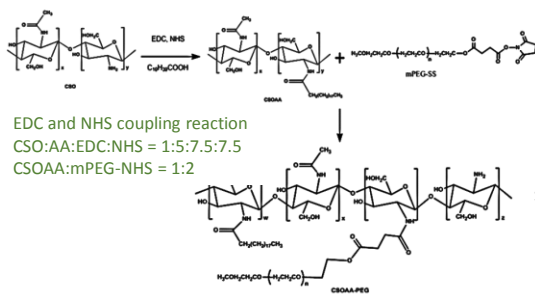

EDC and NHS coupling reaction
CSO:AA:EDC:NHS = 1:5:7.5:7.5
CSOAA:mPEG-NHS = 1:2

Figure. Synthetic scheme of CSOAA-PEG.

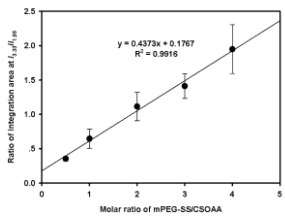

Molar substitution ratio of CSOAA-PEG was 1.82 mole/mole.

Figure. Correlation between the ratio of integration area ($I_{3.3}/I_{1.81}$) and molar ratio of mPEG-SS/CSOAA

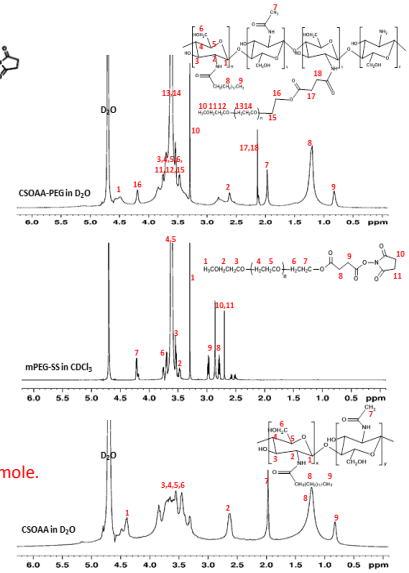

Figure. ^{1}H-NMR spectrum of CSOAA, m-PEG, and CSOAA-PEG.

Preparation and characterization of DOX-loaded nanoparticles

Solvent evaporation method

Table. Characteristics of DOX-loaded CSOAA and CSOAA-PEG nanoparticles.

Formulations (w/w)	Mean diameter (nm)	Polydispersity index	Zeta potential (mV)	Encapsulation efficiency (%)
CSOAA/DOX (7.5 / 1.5)	124.17 ± 2.58	0.20 ± 0.04	27.28 ± 1.50	60.03 ± 2.14
CSOAA-PEG/DOX (7.5 / 1.5)	165.75 ± 6.75	0.19 ± 0.03	21.47 ± 2.05	63.80 ± 3.19

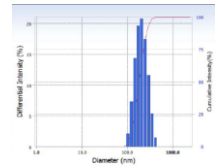

Figure. Size distribution of DOX/CSOAA-PEG nanoparticles.

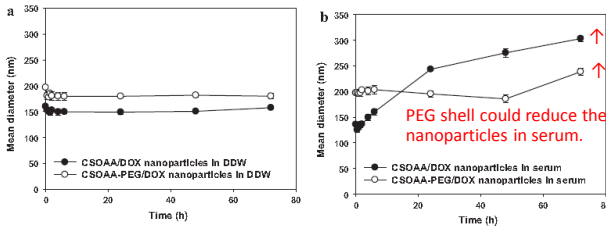

Figure. The change in diameter (nm) of the nanoparticles in (a) DDW and (b) 50% (v/v) serum according incubation time.

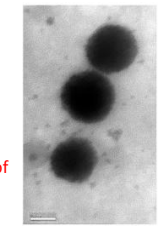

Figure. TEM image of DOX/CSOAA-PEG nanoparticles.

In vitro drug release

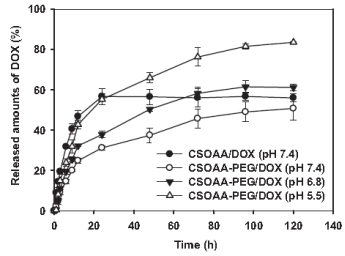

- DOX released from CSOAA and CSOAA-PEG nanoparticles were similar at steady state at pH 7.4.
- CSOAA-PEG nanoparticles show sustained and high drug released rate and amount at acidic pH

Figure. *In vitro* DOX release profiles of CSOAA and CSOAA-PEG-based nanoparticles. Drug release profiles of DOX-loaded CSOAA nanoparticles (pH 7.4) and CSOAA-PEG nanoparticles at pH 5.5, 6.8, and 7.4 are shown. Each point represents the mean ± SD (n = 3).

In vitro cytotoxicity test

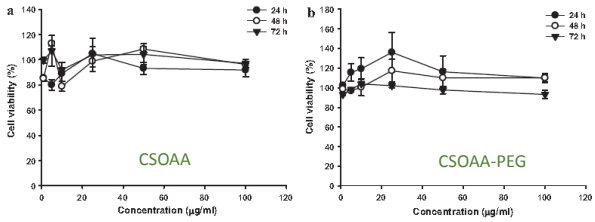

CSOAA and CSOAA-PEG have not serious toxic effects at the tested concentration range in K562 cells.

Figure. *In vitro* cytotoxicity test of CSOAA (a) and CSOAA-PEG (b) in K562 cells. Each conjugate at various concentrations was incubated for 24, 48, and 72 h in the presence of the cells. Each point represents the mean ± SD (n = 4).

In vitro cellular uptake

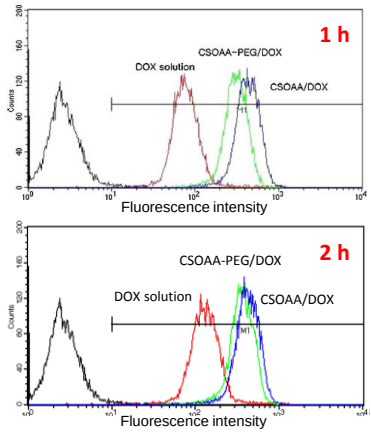

Figure. Flow cytometry analysis of intracellular DOX intensity in K562 cells at 1 and 2 h after exposing the cells to free DOX, DOX-loaded CSOAA or DOX-loaded CSOAA-PEG (DOX concentration 15 μg/ml).

CSOAA > CSOAA-PEG > DOX solution

*PEG shell may

- reduce the electrostatic force between chitosan and cell membrane
- block the internalization of AA into cell membrane

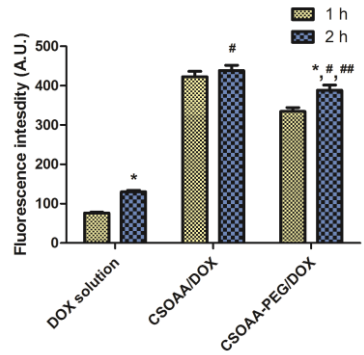

*, p<0.05 compared to 1 h incubation time in each group.
#, p<0.05 compared to DOX solution group.
##, p<0.05 compared to CSOAA/DOX group.

23

In vivo pharmacokinetics in rats

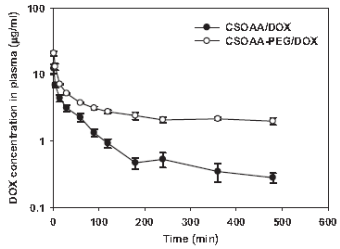

Figure. *In vivo* pharmacokinetic profiles of DOX in rats. Nanoparticles were administered intravenously at a dose of 4 mg/kg. Each point represents the mean ± SD ($n \geq 3$).

Parameter	DOX solution[a]	CSOAA/DOX	CSOAA-PEG/DOX
AUC (μg·min/ml)	65.18 ± 16.47	563.24 ± 33.34$^{\#}$	3128.65 ± 621.52$^{\#,*}$
Terminal $t_{1/2}$ (min)	76.37 ± 8.83	132.50 ± 32.80$^{\#}$	687.19 ± 221.97$^{\#,*}$
CL (ml/min/kg)	63.76 ± 14.18	7.12 ± 0.41$^{\#}$	1.33 ± 0.31$^{\#,*}$

$^{\#}p < 0.05$ compared to DOX solution group.
$^{*}p < 0.05$ compared to CSOAA/DOX nanoparticle group.
Data present as mean ± SD ($n \geq 3$).
[a]Data were cited from our previous report (Cho et al., 2012b).

↑AUC, $t_{1/2}$
↓CL

PEGylation could prolong circulation time of nanoparticles in blood stream.

24

Summary and conclusion

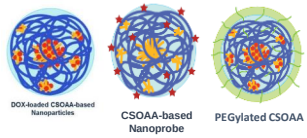

- ✓ Small nanoparticles size (< 100 in blank nanoparticles) with low size distribution and CAC value
- ✓ Enhancing solubility of drugs
- ✓ Improving cellular uptake of drug into cancer cells
- ✓ Improving anticancer activity of anticancer drug
- ✓ Improving contrast efficiency of contrast agents
- ✓ Decreasing *in vivo* clearance of drug and prolonging blood circulation of time of nanoparticles (PEGylated nanoparticles)

The CSOAA-based nanoparticles could be an effective candidate for targeted delivery of anticancer drugs. They could be applied to improve the specific uptake of anticancer drugs at tumor site, thereby optimizing pharmacokinetics and antitumor efficacy. These drug delivery systems could be further developed for safe therapy and diagnosis of cancer.

25

Further study

+ Targeting ligand =

Active targeted drug delivery

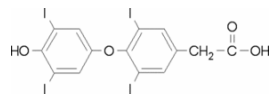

3,3’,5,5’-Tetraiodothyroacetic acid

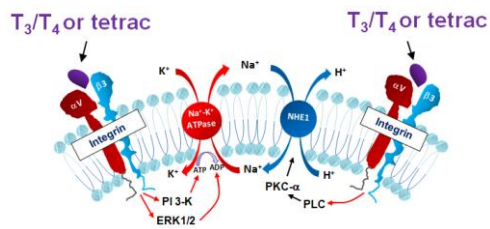

26

References

- Davis ME and Shin DM (2008) Nanoparticle therapeutics: an emerging treatment modality for cancer. *Nature reviews Drug discovery* **7**(9):771-782.
- Du Y-Z, Wang L, Yuan H, Wei X-H and Hu F-Q (2009) Preparation and characteristics of linoleic acid-grafted chitosan oligosaccharide micelles as a carrier for doxorubicin. *Colloids and Surfaces B: Biointerfaces* **69**(2):257-263.
- Du Y-Z, Lu P, Zhou J-P, Yuan H and Hu F-Q (2010) Stearic acid grafted chitosan oligosaccharide micelle as a promising vector for gene delivery system: factors affecting the complexation. *International Journal of Pharmaceutics* **391**(1):260-266.
- Hu F-Q, Wu X-l, Du Y-Z, You J and Yuan H (2008) Cellular uptake and cytotoxicity of shell crosslinked stearic acid-grafted chitosan oligosaccharide micelles encapsulating doxorubicin. *European journal of pharmaceutics and biopharmaceutics* **69**(1):117-125.
- Kamaly N, Xiao Z, Valencia PM, Radovic-Moreno AF and Farokhzad OC (2012) Targeted polymeric therapeutic nanoparticles: design, development and clinical translation. *Chemical Society Reviews* **41**(7):2971-3010.
- Kumar AV, Varadaraj MC, Lalitha RG and Tharanathan R (2004) Low molecular weight chitosans: preparation with the aid of papain and characterization. *Biochimica et Biophysica Acta (BBA)-General Subjects* **1670**(2):137-146.
- Lee J-H, Jung S-W, Kim I-S, Jeong Y-I, Kim Y-H and Kim S-H (2003) Polymeric nanoparticle composed of fatty acids and poly(ethylene glycol) as a drug carrier. *International Journal of Pharmaceutics* **251**(1–2):23-32.
- Noh SM, Han SE, Shim G, Lee KE, Kim C-W, Han SS, Choi Y, Kim YK, Kim W-K and Oh Y-K (2011) Tocopheryl oligochitosan-based self assembling oligomersomes for siRNA delivery. *Biomaterials* **32**(3):849-857.
- Mittal A, Sara U, Ali A and Aqil M (2009) Status of fatty acids as skin penetration enhancers-a review. *Current drug delivery* **6**(3):274-279.
- Schluep, T., Cheng, J., Khin, K. T., & Davis, M. E. (2006). Pharmacokinetics and biodistribution of the camptothecin–polymer conjugate IT-101 in rats and tumor-bearing mice. *Cancer chemotherapy and pharmacology*, *57*(5), 654-662.

Supplementary

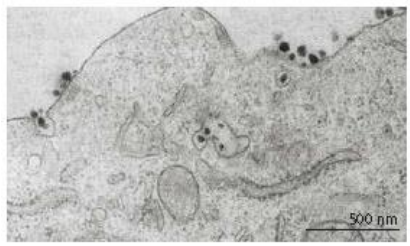

Figure Nanoparticles can enter cells via endocytosis. This figure shows a transmission electron micrograph of nanoparticles at the surface of a cancer cell, entering the cell and within endocytic vesicles.

Davis et.al, 2008.

Table 1 | The function of different inhibitors and the response of NPs and ILNPs to these inhibitors

Inhibitors	Function	NPs	ILNPs
Sodium azide	Energy	+	+
Phenylarsine oxide	Endocytosis	++	++
Sucrose	Blocking agents of clathrin-coated pit formation	+	++
chlorpromazine	Blocking agents of clathrin-coated pit formation		++
Nocodazole	Inhibitor of macropinocytosis	+	
Cytochalsin D	Microtubule-disrupting agent	++	+
Filipin	Inhibitor of caveolae-associated endocytosis		+
BFA	Disrupture of Golgi apparatus		+
Monensin	lysosome inhibitor		+

"+" means positive response to the inhibitors, "++" means greatly positive response to the inhibitors, "" means negative response to the inhibitors.

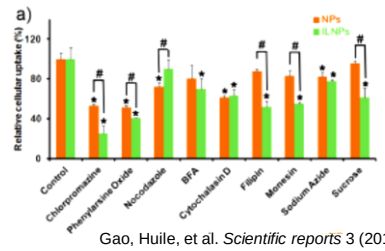

Gao, Huile, et al. *Scientific reports* 3 (2013).

Thank you.

29

International Journal of Pharmaceutics 441 (2013) 373–380

Contents lists available at SciVerse ScienceDirect

International Journal of Pharmaceutics

journal homepage: www.elsevier.com/locate/ijpharm

Pharmaceutical nanotechnology

Chitosan oligosaccharide–arachidic acid-based nanoparticles for anti-cancer drug delivery

Ubonvan Termsarasab[a,1], Hyun-Jong Cho[b,1], Dong Hwan Kim[a], Saeho Chong[a], Suk-Jae Chung[a], Chang-Koo Shim[a], Hyun Tae Moon[a,*], Dae-Duk Kim[a,*]

[a] College of Pharmacy and Research Institute of Pharmaceutical Sciences, Seoul National University, Seoul 151-742, Republic of Korea
[b] College of Pharmacy, Kangwon National University, Chuncheon 200-701, Republic of Korea

ARTICLE INFO

Article history:
Received 6 September 2012
Received in revised form 28 October 2012
Accepted 11 November 2012
Available online 19 November 2012

Keywords:
Arachidic acid
Chitosan oligosaccharide
Doxorubicin
Head and neck cancer
Self-assembly

ABSTRACT

Chitosan oligosaccharide–arachidic acid (CSOAA) conjugate was successfully synthesized and used for the development of self-assembled nanoparticles for doxorubicin (DOX) delivery. The molar substitution of AA on CSO and critical micelle concentration (CMC) of CSOAA were measured. Physicochemical properties of DOX-loaded CSOAA-based nanoparticles, such as particle size, zeta potential and morphology, were also characterized. The DOX-loaded CSOAA-based nanoparticles showed spherical shape with a mean diameter of 130 nm and positive charge. According to the result of *in vitro* release test, DOX-loaded CSOAA-based nanoparticles exhibited sustained and pH-dependent drug release profiles. The CSOAA showed negligible cytotoxicity in FaDu, human head and neck cancer, cells. Cellular uptake of DOX in FaDu cells was higher in the nanoparticle-treated group compared to the free DOX group. The anti-tumor efficacy of DOX-loaded nanoparticles was also verified in FaDu tumor xenografted mouse model. These results suggested that synthesized amphiphilic CSOAA might be used for the preparation of self-assembled nanoparticles for anti-cancer drug delivery.

1. Introduction

Polymeric nanoparticles have been widely investigated as drug carriers for anti-cancer agents (Cho et al., 2011; Choi et al., 2012; Kaida et al., 2010; Kolishetti et al., 2010; Yoon et al., 2012). Self-assembly based on amphiphilic polymer has been widely investigated because it has many interesting properties. Amphiphilic polymers can form stable nanoparticles composed of a hydrophobic core and a hydrophilic shell in an aqueous environment. Poorly water-soluble drugs can be encapsulated in the internal hydrophobic cavity, which can improve their solubility and bioavailability (Aliabadi et al., 2005; Kwon, 2003; Li and Tan, 2008). The nano-size and hydrophilic shell of these self-assembled nanoparticles can impede elimination by the reticuloendothelial system (RES) and have an enhanced permeability and retention (EPR) effect as a passive targeting strategy, leading to effective accumulation of drugs at the tumor region (Maeda et al., 2000).

Doxorubicin (DOX) is an anthracycline antibiotic that is commonly used in the treatment of various types of cancer, such as hematological malignancies, breast carcinomas, ovarian carcinomas, bronchogenic carcinomas, and soft-tissue sarcomas. DOX has also exhibited therapeutic effects for head and neck cancer (Airoldi et al., 2008), which includes several types of tumor localized in the oral cavity, nose, throat, sinuses, and salivary glands (Cho et al., 2012a). The response rate for anti-cancer therapeutics is known to be relatively low in head and neck cancer, with a survival benefit of about 10 weeks for patients with recurrent/metastatic disease (Reuter et al., 2007). Although DOX shows high potential anti-cancer efficacy, its clinical application is limited because of its severe side effects, especially cardiotoxicity and myelosuppression (Kratz et al., 2007; Wildiers et al., 2008). Therefore, it is thought that tumor-targeting strategy can minimize these side effects (Cho et al., 2012b).

Chitosan (CS) is a linear cationic polysaccharide composed of randomly distributed β-(1–4)-linked D-glucosamine and N-acetyl-D-glucosamine units, produced by the deacetylation of chitin. CS has been regarded as an attractive material for the development of drug delivery systems due to its biocompatibility, biodegradability, and low toxicity (Kumar et al., 2004; Muzzarelli and Muzzarelli, 2005). Moreover, CS has free primary amino groups, allowing for further chemical modification. However, the major drawback of CS is its poor solubility at physiological pH. Recently, many researchers have investigated chitosan oligosaccharide (CSO), a low-molecular-weight CS, because it can be soluble in water and several organic solvents under physiologically relevant conditions (Vishu Kumar

* Corresponding authors. Tel.: +82 2 880 7870; fax: +82 2 873 9177.
E-mail addresses: htmoon@snu.ac.kr (H.T. Moon), ddkim@snu.ac.kr (D.-D. Kim).
[1] These authors have equally contributed.

0378-5173/$ – see front matter © 2012 Elsevier B.V. All rights reserved.
http://dx.doi.org/10.1016/j.ijpharm.2012.11.018

et al., 2004). CSO has been modified with hydrophobic residues, such as alkyl groups, cholesterol, tocopherol, and deoxycholic acid (Chae et al., 2005). These hydrophobically modified CSOs can form self-assembled nanoparticles, which can be used as carriers for tumor-targeted drug and gene delivery.

In this study, arachidic acid (AA), as a fatty acid, was conjugated to a CSO backbone to make an amphiphilic CSO derivative. DOX was loaded into the self-assembled nanoparticles based on chitosan oligosaccharide–arachidic acid (CSOAA). The physiochemical properties of DOX-loaded CSOAA-based nanoparticles, such as particle size, zeta potential and morphology, and *in vitro* drug release behavior were investigated. *In vitro* cytotoxicity and cellular uptake efficiency were evaluated in head and neck cancer cells, and *in vivo* anti-tumor efficacy was also assessed in the head and neck cancer xenografted mouse model.

2. Materials and methods

2.1. Materials

Chitosan oligosaccharide (CSO; average molecular weight = 5 kDa, degree of acetylation > 90%) was purchased from Kitto Life Co., Ltd. (Seoul, Korea). Arachidic acid (AA), 1-ethyl-3-(3-dimethylaminopropyl) carbodiimide (EDC), N-hydroxysuccinimide (NHS), and deuterium oxide were purchased from Sigma–Aldrich Co. (St. Louis, MO, USA). Dimethylsulfoxide-d_6 (DMSO-d_6) was purchased from Cambridge Isotope Laboratories Inc. (Andover, MA, USA). Doxorubicin hydrochloride (DOX HCl) was obtained from Boryung Pharmaceutical Co. (Seoul, Korea). Minimum essential medium (MEM), penicillin, streptomycin, and fetal bovine serum (FBS) were obtained from Gibco Life Technologies, Inc. (Grand Island, NY, USA). All other chemicals were of reagent grade and were used without further purification.

2.2. Synthesis and characterization of CSOAA

Amphiphilic CSOAA was synthesized from CSO and AA. Briefly, CSO (0.2 mmol) and AA (0.6 mmol) were dissolved separately in 20 ml DMSO each at 50 °C for 15 min. Carboxyl groups of AA were activated by adding EDC and NHS (1.5 mol/mol AA) and it was stirred at room temperature for 30 min. Then, activated AA solution was dripped into the CSO solution for 5 min. The coupling reaction was conducted for a further 12 h, and then 4 ml of deionized distilled water (DDW) was added. The pH of the mixture was adjusted to 3.5 with 1 N HCl and stirred for 30 min. The mixture was precipitated by adding acetone (ten times the volume of mixture) and centrifuged (8608 × *g*, 30 min) to remove unreacted AA. The precipitation step was repeated three times. Next, the precipitate was dispersed with DDW and dialyzed with dialysis membrane (molecular weight cut-off = 1 kDa; Spectrum Laboratories, Laguna Hills, CA, USA) against DDW for 24 h. The dialyzed products were lyophilized.

The conjugation of CSOAA was confirmed by Fourier transform infrared (FTIR) spectroscopy and ^{1}H-nuclear magnetic resonance (NMR) analyses. FTIR spectra were obtained with a JASCO FTIR 4200 spectrometer (JASCO Company Ltd., Hachioji, Japan) by KBr method. The ^{1}H NMR spectra were obtained using a Varian FT 500-MHz NMR spectrometer (Varian Inc., Palo Alto, CA, USA). Samples (15 mg/ml) were dissolved in DMSO-d_6. The molar substitution (MS) of CSOAA, which is total number of moles of reacted AA per one mole of CSO, was determined by integration of the values of the proton peaks from the ^{1}H NMR spectra. MS of CSOAA was obtained using a linear regression line generated from standard samples with various molar ratios between AA and CSO (0.5:1, 1:1, 2:1, 3:1, and 4:1). The standard samples were prepared by homogeneously mixing CSO and AA in DDW/tetrahydrofuran (THF) mixture (1:1, v/v). THF was removed by evaporation and the resultant was lyophilized. The ratio of integration area (1.23/1.81 ppm) of each standard sample was calculated.

2.3. Preparation and characterization of nanoparticles

To investigate the self-assembly behavior of CSOAA, the critical micelle concentration (CMC) of CSOAA was determined by using pyrene as a fluorescence probe. The fluorescence emission spectrum of pyrene (6×10^{-7} M) was recorded at 360–450 nm in the CSOAA concentration range from 10^{-4} to 1 mg/ml. The excitation wavelength was 334 nm and the slit openings for excitation and emission were set at 10 and 3 nm, respectively. The intensity ratio of the first peak (I_1, 373 nm) to the third peak (I_3, 384 nm) was calculated to determine the CMC.

Blank self-assembled nanoparticles were prepared by dissolving CSOAA in DDW, vortexing for 15 min, and filtering through a 0.2-μm syringe filter (Minisart RC 15; Sartorius Stedim Biotech GmbH, Goettingen, Germany).

DOX base was used as a hydrophobic drug and encapsulated into the CSOAA nanoparticles by a solvent evaporation method. To prepare DOX base according to a reported method (Cho et al., 2012b), DOX HCl was reacted with triethylamine in DMSO for 12 h, and then lyophilized. To make DOX-loaded nanoparticle, DOX base (1 mg) was dissolved in 1 ml DMSO and DDW mixture (1:1, v/v). CSOAA (7.5 mg) was added to that mixture and vortexed for 10 min. The solvent was evaporated under a nitrogen gas stream for 4 h at 70 °C. DOX-loaded CSOAA-based self-assembled nanoparticles were obtained by resuspending the polymer and drug composite film with 1 ml DDW. That suspension was gently stirred for 15 min and further heated at 70 °C for 15 min. Unloaded drug was eliminated with a 0.22-μm syringe filter.

The encapsulation efficiency (EE) of the DOX in nanoparticles was determined by disrupting DOX-loaded nanoparticles with 100× the volume of DMSO. DOX was analyzed quantitatively by Waters high-performance liquid chromatography (HPLC) system (Waters Co., Milford, MA, USA), equipped with a reversed-phase C-18 column (Xbridge RP18, 250 mm × 4.6 mm, 5 μm; Waters Co.), a separation module (Waters e2695), and a fluorescence detector (Waters 2475). The mobile phase consisted of 0.1 M sodium acetate buffer (pH 4.0, adjusted with acetic acid) and acetonitrile (71:29, v/v), and the eluent was monitored at excitation and emission wavelengths of 470 nm and 565 nm, respectively, with a flow rate of 1.0 ml/min. The injection volume for drug analysis was 20 μl. The EE value was calculated using the following equation:

$$\text{EE}\ (\%) = \frac{\text{actual amount of DOX in nanoparticle}}{\text{theoretical amount of DOX in nanoparticle}} \times 100. \quad (1)$$

The mean diameter and zeta potential values of the blank nanoparticles and DOX-loaded nanoparticles were measured by a dynamic light scattering (DLS) method (ELS-Z, Photal; Otsuka Electronics Co. Ltd., Osaka, Japan). The morphological shapes of self-assembled nanoparticles were observed under transmission electron microscopy (TEM; LIBRA 120; Carl Zeiss, Oberkochen, Germany). The samples were placed on a copper grid coated with carbon film, dried at 20 °C, and photographed.

2.4. In vitro DOX release

In vitro release studies were performed in phosphate-buffered saline (PBS; pH 5.5, 6.8, and 7.4, adjusted with phosphoric acid) at 37 °C. DOX-loaded CSOAA-based nanoparticles (150 μl) were placed in a mini GeBA-flex tube (molecular weight cut-off = 12–14 kDa). That tube was then transferred to 10 ml release medium and kept in the horizontal shaker at 37 °C and 50 rpm of rotation speed. An aliquot (0.2 ml) of the release medium was

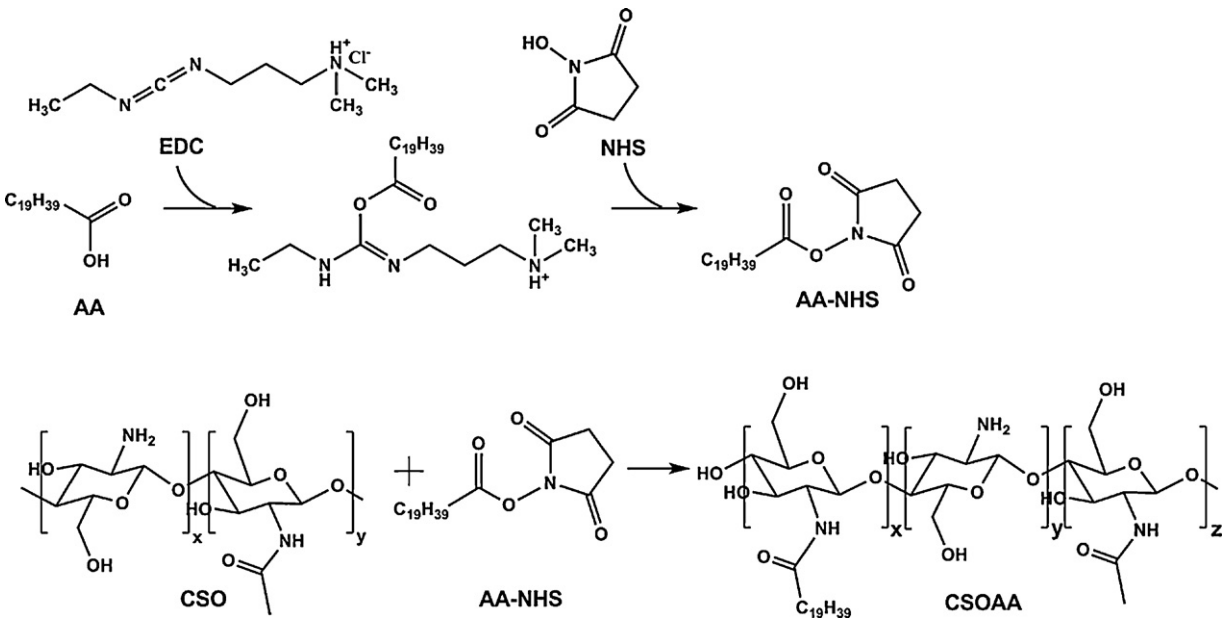

Fig. 1. Synthetic scheme of CSOAA.

periodically collected (at 1, 2, 3, 4, 6, 9, 12, 24, 48, 72, 96, 120, and 144 h) and the same volume of fresh medium was replaced. The released DOX was quantitatively analyzed by HPLC system.

2.5. In vitro cytotoxicity of CSOAA

FaDu cells were purchased from the Korean Cell Line Bank (Seoul, Korea). These cells were cultured in MEM containing 10% FBS, 100 U/ml penicillin, and 100 μg/ml streptomycin at 37 °C under 5% CO_2 atmosphere and 95% relative humidity. The cytotoxicity of CSOAA was determined by a 3-(4,5-dimethylthiazol-2-yl)-5(3-carboxymethonyphenol)-2-(4-sulfophenyl)-2H-tetrazolium (MTS)-based assay. Cells were seeded in 96-well plates at a density of 1.0×10^4 cells per well. After 24 h of incubation, the cell culture medium was replaced with 200 μl medium containing various concentrations (5–500 μg/ml) of CSOAA and incubated for 12 and 24 h. After discarding the culture medium, cells were treated with the MTS-based CellTiter 96 AQ_{ueous} One Solution Cell Proliferation Assay Reagent (Promega Corp., Madison, WI, USA) at 37 °C for 4 h, according to the manufacturer's protocol. The spectrophotometric absorbance of samples was measured at a wavelength of 490 nm using an EMax Precision Microplate Reader (Molecular Devices, Sunnyvale, CA, USA).

2.6. In vitro cellular uptake

Cellular uptake efficiency was evaluated by flow cytometry analysis. FaDu cells were seeded in 6-well plates at a density of 6×10^5 cells per well and grown overnight at 37 °C. The culture medium was then removed, and the cells were incubated with free DOX or the DOX-loaded CSOAA-based nanoparticles at an equivalent DOX concentration (50 μg/ml) for 1 h. After washing with PBS (pH 7.4) at least three times, the cells were detached and centrifuged. The supernatant was then removed and the cell pellets were resuspended with PBS containing 2% (v/v) FBS. DOX uptake was analyzed using a Calibur fluorescence-activated cell sorter equipped with CELLQuest software (Becton Dickinson Biosciences, San Jose, CA, USA).

2.7. In vivo anti-tumor efficacy

Female BALB/c nude mice (5 weeks old; Charles River) were used to prepare a tumor-bearing mouse model for evaluating anticancer efficacy. Mice were maintained in a light-controlled room kept at a temperature of 22 ± 2 °C and a relative humidity of 55 ± 5% (Animal Center for Pharmaceutical Research, College of Pharmacy, Seoul National University, Seoul, Korea). Experimental protocols used were approved by the Animal Care and Use Committee of the College of Pharmacy, Seoul National University. BALB/c nude mice bearing FaDu tumors were prepared by subcutaneous injection of 3×10^6 cells in the right back. Tumor size was measured with Vernier calipers and tumor volume (mm^3) was calculated according to the following formula: volume = 0.5 × longest diameter × shortest diameter^2. Measuring tumor volume and weighing body weight started 10 days post-inoculation, when the tumor volume reached about 50–100 mm^3. The mice were divided into three groups: control, DOX solution, and DOX-loaded CSOAA-based nanoparticles. Both DOX solution and DOX-loaded nanoparticles were injected intravenously at a dose of 25 mg/kg on days 6, 8, 11, and 13. The tumor volume and body weight were monitored for 18 days.

2.8. Statistical analysis

Statistical analyses were performed using analysis of variance. All experiments were performed at least three times and the data are presented as mean ± standard deviation (SD).

3. Results

3.1. Synthesis and characterization of CSOAA

The CSOAA conjugate was synthesized by EDC- and NHS-mediated amide bond formation between the carboxylic group of AA and the amine group of CSO. The synthesis scheme is shown in Fig. 1. EDC can react with the carboxylic group of AA to form an EDC active ester, and the NHS ester intermediate forms rapidly. The intermediate can then react with the primary amine of CSO to form an amide bond.

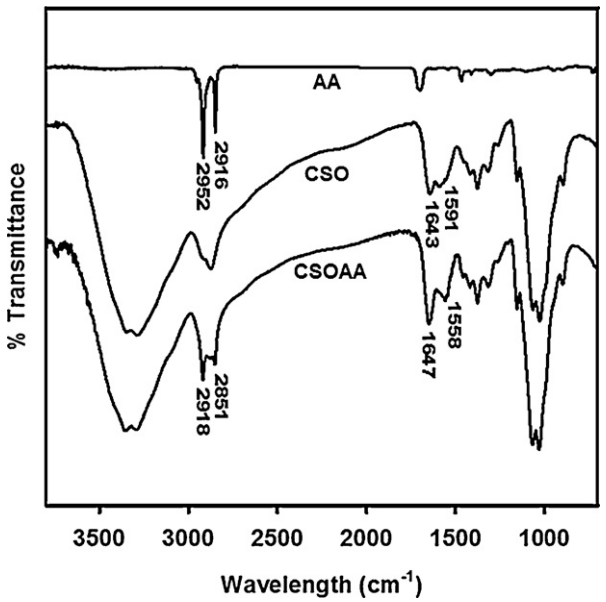

Fig. 2. FTIR spectra of AA, CSO, and CSOAA.

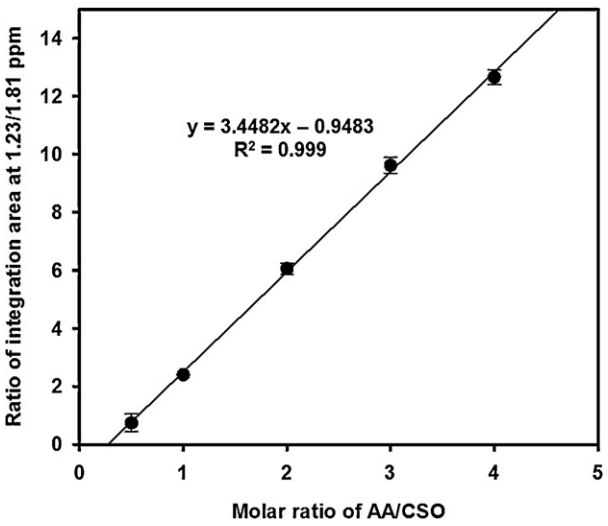

Fig. 4. The correlationship between the ratio of integration area (1.23/1.81 ppm) and molar ratio of AA/CSO based on their physical mixture. Each point represents the mean ± SD ($n = 3$).

The structural characterization of CSOAA was performed using FTIR and ^{1}H NMR. The FTIR spectrum (Fig. 2) confirmed the synthesis of the CSOAA conjugate. Absorption bands of CSO at 1591 and 1643 cm^{-1} were assigned to N—H bending of the deacetylated amine (—NH_2) and carbonyl stretching of a non-deacetylated amide (NHC=OCH_3; amide I band), respectively. After the reaction, the amine peak at 1591 cm^{-1} of CSO disappeared and a new absorption band at 1558 cm^{-1} in the spectrum of CSOAA was observed, which was associated with the formation of a new amide bond (amide II band). Additionally, absorption bands at 2918 and 2851 cm^{-1} of CSOAA represented stretching vibrations of the acyl chain, —CH_2— and —CH_3 of AA, respectively. The conjugation of AA to CSO was also confirmed by ^{1}H NMR analysis (Fig. 3). The ^{1}H NMR spectrum of CSOAA exhibited proton signals for both CSO and AA. Although the proton peaks of the glucosamine ring of CSO overlapped with the DMSO-d_6 solvent, the proton peaks at 0.86 and 1.23 ppm indicated a terminal methyl group (—CH_3) and an alkyl chain (—CH_2—) of AA, respectively. Furthermore, a new proton peak of —CH_2— of AA linked with a carbonyl group was seen at 2.07 ppm in the ^{1}H NMR spectrum of the CSOAA conjugate, whereas that peak was absent in the spectrum of a physical mixture of CSO and AA (Supplementary Fig. 1S). This result indicated that AA was successfully conjugated to the CSO backbone *via* amide bond formation.

To calculate the MS of CSOAA, the homogeneous physical mixtures of CSO and AA (at different molar ratios) were prepared as standard samples and analyzed by ^{1}H NMR. As shown in Fig. 4, the linear regression line was generated by plotting the ratio of integration area between peak of the alkyl chain protons of AA ($\delta = 1.23$ ppm; —CH_2—) and the N-acetyl protons of CSO ($\delta = 1.81$ ppm; NH—CO—CH_3) according to the molar ratio of AA/CSO. The MS of CSOAA was 1 (mole of AA/mole of CSO), calculated from the equation of regression line with its ^{1}H NMR integration ratio (1.23/1.81 ppm), when the initial molar ratio

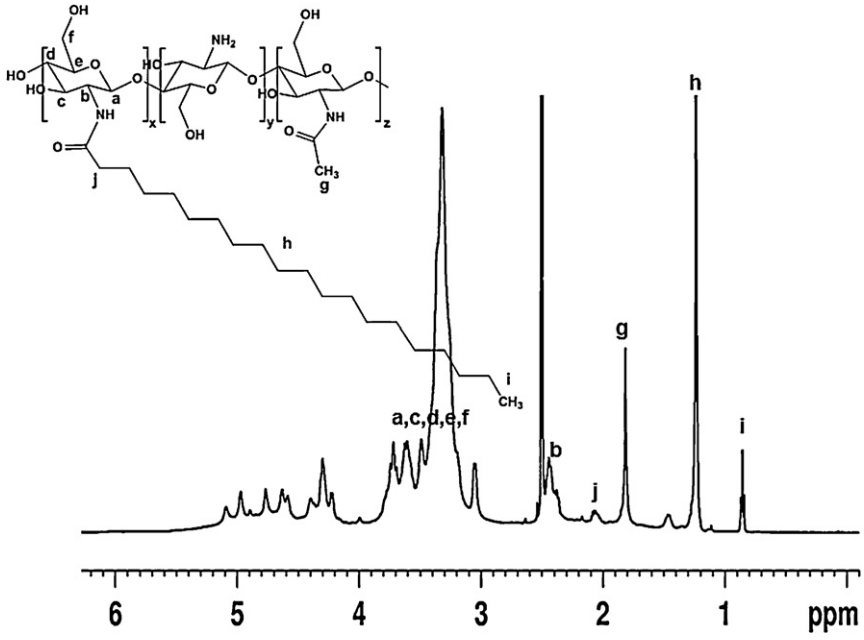

Fig. 3. ^{1}H NMR spectrum of CSOAA. CSOAA was dissolved in DMSO-d_6 for ^{1}H NMR analysis.

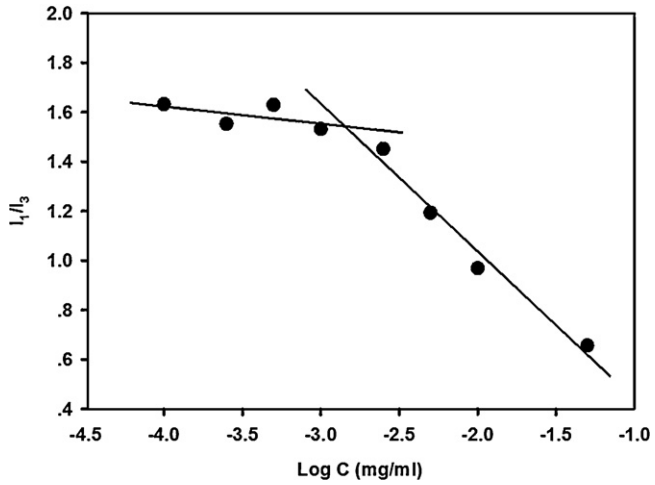

Fig. 5. Determination of the CMC of CSOAA. Fluorescence intensity ratio (I_{373}/I_{384}) was plotted against CSOAA concentration.

(AA/CSO) was 3 in the conjugation reaction. The chemical yield of CSOAA was 61.2%.

The self-assembly behavior of CSOAA in the aqueous phase was investigated by fluorescence measurements, using pyrene as a fluorescence probe (Fig. 5). CMC can be determined by measuring the intensity ratio (I_1/I_3) between the first (373 nm) and third (384 nm) emission peaks of pyrene according to the CSOAA concentration. As shown in Fig. 5, the CMC of CSOAA was 1.42 μg/ml.

3.2. Preparation and characterization of CSOAA-based self-assembled nanoparticles

Blank self-assembled nanoparticles (without drug loading) were prepared by dissolving CSOAA in the aqueous solution. The formation of nanoparticles was confirmed by measuring particle size and zeta potential values. To load DOX into the CSOAA-based nanoparticles, a solvent evaporation method was used. The mean diameter and zeta potential values were measured by DLS and are shown in Table 1. The mean diameter of blank nanoparticles was smaller than that of DOX-loaded nanoparticles (73.67 ± 3.91 nm *vs.* 130.00 ± 5.76 nm). The polydispersity index of the DOX-loaded nanoparticles was 0.23 ± 0.02, indicating a narrow size distribution of nanoparticles (Fig. 6a). The zeta potential value was also increased slightly after loading DOX into the nanoparticles (from 7.58 ± 0.62 mV to 12.98 ± 0.55 mV). The spherical shape of the DOX-loaded CSOAA-based nanoparticles was observed by TEM (Fig. 6b). No aggregation of CSOAA-based nanoparticles was observed in that image. The loading amount of DOX in the nanoparticles was measured by HPLC analysis and the EE was $53.12 \pm 2.60\%$.

3.3. In vitro DOX release

DOX release patterns from nanoparticles were investigated under different pH conditions (pH 5.5, 6.8 and 7.4) at 37 °C (Fig. 7). DOX release from the CSOAA-based nanoparticles was monitored for 6 days. Sustained drug release was observed and it was dependent on the pH of the release medium. About 30% of DOX was released in the first 12 h under all pH conditions. After that, the amounts of DOX released from CSOAA-based nanoparticles increased as the pH value of the releasing medium decreased. After 6 days, DOX was completely released at pH 5.5; in contrast, 78% and 64% of DOX was released at pH 6.8 and 7.4, respectively.

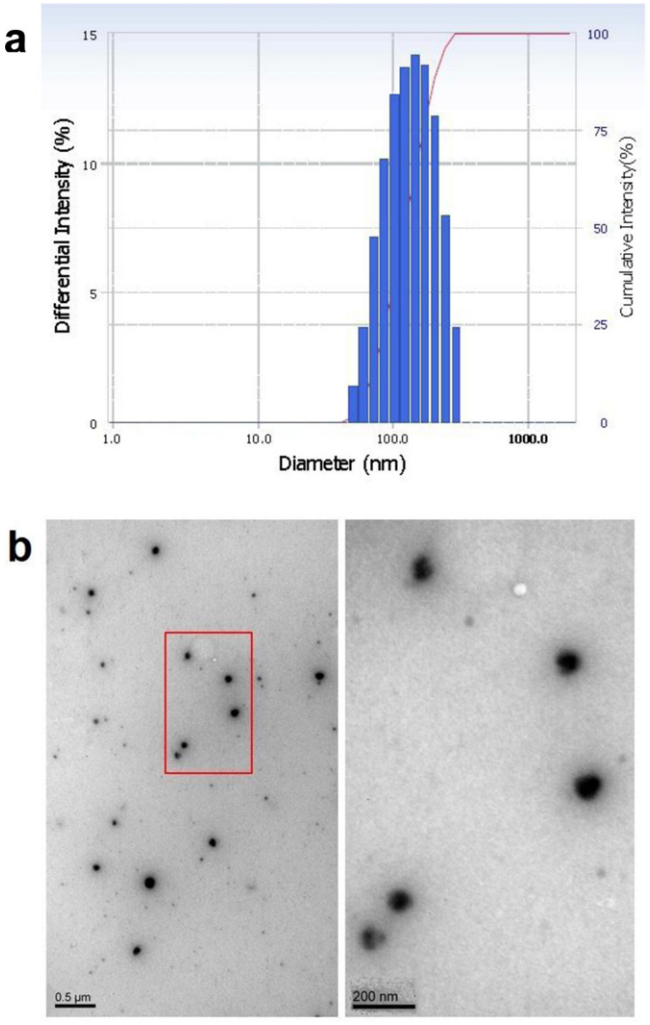

Fig. 6. Morphology and size distribution of DOX-loaded CSOAA-based nanoparticles. (a) The size distribution of DOX-loaded CSOAA-based nanoparticles was determined by dynamic light scattering. The CSOAA:DOX weight ratio was 7.5:1. (b) TEM images of DOX-loaded CSOAA-based nanoparticles were shown. Bar lengths are 500 (left) and 200 (right) nm, respectively.

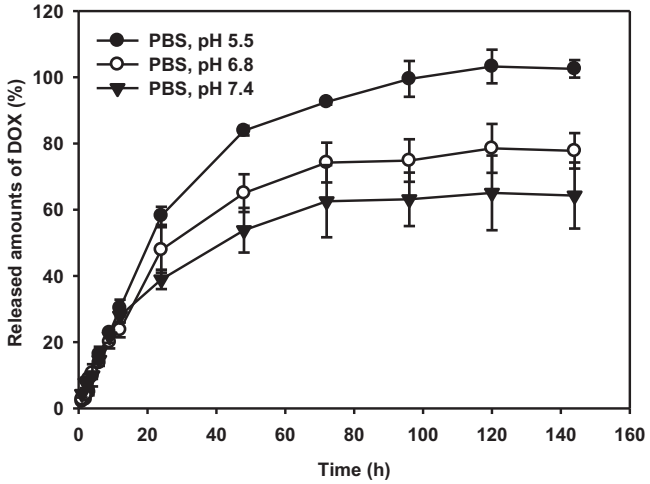

Fig. 7. *In vitro* DOX release profiles from CSOAA-based self-assembled nanoparticles. Drug release profiles from CSOAA:DOX = 7.5:1 formulation at different pH conditions (pH 5.5, 6.8, and 7.4) are shown. Each point represents the mean ± SD ($n = 3$).

Table 1
Characteristics of CSOAA-based nanoparticles.

Formulation	Mean diameter (nm, mean ± SD)	Polydispersity index	Zeta potential (mV)	Encapsulation efficiency (%)
Blank nanoparticles	73.67 ± 3.91	0.32 ± 0.01	7.58 ± 0.62	–
CSOAA:DOX (7.5:1)	130.00 ± 5.76	0.23 ± 0.02	12.98 ± 0.55	53.12 ± 2.60

Values are presented as mean ± SD ($n \geq 3$).

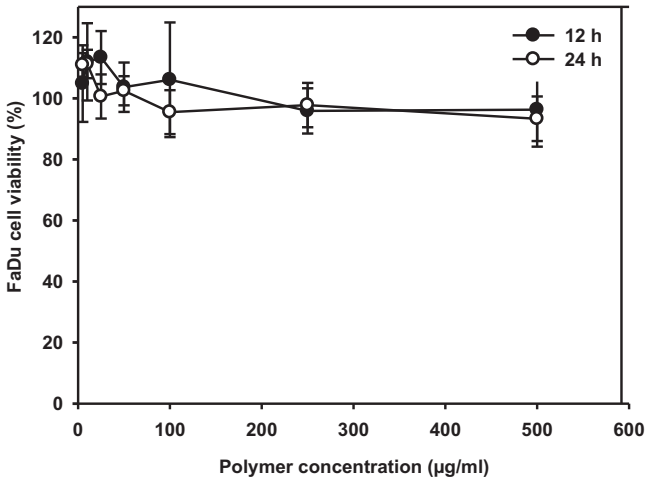

Fig. 8. *In vitro* cytotoxicity tests of CSOAA in FaDu cells. Various concentrations of CSOAA were incubated for 12 and 24 h in FaDu cells. Cell viability (%) was determined by an MTS-based assay. Each point represents the mean ± SD ($n = 4$).

3.4. In vitro cytotoxicity test

To examine the cytotoxicity of CSOAA, cell viability was measured in FaDu cells, a head and neck cancer cell line. The cells were treated with various concentrations of CSOAA for 12 and 24 h. As shown in Fig. 8, FaDu cell viability (%) was over 90% for all CSOAA concentrations tested. Thus, it can be concluded that CSOAA had no severe toxicity for FaDu cells.

3.5. In vitro cellular uptake study

The cellular uptake efficiency of DOX in FaDu cells was investigated by flow cytometry. Fluorescence intensity was assumed to be proportional to the amount of DOX internalized into the cells. Fig. 9 shows that higher amount of DOX from CSOAA-based nanoparticles was taken up into the cells than from the DOX solution group.

3.6. In vivo anti-tumor efficacy

In vivo anti-tumor efficacy of DOX-loaded nanoparticles was assessed in a FaDu tumor-bearing mouse model. DOX solution and DOX-loaded CSOAA-based nanoparticles were injected intravenously on days 6, 8, 11, and 13. Tumor volume (mm^3) and body weight (g) were monitored for 18 days. As shown in Fig. 10a, tumor growth inhibition in the DOX-loaded nanoparticle-treated group was significantly higher than in either the DOX solution-treated group or the control group ($p < 0.05$). After 18 days of treatment with DOX solution or DOX-loaded nanoparticles, tumor volumes were 44.63 ± 9.02% and 25.24 ± 5.61% of that for control group. No significant difference in body weight change was observed among the three groups; control, DOX solution-, and DOX-loaded nanoparticle-treated groups (Fig. 10b).

4. Discussion

In this study, CSOAA was successfully synthesized as a hydrophobically modified CSO for the preparation of self-assembled nanoparticles. The synthesis of CSOAA conjugate was confirmed by ^{1}H NMR analysis, but accurate substitution ratio (AA to CSO) might not be obtained from ^{1}H NMR spectrum of CSOAA. From ^{1}H NMR analysis of CSOAA, the proton peak of the glucosamine ring of CSO could be overlapped with the solvent peak and deacetylation degree of CSO was not obviously determined. Because of these limitations, the correlation between the integration ratio (1.23/1.81 ppm) and molar ratio of AA/CSO, based on physical mixture, was evaluated in this investigation (Fig. 4). With the input of the integration ratio (1.23/1.81 ppm) of CSOAA conjugate into this regression line, the stoichiometric ratio of CSOAA can

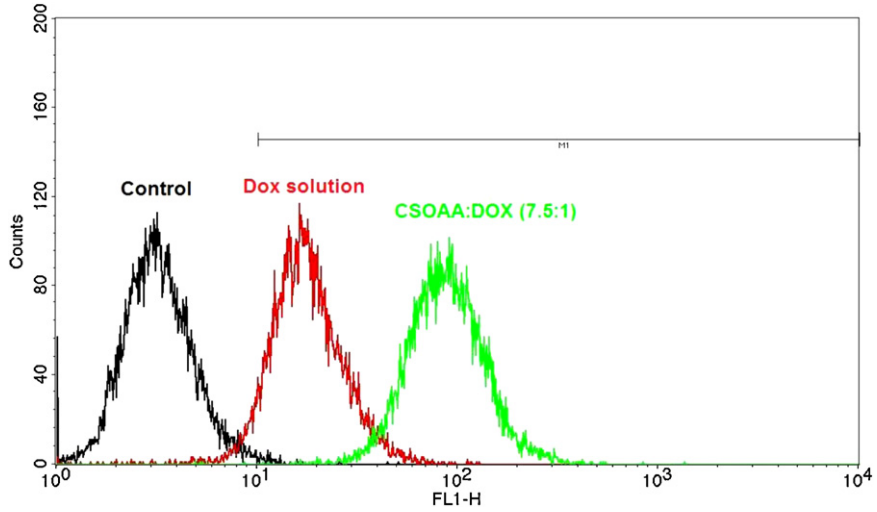

Fig. 9. Cellular uptake efficiency of DOX analyzed by flow cytometry. DOX solution and DOX-loaded nanoparticles were incubated for 1 h. The colors indicate each experimental group (*black*: control, *red*: DOX solution group, *green*: DOX-loaded nanoparticle group). (For interpretation of the references to color in this figure legend, the reader is referred to the web version of this article.)

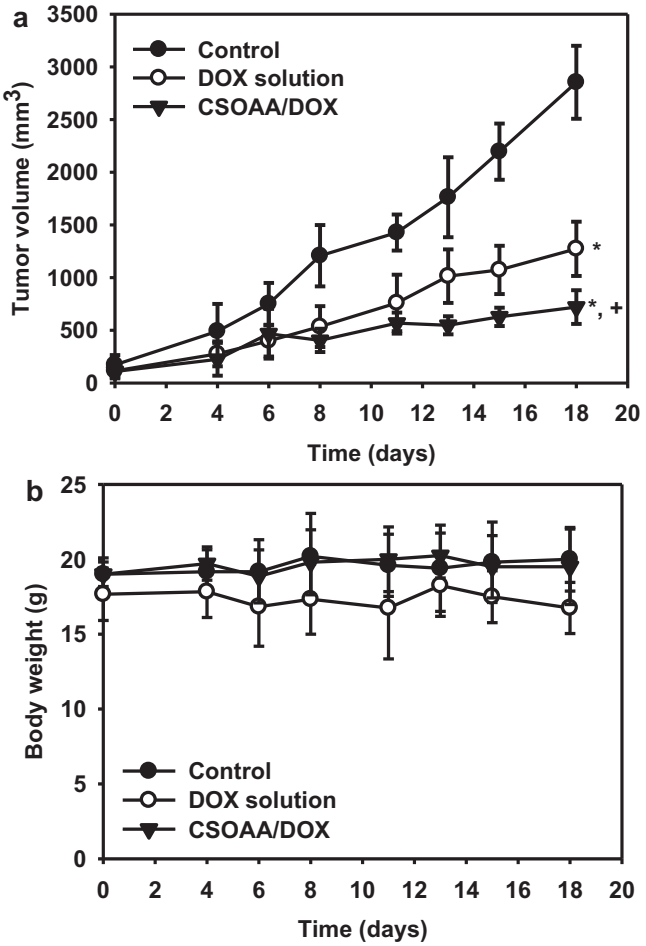

Fig. 10. Anti-tumor efficacy test of DOX-loaded CSOAA-based nanoparticles in a FaDu tumor-bearing BALB/c nude mouse model. (a) Tumor volume (mm^3) profiles according to the time (days) for 18 days were shown. DOX solution and DOX-loaded nanoparticles were injected intravenously on days 6, 8, 11, and 13. Each point indicates the mean ± SD ($n \geq 4$). (b) Body weight (g) was monitored. Each point indicates the mean ± SD ($n \geq 4$). $^*P < 0.05$ *vs.* control group; $^+P < 0.05$ *vs.* DOX solution group.

be determined more accurately. It is assumed that established assay (Fig. 4) could help identify the synthesis of CSOAA and calculate substitution ratio. The CMC value is also an important characteristic of micellar structured nanoparticle. The CMC value of CSOAA was significantly lower than those of low-molecular-weight surfactants in water (Lee et al., 1998). It can be concluded that CSOAA can form stable nanoparticulate structures at its low concentration after dilution with a large volume of body fluids.

The CSOAA synthesized could readily produce self-assembled nanoparticles in aqueous solution because of its amphiphilic property. The AA part could constitute an internal hydrophobic core, while CSO could provide a hydrophilic outer shell of the nanoparticles. The DOX-loaded CSOAA-based self-assembled nanoparticles were prepared by a solvent evaporation method. This method can provide several advantages over dialysis methods, such as the short preparation period and high drug loading efficiency (Park et al., 2004). DOX-loaded CSOAA-based nanoparticles exhibited <200 nm of mean diameter and narrow size distribution, high drug encapsulation efficiency, and negligible cytotoxicity. Because of these properties, it is assumed that DOX-loaded CSOAA-based nanoparticles can effectively accumulate in the tumor region *via* the EPR effect and exhibit reduced uptake by RES (Maeda et al., 2000; Yuan et al., 1995).

The sustained and pH-dependent drug release patterns from the CSOAA-based nanoparticles developed were observed (Fig. 7). Sustained drug release can lead to reduced *in vivo* drug clearance and maintenance of effective drug concentrations for tumor growth inhibition. Additionally, larger amount of DOX was released at acidic pH, simulating the endocytic compartment of cancer cells, compared with normal pH condition (pH 7.4). This difference may have been due to the slack structure of the nanoparticle, following protonation of amino groups in CSO and the higher solubility of DOX at an acidic pH. These results indicate that DOX-loaded CSOAA-based nanoparticles can be highly accumulated and release a large amount of drug in tumor tissues, with less DOX delivery to non-tumor regions. Moreover, enhanced drug release at pH 5.5 can imply endosomal escape of the drug and its improved transport to the cell nucleus.

As shown in Fig. 9, larger amount of DOX from nanoparticle-treated group was taken up to the cells compared to that from DOX solution group. This result may be explained by the interaction between the positively charged surface of the CSOAA-based nanoparticle and the negatively charged cellular membrane, and subsequent endocytosis of nanoparticles (Chavanpatil et al., 2006; Lee et al., 2011; Zauner et al., 1998). Furthermore, fatty acid-modified CS nanoparticles have been reported to form self-assembled nanoparticles with a multi-hydrophobic core (You et al., 2007). A hydrophobic minor core may help the internalization of nanoparticles into the cells by inserting fatty acids into the cell membrane.

FaDu cells were selected as a head and neck cancer cell line for this investigation. As shown in Fig. 10a, DOX-loaded CSOAA-based nanoparticles exhibited significant inhibitory effects on FaDu tumor growth, compared with both the control and DOX solution-treated groups. The physicochemical properties of drug-loaded nanoparticles, sustained drug release, and passive targeting, *via* mainly an EPR effect, may explain the efficient tumor growth inhibition by DOX-loaded CSOAA-based nanoparticles. In conclusion, the self-assembled CSOAA-based nanoparticle developed can be used as an anti-cancer drug delivery system, especially for head and neck cancer therapy.

5. Conclusions

CSOAA was synthesized for the preparation of self-assembled nanoparticles for DOX delivery. Its CMC value was relatively low and it could form self-assembled nanoparticles in an aqueous environment with a narrow size distribution. DOX-loaded CSOAA-based nanoparticles showed a sustained and pH-dependent drug release profile. It seemed that the nanoparticulate structure and drug release profile of the nanoparticles influenced on the cellular uptake and anti-tumor activity. DOX-loaded CSOAA-based nanoparticles significantly inhibited FaDu tumor growth *in vivo*. Considering all experimental results in this study, CSOAA-based self-assembled nanoparticles may be a promising carrier for anti-cancer drug delivery.

Acknowledgements

This work was supported by the National Research Foundation of Korea (NRF) grant funded by the Korean government (MEST) (No. 2011-0030635) and the MarineBio Research Program (NRF-C1ABA001-2011-0018561).

Appendix A. Supplementary data

Supplementary data associated with this article can be found, in the online version, at http://dx.doi.org/10.1016/j.ijpharm.2012.11.018.

References

Airoldi, M., Cattel, L., Milla, P., Pedani, F., Garzaro, M., Dosio, F., 2008. Paclitaxel and pegylated liposomal doxorubicin in recurrent head and neck cancer: clinical and unexpected pharmacokinetic interactions. Anticancer Res. 28, 2519–2527.

Aliabadi, H.M., Brocks, D.R., Lavasanifar, A., 2005. Polymeric micelles for the solubilization and delivery of cyclosporine A: pharmacokinetics and biodistribution. Biomaterials 26, 7251–7259.

Chae, S.Y., Son, S., Lee, M., Jang, M.K., Nah, J.W., 2005. Deoxycholic acid-conjugated chitosan oligosaccharide nanoparticles for efficient gene carrier. J. Control. Release 109, 330–344.

Chavanpatil, M.D., Khdair, A., Panyam, J., 2006. Nanoparticles for cellular drug delivery: mechanisms and factors influencing delivery. J. Nanosci. Nanotechnol. 6, 2651–2663.

Cho, H.J., Chong, S., Chung, S.J., Shim, C.K., Kim, D.D., 2012a. Poly-L-arginine and dextran sulfate-based nanocomplex for epidermal growth factor receptor (EGFR) siRNA delivery: its application for head and neck cancer treatment. Pharm. Res. 29, 1007–1019.

Cho, H.J., Yoon, H.Y., Koo, H., Ko, S.H., Shim, J.S., Lee, J.H., Kim, K., Kwon, I.C., Kim, D.D., 2011. Self-assembled nanoparticles based on hyaluronic acid-ceramide (HA-CE) and Pluronic® for tumor-targeted delivery of docetaxel. Biomaterials 32, 7181–7190.

Cho, H.J., Yoon, I.S., Yoon, H.Y., Koo, H., Jin, Y.J., Ko, S.H., Shim, J.S., Kim, K., Kwon, I.C., Kim, D.D., 2012b. Polyethylene glycol-conjugated hyaluronic acid-ceramide self-assembled nanoparticles for targeted delivery of doxorubicin. Biomaterials 33, 1190–1200.

Choi, J.S., Seo, K., Yoo, J.W., 2012. Recent advances in PLGA particulate systems for drug delivery. J. Pharm. Invest. 42, 155–163.

Kaida, S., Cabral, H., Kumagai, M., Kishimura, A., Terada, Y., Sekino, M., Aoki, I., Nishiyama, N., Tani, T., Kataoka, K., 2010. Visible drug delivery by supramolecular nanocarriers directing to single-platformed diagnosis and therapy of pancreatic tumor model. Cancer Res. 70, 7031–7041.

Kolishetti, N., Dhar, S., Valencia, P.M., Lin, L.Q., Karnik, R., Lippard, S.J., Langer, R., Farokhzad, O.C., 2010. Engineering of self-assembled nanoparticle platform for precisely controlled combination drug therapy. Proc. Natl. Acad. Sci. U. S. A. 1793, 17939–17944.

Kratz, F., Ehling, G., Kauffmann, H., Unger, C., 2007. Acute and repeat-dose toxicity studies of the (6-maleimidocaproyl) hydrazone derivative of doxorubicin (DOXO-EMCH), an albumin-binding prodrug of the anticancer agent doxorubicin. Hum. Exp. Toxicol. 26, 19–35.

Kumar, M., Muzzarelli, R.A.A., Muzzarelli, C., Sashiwa, H., Domb, A., 2004. Chitosan chemistry and pharmaceutical perspectives. Chem. Rev. 1014, 6017–6084.

Kwon, G.S., 2003. Polymeric micelles for delivery of poorly water-soluble compounds. Crit. Rev. Ther. Drug Carrier Syst. 20, 357–403.

Lee, J.Y., Choi, Y.S., Suh, J.S., Kwon, Y.M., Yang, V.C., Lee, S.J., Chung, C.P., Park, Y.J., 2011. Cell penetrating chitosan/doxorubicin/TAT conjugates for efficient cancer therapy. Int. J. Cancer 128, 2470–2480.

Lee, K., Kwon, I., Kim, Y.H., Jo, W., Jeong, S., 1998. Preparation of chitosan self-aggregates as a gene delivery system. J. Control. Release 51, 213–220.

Li, L., Tan, Y.B., 2008. Preparation and properties of mixed micelles made of Pluronic polymer and PEG-PE. J. Colloid Interface Sci. 317, 326–331.

Maeda, H., Wu, J., Sawa, T., Matsumura, Y., Hori, K., 2000. Tumor vascular permeability and the EPR effect in macromolecular therapeutics: a review. J. Control. Release 65, 271–284.

Muzzarelli, R., Muzzarelli, C., 2005. Chitosan chemistry: relevance to the biomedical sciences. Adv. Polym. Sci. 186, 151–209.

Park, J.H., Kwon, S., Nam, J.O., Park, R.W., Chung, H., Seo, S.B., Kim, I.S., Kwon, I.C., Jeong, S.Y., 2004. Self-assembled nanoparticles based on glycol chitosan bearing 5 beta-cholanic acid for RGD peptide delivery. J. Control. Release 95, 579–588.

Reuter, C.W., Morgan, M.A., Eckardt, A., 2007. Targeting EGF-receptor-signalling in squamous cell carcinomas of the head and neck. Br. J. Cancer 96, 408–416.

Vishu Kumar, A.B., Varadaraj, M.C., Lalitha, R.G., Tharanathan, R.N., 2004. Low molecular weight chitosans: preparation with the aid of papain and characterization. Biochim. Biophys. Acta 1670, 137–146.

Wildiers, H., Jurcut, R., Ganame, J., Herbots, L., Neven, P., De Backer, J., Denys, H., Cocquyt, V., Rademakers, F., Voigt, J.U., 2008. A pilot study to investigate the feasibility and cardiac effects of pegylated liposomal doxorubicin (PL-DOX) as adjuvant therapy in medically fit elderly breast cancer patients. Crit. Rev. Oncol. Hematol. 67, 133–138.

Yoon, H.Y., Koo, H., Choi, K.Y., Lee, S.J., Kim, K., Kwon, I.C., Leary, J.F., Park, K., Yuk, S.H., Park, J.H., Choi, K., 2012. Tumor-targeting hyaluronic acid nanoparticles for photodynamic imaging and therapy. Biomaterials 33, 3980–3989.

You, J., Hu, F.Q., Du, Y.Z., Yuan, H., Ye, B.F., 2007. High cytotoxicity and resistant-cell reversal of novel paclitaxel loaded micelles by enhancing the molecular-target delivery of the drug. Nanotechnology 18, 495101.

Yuan, F., Dellian, M., Fukumura, D., Leunig, M., Berk, D.A., Torchilin, V.P., Jain, R.K., 1995. Vascular permeability in a human tumor xenograft: molecular size dependence and cutoff size. Cancer Res. 55, 3752–3756.

Zauner, W., Ogris, M., Wagner, E., 1998. Polylysine-based transfection systems utilizing receptor-mediated delivery. Adv. Drug Deliv. Rev. 30, 97–113.

Colloids and Surfaces B: Biointerfaces 109 (2013) 280–286

Contents lists available at SciVerse ScienceDirect

Colloids and Surfaces B: Biointerfaces

journal homepage: www.elsevier.com/locate/colsurfb

Self-assembled magnetic resonance imaging nanoprobes based on arachidyl chitosan for cancer diagnosis

Ubonvan Termsarasab[a,1], Hyun-Jong Cho[b,1], Hyun Tae Moon[a], Ju-Hwan Park[a], In-Soo Yoon[c], Dae-Duk Kim[a,*]

[a] College of Pharmacy and Research Institute of Pharmaceutical Sciences, Seoul National University, Seoul 151-742, Republic of Korea
[b] College of Pharmacy, Kangwon National University, Chuncheon 200-701, Republic of Korea
[c] College of Pharmacy and Natural Medicine Research Institute, Mokpo National University, Jeonnam 534-729, Republic of Korea

ARTICLE INFO

Article history:
Received 21 January 2013
Received in revised form 8 March 2013
Accepted 30 March 2013
Available online 17 April 2013

Keywords:
Arachidyl chitosan
Gadolinium
Head and neck cancer
Magnetic resonance imaging
Nanoprobe

ABSTRACT

Arachidyl chitosan (chitosan oligosaccharide–arachidic acid; CSOAA)-based self-assembled nanoprobes for magnetic resonance imaging (MRI) of neoplastic lesions was developed and evaluated *in vitro*. Diethylenetriaminepentaacetic dianhydride (DTPA) was conjugated to chitosan oligosaccharide (CSO) and Gd^{3+} was chelated to the resulting ligand. DTPA conjugation and Gd^{3+} chelation were confirmed primarily by Fourier transform infrared spectroscopy (FT-IR) and zeta potential measurement. A spherical nanoprobe of around 150 nm mean diameter in the tested concentration range was formed in an aqueous environment by simple dissolution. The critical aggregation concentration (CAC) of the CSOAA-based nanoprobe was 3.86 μg/ml, indicating its stability after dilution in body fluid. The nanoprobe had negligible toxicity in head and neck cancer cell lines (Hep-2 and FaDu cells). The amount of Cy5.5-labeled nanoprobe taken-up by cells, as observed by confocal laser scanning microscopy (CLSM), increased according to incubation time (up to 12 h). A phantom study showed a T_1-positive contrast-enhancing effect of the developed CSOAA-based nanoprobe, compared to that of the commercial formulation (Gd-DTPA; Magnevist). These results indicate that the CSOAA-based nanoprobe can be used for efficient MR imaging of neoplastic cells.

1. Introduction

Alongside innovations in drug delivery for cancer therapy, imaging techniques for cancer diagnosis have also evolved. Progress in imaging agents and apparatus used for magnetic resonance imaging (MRI), computed tomography (CT), positron emission tomography (PET), single-photon emission computed tomography (SPECT) and ultrasound have contributed to more accurate diagnosis of cancer. MRI is one of the most powerful imaging techniques for diagnosis and has several advantages, such as high resolution of specific tissues and organs and deep penetration into the soft tissues [1–3]. MRI can provide abundant information on the anatomical and physiological state of the body [4]. Additionally, contrast agents are used to improve sensitivity resulting from the interaction with surrounding water protons and shortening of the proton relaxation time to enhance contrast [5]. Contrast agents can be classified into the T_1-weighted type (paramagnetic gadolinium chelates) and the T_2-weighted type (superparamagnetic iron oxide nanoparticles; SPION), which could enhance the contrast of regions of interest positively or negatively, respectively [2,3]. In particular, the T_1 contrast agents (paramagnetic Gd^{3+} chelates) have several advantages: high magnetic moment, suitable electron relaxation time, and a positive contrast enhancing effect [2,6]. Clinically relevant Gd^{3+} chelates are as follows [6]: Gd-diethylenetriaminepentaacetic acid (Gd-DTPA), Gd-1,4,7,10-tetra-azacyclododecane-1,4,7,10-tetraacetic acid (Gd-DOTA), and Gd-10-(2-hydroxypropyl)-1,4,7,10-tetra-azacyclododecane-1,4,7-triacetic acid (Gd-HP-DO3A). Although these Gd^{3+} chelates have been used successfully clinically, they have some problems; reduction of relaxivity (r_1) by chelation (mainly due to the decreased number of coordination sites for water proton exchange), lack of specificity for certain tissues or organs, and rapid clearance from the blood due to renal excretion [7,8]. Therefore, acquisition of enough spatial information on long-term application and disease targeting is difficult. It is expected that development of polymeric nanoparticles-based imaging agents will solve these problems.

Recently, polysaccharide-based nanoprobes for MR imaging have been investigated [4,9–11]. Various MR imaging probes based on chitosan or its derivatives have been developed [12–14]. Pure chitosan does not include any tumor-targeting ligand for

* Corresponding author. Tel.: +82 2 880 7870; fax: +82 2 873 9177.
E-mail address: ddkim@snu.ac.kr (D.-D. Kim).
[1] These authors are contributed equally.

0927-7765/$ – see front matter © 2013 Elsevier B.V. All rights reserved.
http://dx.doi.org/10.1016/j.colsurfb.2013.03.058

cancer diagnosis, but chitosan nanoparticles can accumulate in the tumor region after intravenous injection, mainly due to the enhanced permeability and retention (EPR) effect. In our previous study [15], chitosan oligosaccharide–arachidic acid (CSOAA), as an amphiphilic CSO derivative, was synthesized and used to prepare self-assembled nanoparticles. A hydrophobic anti-cancer drug was incorporated into the hydrophobic internal cavity of nanoparticles and injected intravenously into a head and neck cancer xenografted mouse model to evaluate *in vivo* anti-tumor efficacy. Herein, we report the development and *in vitro* evaluation of CSOAA-DTPA-Gd nanoprobes for MR imaging of cancer. DTPA was conjugated to CSO, after which Gd^{3+} was chelated to the DTPA ligand. It is expected that self-assembled CSOAA can form a nano-sized MRI probe (mean diameter, ~150 nm) in an aqueous environment, and thus can act as a useful MR imaging probe for cancer diagnosis.

2. Materials and methods

2.1. Materials

Chitosan oligosaccharide (average molecular weight = 5 kDa, degree of deacetylation >90%) was purchased from Kitto Life Co., Ltd. (Seoul, Korea). Arachidic acid (AA), 1-ethyl-3-(3-dimethylaminopropyl) carbodiimide (EDC), N-hydroxysuccinimide (NHS), pyrene, diethylenetriaminepentaacetic dianhydride (DTPA), and gadolinium (III) chloride hexahydrate ($GdCl_3 \bullet 6H_2O$) were purchased from Sigma Chemical Co. (St. Louis, MO, USA). Cy5.5 NHS ester was purchased from Amersham Biosciences (Piscataway, NJ, USA). Dulbecco's modified Eagle's medium (DMEM), minimum essential medium (MEM), penicillin, streptomycin, and heat-inactivated fetal bovine serum (FBS) were obtained from Gibco Life Technologies, Inc. (Grand Island, NY, USA). All other chemicals were of reagent grade and used without further purification.

2.2. Synthesis of CSOAA-DTPA-Gd

CSOAA was synthesized according to our previous method [15]. In brief, CSO (0.2 mmol) and AA (0.6 mmol) were dissolved separately in 20 ml dimethyl sulfoxide (DMSO) at 50 °C for 15 min. The carboxyl groups of AA were activated by adding EDC and NHS (molar ratio for AA = 1.5:1) and stirring for 30 min at room temperature. The activated AA solutions were added to the CSO solution for 5 min, then allowed to react for a further 12 h, after which double-distilled water (DDW) at a volume ratio of 10% was added. The pH of mixed solutions was adjusted to 3.5 with 1 N HCl and stirred for 30 min. The solution was precipitated with acetone (ten times the volume of the mixture, v/v) and centrifuged at 7500 rpm for 30 min to eliminate unreacted AA. The precipitation step was repeated three times. After precipitation, the precipitates were dispersed with DDW and dialyzed against DDW with a dialysis membrane (molecular weight cut-off: 1 kDa, Spectrum Laboratories, Laguna Hills, CA, USA) for 1 day. Dialysis products were obtained by freeze-drying.

DTPA was conjugated to CSO by amide bond formation between the carboxylic group of DTPA and the amine group of CSO. DTPA (0.1 mmol) was dissolved in DDW (15 ml), and EDC (0.2 mmol) and NHS (0.2 mmol) were added. After stirring for 30 min, the solution was slowly added to CSOAA (0.02 mmol) solution in DDW (20 ml). It was further stirred for 12 h at room temperature and dialyzed with a dialysis membrane (molecular weight cut-off: 3.5 kDa) against DDW for 3 days. CSOAA-DTPA was obtained by lyophilization. For Gd^{3+} chelation, $GdCl_3 \bullet 6H_2O$ (0.05 mmol) dissolved in 5 ml of DDW was slowly added to CSOAA-DTPA (0.01 mmol) dissolved in 30 ml DDW and the pH was adjusted to 7 by 1 N NaOH. It was stirred for 24 h and dialyzed for 3 days against DDW to remove free Gd^{3+}. CSOAA-DTPA-Gd was obtained by freeze-drying. DTPA conjugation to CSOAA was identified by ^1H NMR analysis (500 MHz). CSOAA-DTPA was solubilized in deuterium oxide (D_2O) for ^1H NMR analysis. DTPA conjugation and Gd^{3+} chelation were also confirmed by FT-IR analysis with a JASCO FT-IR 4200 spectrometer (JASCO Company Ltd., Hachioji, Japan). Gd content in the CSOAA-based nanoprobe was determined by an inductive coupled plasma-atomic emission spectrometer (ICP-AES, Optima 4300 DV, PerkinElmer Inc., Wellesley, MA, USA).

2.3. Characteristics of the CSOAA-based nanoprobe

To produce CSOAA-based nanoprobes, CSOAA-DTPA-Gd was solubilized in DDW, phosphate buffered saline (PBS, pH 7.4) or 50% (v/v) FBS solution (in PBS pH 7.4). After dissolving at a predetermined concentration, the sample was sonicated using a probe-type sonicator (Vibra-Cell VC 750 ultrasonic processor, Sonics & Materials, CT, USA) for 1 min. Mean diameter, polydispersity index, and zeta potential values of the nano-sized probe were measured using a light-scattering spectrophotometer (ELS-Z; Otsuka Electronics, Tokyo, Japan) according to the manufacturer's protocol. The morphology of the CSOAA-based nanoprobe was observed by transmission electron microscopy (TEM). The nanoprobes were placed on copper grids with films. After air-drying for 10 min, they were observed by TEM (JEM 1010; JEOL, Tokyo, Japan). The scale bar in the images represents 1 μm. Critical aggregation concentration (CAC) of the CSOAA-based nanoprobe was determined using a fluorescence spectrophotometer with pyrene as a hydrophobic substance. Pyrene dissolved in acetone (2×10^{-6} M) was prepared and 0.3 ml of that solution was transferred to each 1.5 ml tube. Acetone was evaporated under a gentle nitrogen (N_2) gas stream for 1 h at 60 °C. The nanoprobe solution in DDW (1 ml), the concentration of which ranged from 0.1–1000 μg/ml, was added to each tube to make a 6×10^{-7} M pyrene concentration. The emission spectrum (310–550 nm) was obtained at a fixed 334 nm excitation wavelength with a fluorescence spectrometer FP-6500 (JASCO Co., Tokyo, Japan).

2.4. In vitro cytotoxicity of the nanoprobe

Hep-2 and FaDu cells were purchased from Korean Cell Line Bank (KCLB, Seoul, Korea). Hep-2 cells were cultured with DMEM supplemented with 10% FBS, 100 U/ml penicillin, and 100 μg/ml streptomycin, and FaDu cells were cultured with MEM containing 10% FBS, 100 U/ml penicillin, and 100 μg/ml streptomycin, in a 5% CO_2 atmosphere with 95% relative humidity at 37 °C. After Hep-2 and FaDu cells reached 70–80% confluency, they were trypsinized and seeded in a 96-well plate at a density of 1.0×10^4 per well. After incubation for 24 h, the culture medium was removed. After 12 and 24 h incubation of CSOAA-DTPA and CSOAA-DTPA-Gd (15–300 μg/ml) with both cell types at 37 °C, 5% CO_2 and 95% relative humidity, the cell viability (%) was determined using the MTS-based CellTiter 96 AQ_{ueous} One Solution Cell Proliferation Assay Reagent (Promega Corp., WI, USA) at 37 °C for 4 h, according to the manufacturer's protocol. The absorbance at 490 nm was measured using an Emax Precision Microplate Reader (Molecular Devices, Sunnyvale, CA, USA).

2.5. In vitro cellular uptake

To monitor the intracellular uptake of nanoprobes, Cy5.5, a near-infrared fluorescence (NIRF) dye for observation by confocal laser scanning microscopy (CLSM), was conjugated to a CSO backbone by amide bond formation. The CSOAA-DTPA conjugate (100 mg) was dissolved in 50 ml carbonate/bicarbonate buffer (50 mM, pH 9.6).

Cy5.5 NHS ester (0.2 mg) dissolved in 0.02 ml DMSO was slowly added to a CSOAA-DTPA-containing buffer and stirred for 3 h at room temperature. Free Cy5.5 was removed by dialysis against DDW for 3 days. The final product was obtained by lyophilization. For Gd^{3+} chelation, the previously described synthesis method was used. In brief, $GdCl_3{\bullet}6H_2O$ (0.05 mmol) dissolved in 5 ml DDW was slowly added to Cy5.5-CSOAA-DTPA (0.01 mmol) dissolved in 30 ml DDW and the pH was adjusted to 7 using 1 N NaOH. The solution was stirred for 24 h and dialyzed for 3 days against DDW to remove free Gd^{3+}. Cy5.5-CSOAA-DTPA-Gd was obtained by freeze-drying. The Cy5.5 content in the Cy5.5-labeled CSOAA-based nanoprobe was determined by measuring absorbance at 650 nm with a UV/vis spectrophotometer (Emax Precision Microplate Reader, Molecular Devices, Sunnyvale, CA, USA). Linearity was established in the range 1–25 μg/ml Cy5.5.

After Hep-2 and FaDu cells acquired 70–80% confluency, the cells were trypsinized and seeded onto culture slides (BD Falcon, Bedford, MA) at a density of 1.0×10^5 per well (surface area of 1.7 cm^2 per well, four-chamber slides) and incubated for 24 h at 37 °C. The Cy5.5-labeled nanoprobe (1 mg/ml) was incubated for 0.5, 8 and 12 h at 37 °C. The cells were then washed with phosphate-buffered saline (PBS, pH 7.4) at least three times and fixed with a 4% formaldehyde solution for 5 min. VECTASHIELD mounting medium with 4′,6-diamidino-2-phenylindole (DAPI) (H-1200; Vector Laboratories, Inc., Burlingame, CA, USA) was added to stain nuclei and prevent the fading of fluorescence. The preparations were observed by CLSM (LSM 710; Carl-Zeiss, Thornwood, NY, USA).

2.6. In vitro MRI study

All MRI studies were performed with a 4.7-T MRI apparatus (Bruker BioSpec 47/40, Karlsruhe, Germany). T_1 contrast intensities of Gd-DTPA (Magnevist®, Bayer Schering Pharma AG, Berlin, Germany) and the CSOAA-based nanoprobe were scanned at 5–100 μM Gd concentrations. Specific parameters were as follows: echo time (TE) = 6.5 ms, repetition time (TR) = 1000 ms, field of view (FOV) = 5 × 4 cm, matrix = 128 × 128, slice thickness = 2 mm.

The proton relaxation enhancement can be expressed using the following formula:

$$\left(\frac{1}{T_1}\right)_{obs} = \left(\frac{1}{T_1}\right)_{d} + R_1[M] \quad (1)$$

where $(1/T_1)_{obs}$ and $(1/T_1)_d$ are the relaxation rates of the protons in the presence and absence of paramagnetic species (Gd), respectively, and $[M]$ is the concentration of the paramagnetic species (Gd).

2.7. Data analysis

All experiments were performed at least three times and the data were represented as mean ± standard deviation (SD).

3. Results and discussion

3.1. Synthesis of the CSOAA-based nanoprobe

CSOAA was synthesized, as an amphiphilic CSO derivative, to prepare self-assembled nanoparticles according to the reported method [15]. CSOAA was synthesized by amide bond formation between the carboxylic group of AA and the amine bond of CSO by an EDC-coupled reaction (Fig. 1A). Synthesis was identified by ^{1}H NMR analysis. Though the proton peaks for the glucosamine ring of CSO overlapped those of the solvent, the proton peaks at 0.86 and 1.23 ppm indicated that the terminal methyl group (—CH_3) and alkyl chain (—CH_2—) of AA were present [15]. In particular, the proton peak of —CH_2— of AA linked with the carbonyl group without conjugation (2.21 ppm) was shifted after amide bond formation (2.16 ppm). According to our previous report [15], conjugation of AA to the CSO backbone was also confirmed by FT-IR analysis. In particular, the amide II band was shifted from 1591 cm^{-1} in the CSO spectrum to 1558 cm^{-1} in the CSOAA spectrum. Prior to Gd chelation, DTPA was conjugated to CSOAA, as confirmed by ^{1}H NMR and FT-IR analysis. An amide bond was formed between the amine group of CSO and the carboxylic group of DTPA by an EDC-coupled reaction (Fig. 1A). As shown in Fig. 1S, peaks indicating DTPA (3.3 ppm) and CSO (2.0 ppm) were presented in the ^{1}H NMR spectrum of CSOAA-DTPA. The FT-IR spectra also revealed the conjugation of DTPA to CSOAA (Fig. 1B). The FT-IR spectrum of CSOAA was reported in our previous study [15]. Considering the FT-IR spectrum of CSOAA, the amide I band was shifted from 1648 cm^{-1} in the CSOAA spectrum to 1632 cm^{-1} in the CSOAA-DTPA spectrum (Fig. 1B). In particular, the amide II band at 1558 cm^{-1} in the spectrum of CSOAA was altered in the spectrum of CSOAA-DTPA. Absorption intensity of the C—O stretching band in CSOAA-DTPA at 1075 cm^{-1} was attenuated in the spectrum of CSOAA-DTPA-Gd by coordination of Gd^{3+} to DTPA. Furthermore, the Gd content in the CSOAA-based nanoprobe measured by ICP-AES was 5.43% (w/w). Synthesis of CSOAA-DTPA-Gd was also evaluated by measurement of zeta potential, as reported previously [4,11]. As shown in Table 1, the zeta potential was decreased by DTPA conjugation from 12.50 ± 0.81 mV (CSOAA) to 9.21 ± 0.85 mV (CSOAA-DTPA). It may be induced by ionization of the carboxylic group of DTPA. After chelation of Gd^{3+} to CSOAA-DTPA, its zeta potential was slightly increased to 11.19 ± 0.39 mV. The zeta potential can be altered by several factors, such as nanoprobe concentration, DTPA conjugation degree, and Gd content.

3.2. Characteristics of the nanoprobe

A nano-sized CSOAA-based probe was prepared using the self-assemble property of CSOAA. The mean diameter, polydispersity index, and zeta potentials of the nanoprobes were measured. As shown in Table 1, the mean diameter of the CSOAA-DTPA-Gd nanoprobe was 146.30 ± 5.51 nm (at 1 mg/ml concentration of the nanoprobe) and was around 150 nm within 5 mg/ml concentration in DDW (Fig. 2A). Mean diameter of CSOAA-based nanoprobe (at 5 mg/ml concentration) was 248.97 ± 6.70 and 167.70 ± 0.92 nm in 50% (v/v) FBS solution (in PBS pH 7.4) and PBS (pH 7.4), respectively (Fig. 2S). The mean diameters of nanoprobes in both media were maintained constantly for 4 h. Although the particle size of nanoprobe in 50% FBS solution slightly increased compared to that in DDW or PBS, it is still considered to be suitable for the cellular uptake and passive tumor targeting. The morphology was observed by TEM to be spherical (Fig. 2B). The CSOAA-based nanoprobe also exhibited a narrow size distribution (Fig. 2C). The CAC value of CSOAA was 1.42 μg/ml [15] and that of CSOAA-DTPA-Gd was 3.86 μg/ml (Fig. 2D); the lower value implies that the CSOAA-based nanoprobe may be more stable after dilution in body fluids.

Gd-DTPA (Magnevist) has a terminal elimination half-life of about 20 min [16]. Considering the higher molecular weight and larger particle size of the developed polymeric nanoprobe, a polymeric nanoprobe including Gd-DTPA likely exhibits reduced *in vivo* clearance, thereby increasing its blood circulation time compared to the commercial contrast agent (Magnevist). Moreover, the EPR effect can improve accumulation of nanoprobes in the tumor region. In our previous report, the nano-sized polymeric probe exhibited MR signal-enhancing effects in the tumor region compared to the commercial formulation [4]. The particle size (~150 nm) of the experimental nanoprobe in this study may yield improved tumor targetability and cancer diagnosis.

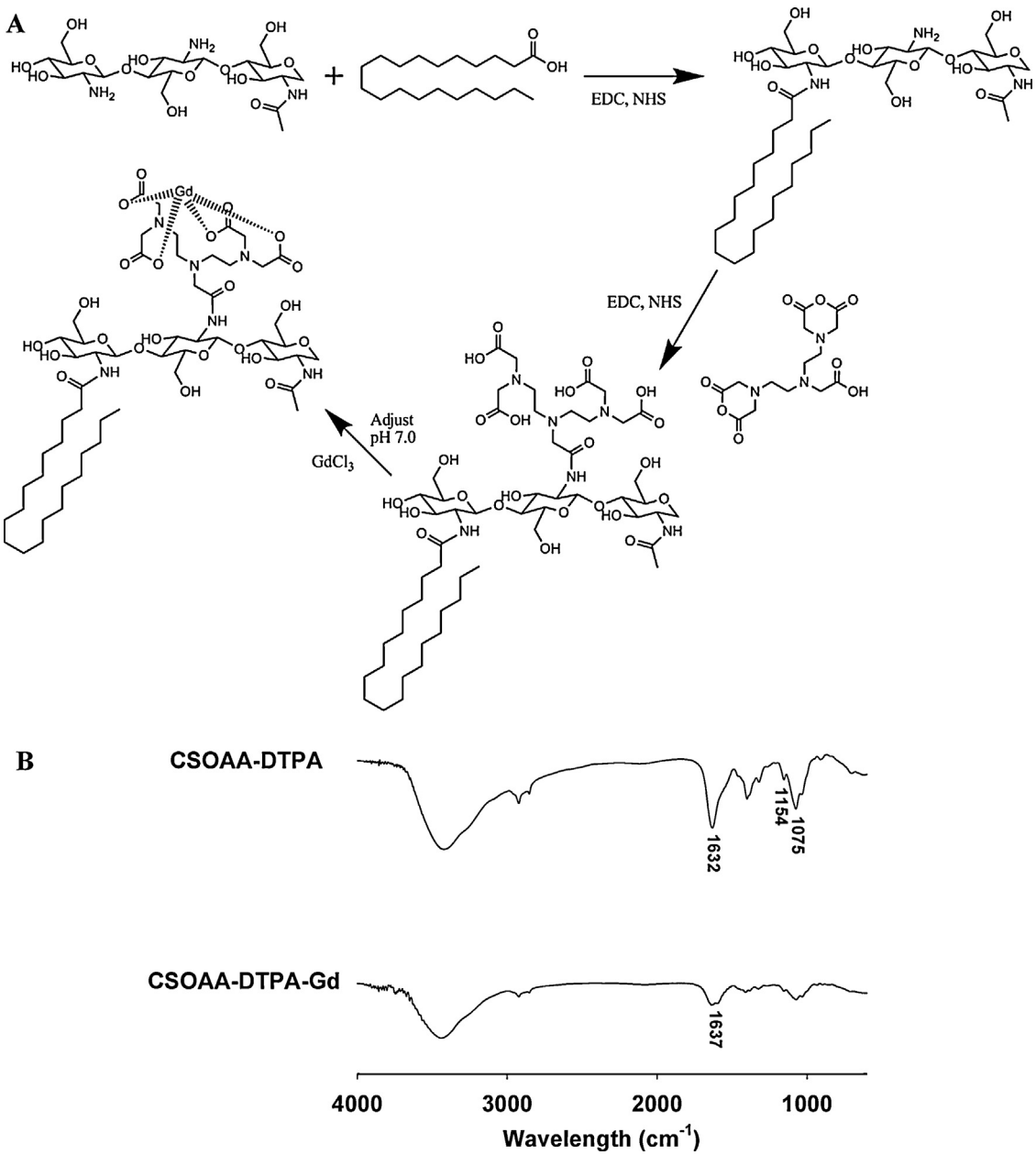

Fig. 1. Synthesis and characteristics of the CSOAA-based nanoprobe. (A) Synthesis of CSOAA-DTPA-Gd. (B) FT-IR spectra of CSOAA-DTPA and CSOAA-DTPA-Gd.

3.3. *In vitro cytotoxicity*

The cytotoxicity of the CSOAA-based nanoprobe (CSOAA-DTPA and CSOAA-DTPA-Gd) was evaluated in cancer cells according to nanoprobe concentration and incubation time. In this investigation, Human laryngeal and pharyngeal cancer (Hep-2 and FaDu) cells were used. These two cell types have previously been used for head and neck cancer research [15,17]. CSOAA showed no severe cytotoxicity in FaDu cells in a previous report [15]; therefore, its cytotoxicity was not evaluated in this study. Viability (%) in both cell types was assessed by MTS-based assay. As shown in Fig. 3, the cytotoxicity of CSOAA-DTPA and CSOAA-DTPA-Gd seemed to be inconsequential in both cell lines at the probe concentrations and incubation times (12 and 24 h) used. Although Gd has been used as a representative T_1-weighted contrast agent, the aqueous Gd^{3+} ion exhibited severe cytotoxicity [7]. Therefore, organic linear

Table 1
Characteristics of CSOAA, CSOAA-DTPA and CSOAA-DTPA-Gd nanoprobes.

Nanoprobe	Mean diameter (nm)	Polydispersity index	Zeta potential (mV)
CSOAA	177.03 ± 2.75	0.20 ± 0.02	12.50 ± 0.81
CSOAA-DTPA	177.90 ± 18.79	0.09 ± 0.01	9.21 ± 0.85
CSOAA-DTPA-Gd	146.30 ± 5.51	0.20 ± 0.05	11.19 ± 0.39

Values are presented as means ± standard deviation (SD) ($n = 3$).
Concentration of all samples was 1 mg/ml.

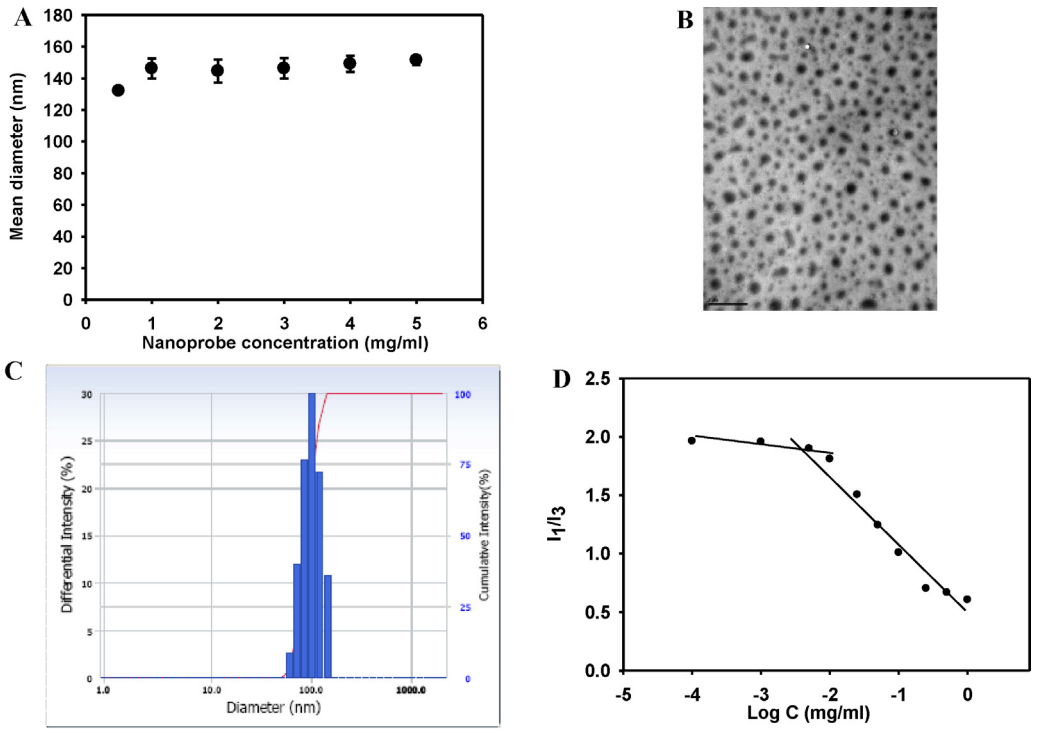

Fig. 2. Characteristics of the CSOAA-based nanoprobe. (A) The mean diameter of the nanoprobe was plotted according to its concentration (0.5–5 mg/ml). Data are expressed as means ± SD ($n = 3$). (B) TEM image of the nanoprobe (2.5 mg/ml). The scale bar in TEM images represents 1 μm. (C) The size distribution of the nanoprobe (2.5 mg/ml). (D) CAC determination of the CSOAA-based nanoprobe. The fluorescence intensity ratio (I_{373}/I_{383}, I_1/I_3) was plotted according to nanoprobe concentration and the CAC was estimated from the threshold concentration of the nanoprobe.

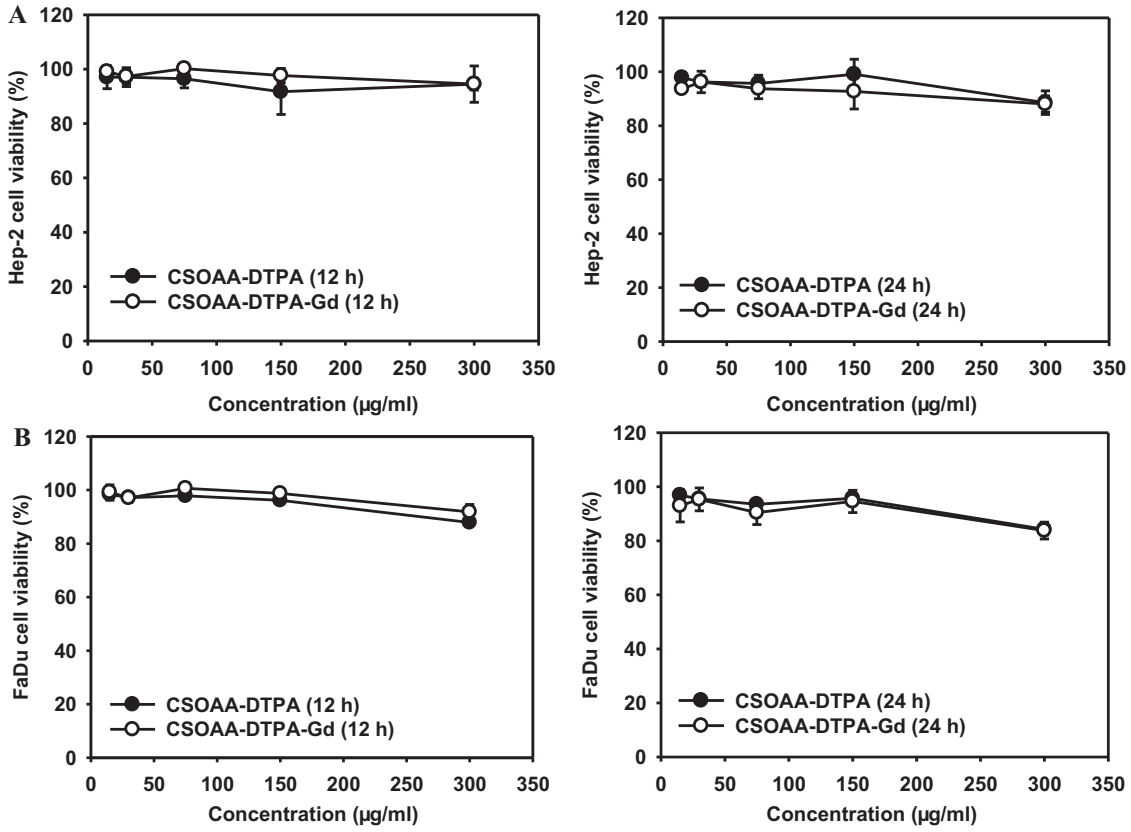

Fig. 3. *In vitro* cytotoxicity tests of the CSOAA-based nanoprobe in (A) Hep-2 and (B) FaDu cells after 12 and 24 h of incubation. Cell viability (%) was measured by MTS-based assay according to nanoprobe concentration. Data are expressed as means ± SD ($n = 4$).

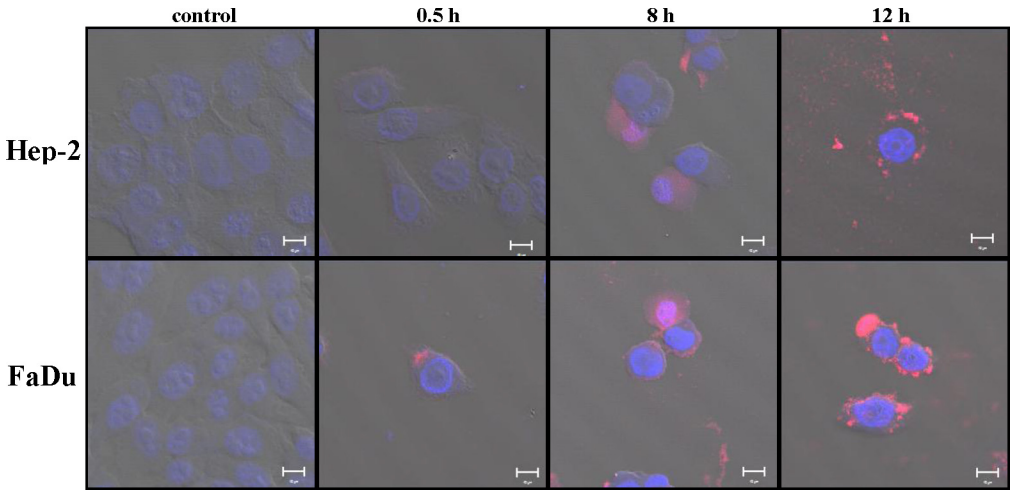

Fig. 4. Cellular uptake studies of the nanoprobe in Hep-2 and FaDu cells. Intracellular uptake and distribution of the Cy5.5-labeled nanoprobe were visualized by CLSM. Merged images of the control (no treatment), and 0.5 h, 8 h and 12 h incubation groups are shown. Red and blue indicate Cy5.5 and DAPI, respectively. The bar in the picture represents 10 μm.

and macrocyclic ligands (*e.g.* DTPA) are required to chelate Gd^{3+} to reduce toxicity [7,18]. CSOAA-DTPA-Gd exhibited no severe cytotoxicity in head and neck cancer cells (Fig. 3), implying that this nanoprobe is safe for MR imaging.

3.4. In vitro cellular uptake

The cellular uptake efficiency of the experimental nanoprobe was determined by CLSM. The nanoprobe was labeled with Cy5.5 and its intracellular uptake and distribution were observed. Cy5.5 was used as a NIRF imaging dye for *in vivo* tumor imaging in our previous studies [4,19,20]. The Cy5.5 NHS ester was conjugated to the amine group of CSO by amide bond formation; the Cy5.5 content of the Cy5.5-labeled CSOAA-based nanoprobe was 0.13% (w/w). Cellular uptake and distribution patterns of Cy5.5-labeled nanoprobe were monitored up to 12 h in both Hep-2 and FaDu cells. The Cy5.5 fluorescence intensity, indicating the amount of nanoprobe taken up by cells, increased according to incubation time in both cell types (Fig. 4).

The physicochemical properties of nanoparticles, such as mean diameter, surface charge, morphology and composition, can influence their cellular uptake and distribution [21]. Though smaller nanoparticles with a uniform size distribution exhibit increased uptake, other factors can play important roles in cellular uptake of chitosan-based nanoparticles [22–24]. The surface charge of a nanoparticle can affect its cellular uptake and subsequent cellular distribution. Electrostatic interaction between positively charged chitosan-based nanoparticles and the negatively charged cellular membrane can facilitate cellular binding and uptake of nanoparticles. The positive charge of a chitosan-based nanoparticle promoted its internalization rate and level in eight cell lines [25]. In addition, some positively charged nanoparticles escaped the lysosome and localized perinuclearly. Endocytosis of the nanoprobe is thought to be governed by its particle size (~150 nm) and positive zeta potential (Table 1).

3.5. Phantom study

In vitro paramagnetism of Gd-DTPA (Magnevist) and CSOAA-DTPA-Gd was evaluated by 4.7-T MRI. In Fig. 5A, T_1-weighted MR images of both formulations according to the Gd concentration (5–100 μM) are shown. As Gd concentration increased, MR signals were also enhanced, as indicated by the brightness in both groups. The MR signals were analyzed quantitatively and a linear relationship between the proton longitudinal relaxation rate ($1/T_1$) and Gd concentration was identified. T_1 relaxivity (r_1) was calculated using Eq. (1). T_1 relaxivity of the CSOAA-based nanoprobe was 15.28 $mM^{-1}\ s^{-1}$, 2.43-fold higher than that of Gd-DTPA (Magnevist) in this investigation (Fig. 5B). In our previous report [4], a contrast-enhancing effect of a hyaluronic acid derivative-based nanoprobe compared to the commercial formulation (Magnevist) was found. CSOAA also has several hydroxyl groups in its glucose ring unit that can attract adjacent water molecules, thereby improving the local density of water molecules [4]. This may increase the water exchange rate in Gd molecules and lead to enhanced T_1 relaxivity [11,26].

Although therapeutic drugs were not incorporated in this study, the formation of an internal hydrophobic core due to the AA segment is expected to facilitate loading of hydrophobic drugs. Anti-cancer drug delivery using an unmodified CSOAA nanoparticle and its anti-tumor efficacy in a head and neck cancer model have

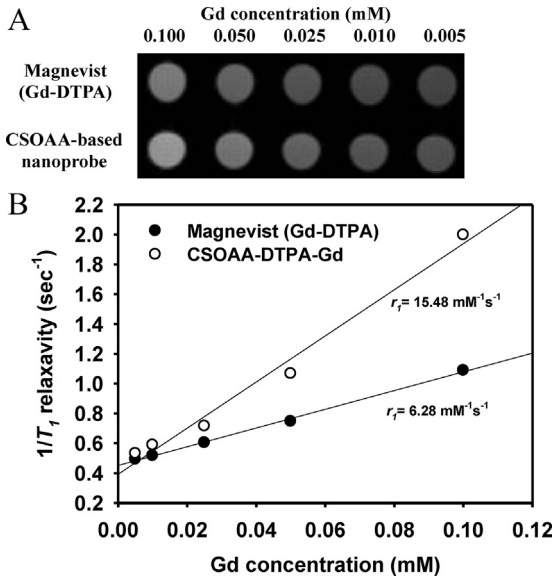

Fig. 5. *In vitro* MRI test of Magnevist (Gd-DTPA) and CSOAA-DTPA-Gd at 4.7-T. (A) T_1-weighted phantom image with 5–100 μM Gd concentrations was shown. (B) Longitudinal relaxation ($1/T_1$) according to the Gd concentration was plotted.

been reported previously [15]. Therefore, although it is expected that the theranostic nanoparticle based on CSOAA is feasible for cancer therapy and diagnosis, further studies of its usefulness are required.

4. Conclusions

Self-assembled CSOAA-based nanoprobes including a T_1 contrast agent was developed for MR imaging. DTPA was conjugated to CSOAA *via* an amide bond and Gd^{3+} was chelated to the DTPA ligand. This created a spherical nanoprobe of ~150 nm mean diameter with a positive zeta potential. The CSOAA-based nanoprobe exhibited negligible cytotoxicity in head and neck cancer cell lines. Cellular uptake and distribution of the Cy5.5-labeled nanoprobe were also observed by CLSM and the amount of nanoprobe taken up in head and neck cancer cells increased according to incubation time. The T_1 contrast-enhancing effect of the CSOAA-based nanoprobe, compared to the commercial formulation (Magnevist), was demonstrated in a phantom study. These results suggest that the CSOAA-based nanoprobe is a promising MR imaging probe for cancer diagnosis.

Acknowledgements

This research was supported by the National Research Foundation of Korea (NRF) funded by the Ministry of Education, Science and Technology (No. 2009-0083533 and 2012038944).

Appendix A. Supplementary data

Supplementary data associated with this article can be found, in the online version, at http://dx.doi.org/10.1016/j.colsurfb.2013.03.058.

References

[1] S.M. Janib, A.S. Moses, J.A. MacKay, Adv. Drug Deliv. Rev. 62 (2010) 1052.
[2] T. Liu, X. Li, Y. Qian, X. Hu, S. Liu, Biomaterials 33 (2012) 2521.
[3] A.J.L. Villaraza, A. Bumb, M.W. Brechbiel, Chem. Rev. 110 (2010) 2921.
[4] H.J. Cho, H.Y. Yoon, H. Koo, S.H. Ko, J.S. Shim, J.H. Cho, J.H. Park, K. Kim, I.C. Kwon, D.D. Kim, J. Control. Release 162 (2012) 111.
[5] N.J.J. Johnson, W. Oakden, G.J. Stanisz, R.S. Prosser, F.C.J.M. van Veggel, Chem. Mater. 23 (2011) 3714.
[6] P. Caravan, J.J. Ellison, T.J. McMurry, R.B. Lauffer, Chem. Rev. 99 (1999) 2293.
[7] J.S. Ananta, B. Godin, R. Sethi, L. Moriggi, X. Liu, R.E. Serda, R. Krishnamurthy, R. Muthupillai, R.D. Bolskar, L. Helm, M. Ferrari, L.J. Wilson, P. Decuzzi, Nat. Nanotechnol. 5 (2010) 815.
[8] H. Kobayashi, N. Sato, A. Hiraga, T. Saga, Y. Nakamoto, H. Ueda, J. Konishi, K. Tokashi, M.W. Brechbiel, Magn. Reson. Med. 45 (2001) 454.
[9] M.J. Ernsting, W.D. Foltz, E. Undzys, T. Tagami, S.D. Li, Biomaterials 33 (2012) 3931.
[10] E.K. Lim, H.O. Kim, E. Jang, J. Park, K. Lee, J.S. Suh, Y.M. Huh, S. Haam, Biomaterials 32 (2011) 7941.
[11] H. Yim, S.G. Yang, Y.S. Jeon, I.S. Park, M. Kim, D.H. Lee, Y.H. Bae, K. Na, Biomaterials 32 (2011) 5187.
[12] J.J. Cheng, J. Zhu, X.S. Liu, D.N. He, J.R. Xu, L.M. Wu, J. Zhou, Q. Feng, Acta Radiol. 53 (2012) 900.
[13] J. Key, C. Cooper, A.Y. Kim, D. Dhawan, D.W. Knapp, K. Kim, J.H. Park, K. Choi, I.C. Kwon, K. Park, J.F. Leary, J. Control. Release 163 (2012) 249.
[14] S.H. Yuk, K.S. Oh, S.H. Cho, B.S. Lee, S.Y. Kim, B.K. Kwak, K. Kim, I.C. Kwon, Biomacromolecules 12 (2011) 2335.
[15] U. Termsarasab, H.J. Cho, D.H. Kim, S. Chong, S.J. Chung, C.K. Shim, H.T. Moon, D.D. Kim, Int. J. Pharm. 441 (2013) 373.
[16] H.J. Weinmann, R.C. Brasch, W.R. Press, G.E. Wesbey, Am. J. Roentgenol. 142 (1984) 619e24.
[17] H.J. Cho, S. Chong, S.J. Chung, C.K. Shim, D.D. Kim, Pharm. Res. 29 (2012) 1007.
[18] M.E. Bartolini, J. Pekar, D.R. Chettle, F. McNeill, A. Scott, J. Sykes, F.S. Prato, G.R. Moran, Magn. Reson. Imaging 21 (2003) 541.
[19] H.J. Cho, H.Y. Yoon, H. Koo, S.H. Ko, J.S. Shim, J.H. Lee, K. Kim, I.C. Kwon, D.D. Kim, Biomaterials 32 (2011) 7181.
[20] H.J. Cho, I.S. Yoon, H.Y. Yoon, H. Koo, Y.J. Jin, S.H. Ko, J.S. Shim, K. Kim, I.C. Kwon, D.D. Kim, Biomaterials 33 (2012) 1190.
[21] A.K.M.D. Chavanpatil, J. Panyam, J. Nanosci. Nanotechnol. 6 (2006) 2651.
[22] M.P. Desai, V. Labhasetwar, G.L. Amidon, R.J. Levy, Pharm. Res. 13 (1996) 1838.
[23] Y.H. Kim, S.H. Gihm, C.R. Park, K.Y. Lee, T.W. Kim, I.C. Kwon, H. Chung, S.Y. Jeong, Bioconjug. Chem. 12 (2001) 932.
[24] H.Y. Nam, S.M. Kwon, H. Chung, S.Y. Lee, S.H. Kwon, H. Jeon, Y. Kim, J.H. Park, J. Kim, S. Her, Y.K. Oh, I.C. Kwon, K. Kim, S.Y. Jeong, J. Control. Release 135 (2009) 259.
[25] Z.G. Yue, W. Wei, P.P. Lv, H. Yue, L.Y. Wang, Z.G. Su, G.H. Ma, Biomacromolecules 12 (2011) 2440.
[26] P. Caraban, Chem. Soc. Rev. 35 (2006) 512.

International Journal of Pharmaceutics 464 (2014) 127–134

Contents lists available at ScienceDirect

International Journal of Pharmaceutics

journal homepage: www.elsevier.com/locate/ijpharm

Pharmaceutical Nanotechnology

Polyethylene glycol-modified arachidyl chitosan-based nanoparticles for prolonged blood circulation of doxorubicin

Ubonvan Termsarasab[a], In-Soo Yoon[b], Ju-Hwan Park[a], Hyun Tae Moon[a], Hyun-Jong Cho[c,*], Dae-Duk Kim[a,**]

[a] College of Pharmacy and Research Institute of Pharmaceutical Sciences, Seoul National University, Seoul 151-742, Republic of Korea
[b] College of Pharmacy and Natural Medicine Research Institute, Mokpo National University, Jeonnam 534-729, Republic of Korea
[c] College of Pharmacy, Kangwon National University, Chuncheon 200-701, Republic of Korea

ARTICLE INFO

Article history:
Received 7 October 2013
Received in revised form
24 December 2013
Accepted 12 January 2014
Available online 19 January 2014

Keywords:
Arachidyl chitosan
Polyethylene glycol
Doxorubicin
Leukemia
Prolonged blood circulation

ABSTRACT

Doxorubicin (DOX)-loaded nanoparticles based on polyethylene glycol-conjugated chitosan oligosaccharide-arachidic acid (CSOAA-PEG) were explored for potential application to leukemia therapy. PEG was conjugated with CSOAA backbone *via* amide bond formation and the final product was verified by ^{1}H NMR analysis. Using the synthesized CSOAA-PEG, nanoparticles having characteristics of a 166-nm mean diameter, positive zeta potential, and spherical shape were produced for the delivery of DOX. The mean diameter of CSOAA-PEG nanoparticles in the serum solution (50% fetal bovine serum) remained relatively constant over 72 h as compared with CSOAA nanoparticles (changes of 20.92% and 223.16%, respectively). The sustained release pattern of DOX from CSOAA-PEG nanoparticles was displayed at physiological pH, and the release rate increased under the acidic pH conditions. The cytotoxicity of the CSOAA-PEG conjugate was negligible in human leukemia cells (K562) at the concentrations tested (~100 μg/ml). The uptake rate of DOX from the nanoparticles by K562 cells was higher than that from the solution. Judging from the results of pharmacokinetic studies in rats, *in vivo* clearance rate of DOX from the CSOAA-PEG nanoparticle group was slower than other groups, subsequently extending the circulation period. The PEGylated CSOAA-based nanoparticles could represent an effective nano-sized delivery system for DOX which has been used for the treatment of blood malignancies.

1. Introduction

Nano-sized carriers have been developed for anti-cancer drug delivery to tumor regions to overcome the intrinsic drawbacks of using the pure drug, which include a short half-life and undesired distribution to normal tissues and organs (Bae et al., 2007; Cho et al., 2011; ElBayoumi and Torchilin, 2009; Jin et al., 2012; Mu et al., 2010; Xiao et al., 2012; Yang et al., 2007). Several approaches for modifying the surfaces of nanovehicles to modulate the pharmacokinetic and pharmacodynamic properties of drugs have been investigated. Shielding groups, adsorbed or conjugated to the surface of nanoparticles, can disturb the electrostatic and hydrophobic interactions between opsonins and nanoparticles (Owens and Peppas, 2006). Among them, PEG has been grafted or adsorbed onto the drug itself or polymers (Cho et al., 2012b; Kaminskas et al., 2013; Veronese et al., 2005). It is known that an outer PEG shell can prevent the opsonization of nanoparticles in the blood and maintain their camouflage for phagocytosis (Owens and Peppas, 2006). Thus, this "stealth effect" can enhance systemic drug exposure and prolong circulation of nanocarriers in the blood stream. It has also been reported that the density of the PEG chain on the surface of nanoparticles may affect their interaction with blood components and macrophages (Owens and Peppas, 2006). Studies of the influence of PEG conjugation to various polymeric nanoparticles, for anti-cancer drug delivery, on the blood circulation time and anti-tumor efficacy have been reported (Cho et al., 2012b; Lv et al., 2012; Qu et al., 2009; Yadav et al., 2011). Moreover, a PEG shell on nanoparticles containing anti-cancer agents reduced their hematological toxicity after intravenous administration (Jain et al., 2012); thus, it can be used to mask the toxicity of polymeric matrix in the blood stream.

Natural polymers and their derivatives have been widely used for the development of self-assembled nanoparticles for cancer therapy and diagnosis (Cho et al., 2012a; Chung et al., 2013; Lee et al., 2011; Nogueira et al., 2013). In our previous reports (Termsarasab et al., 2013a,b), chitosan oligosaccharide-arachidic acid (CSOAA), as an amphiphilic chitosan oligosaccharide derivative, was synthesized, and self-assembled nanoparticles based on

* Corresponding author. Tel.: +82 33 250 6916; fax: +82 33 259 5631.
** Corresponding author. Tel.: +82 2 880 7870; fax: +82 2 873 9177.
E-mail addresses: hjcho@kangwon.ac.kr (H.-J. Cho), ddkim@snu.ac.kr (D.-D. Kim).

0378-5173/$ – see front matter © 2014 Elsevier B.V. All rights reserved.
http://dx.doi.org/10.1016/j.ijpharm.2014.01.015

CSOAA were prepared. CSOAA-based nanoparticles were developed for delivery of anti-cancer drugs to the tumor region and cancer diagnosis. Although anti-tumor efficacy after intravenous injection based on passive targeting strategy, mainly due to the enhanced permeability and retention (EPR) effect, has been achieved in a head and neck cancer xenograft mouse model, the nanoparticles developed may exhibit greater *in vivo* anti-tumor efficacy as a result of the surface modification. Here, PEGylated CSOAA-based nanoparticles were prepared in an effort to prolong their circulation in the blood stream after intravenous administration. CSOAA-PEG conjugate was synthesized, and the physicochemical properties of CSOAA-PEG nanoparticles were investigated. Their application for leukemia therapy was tried and the alterations in the pharmacokinetic properties of the drug were assessed in an animal model.

2. Materials and methods

2.1. Materials

Chitosan oligosaccharide (CSO; average molecular weight = 5 kDa, deacetylation degree > 90%) was obtained from Kitto Life Co., Ltd. (Seoul, Korea). Arachidic acid (AA), 1-ethyl-3-(3-dimethylaminopropyl) carbodiimide (EDC), N-hydroxysuccinimide (NHS), deuterochloroform ($CDCl_3$) and deuterium oxide (D_2O) were purchased from Sigma–Aldrich Co. (St. Louis, MO, USA). Methoxypolyethylene glycol succinimidyl succinate (mPEG-SS; molecular weight = 2 kDa) was provided by Sunbio Co. (Anyang, Korea). Doxorubicin hydrochloride (DOX HCl) was purchased from Boryung Pharmaceutical Co., Ltd. (Seoul, Korea). RPMI 1640 medium, penicillin, streptomycin, and heat-inactivated fetal bovine serum (FBS) were purchased from Gibco Life Technologies Inc. (Grand Island, NY, USA). All other reagents were of analytical grade and were obtained from commercial sources.

2.2. Synthesis and characterization of CSOAA-PEG

CSOAA was synthesized as described in our previous report, with slight modifications (Termsarasab et al., 2013a). Briefly, CSO (0.2 mmol) and AA (1 mmol) were solubilized in 25 ml dimethyl sulfoxide (DMSO) separately at 50 °C for 15 min and cooled to room temperature. EDC (1.5 mmol) and NHS (1.5 mmol) were added to the AA solution and stirred for 30 min. Then, the AA solution was added to the CSO solution; the reaction was conducted for 12 h with stirring. That solution was then adjusted to pH 3.5 with 1 N HCl, prior to precipitating with 450 ml acetone three times to remove unreacted AA. The precipitate was collected by centrifugation (8608 × *g*, 30 min), and resuspended in 50-ml double-distilled water (DDW). This solution was dialyzed (dialysis membrane molecular weight cut-off = 1 kDa; Spectrum Laboratories, Laguna Hills, CA, USA) against DDW for 2 days. CSOAA was obtained after freeze-drying.

To synthesize CSOAA-PEG, CSOAA (0.125 mmol) was solubilized in 30-ml DMSO, followed by addition of mPEG-SS (0.25 mmol). After stirring for 12 h, the solution was dialyzed (dialysis membrane molecular weight cut-off = 3.5 kDa) against DDW for 1 day and then freeze-dried. The freeze-dried product was precipitated by adding excess acetone to remove unreacted mPEG-SS. The precipitate was collected by filtering and dried at 60 °C. The conjugations of CSOAA and CSOAA-PEG were confirmed by ^{1}H NMR analysis (Varian FT 500-MHz, Varian Inc., Palo Alto, CA, USA). To prepare the ^{1}H NMR samples (15 mg/ml concentration), CSOAA and CSOAA-PEG were dissolved in D_2O and mPEG-SS was solubilized in $CDCl_3$, respectively. Standard samples were prepared by mixing mPEG-SS and CSOAA at various molar ratios (0.5:1, 1:1, 1:2, 1:3, and 1:4) and freeze-drying for the determination of molar substitution (MS) of CSOAA-PEG. The MS of CSOAA-PEG was calculated based on the ratio of the integration values of the CSOAA and mPEG-SS ^{1}H NMR spectra. Those substances were dissolved in DMSO-d_6.

2.3. Preparation and characterization of DOX-loaded nanoparticles

DOX-loaded CSOAA and CSOAA-PEG nanoparticles were prepared by a solvent evaporation method as reported previously (Termsarasab et al., 2013a). DOX base was prepared by the reaction between DOX HCl and triethylamine in DMSO for 12 h and lyophilization. CSOAA or CSOAA-PEG and DOX base (7.5:1.5, w/w) were dissolved in DMSO and DDW mixture (1:1, v/v). The solvent was removed under a nitrogen gas stream at 70 °C for 4 h. The drug and polymer film coated-tube was hydrated with DDW, followed by sonication using a probe sonicator (Vibra-Cell, Sonics & Materials Inc., CT, USA) for 5 min. The nanoparticle suspension was then filtered through a syringe filter with 0.45-μm pore size (Minisart RC 15; Satorius Stedim Biotech GmbH, Gottingen, Germany) to remove unloaded DOX.

The average mean diameter, polydispersity index, and zeta potential values of DOX-loaded CSOAA and CSOAA-PEG nanoparticles in DDW were measured using a dynamic light scattering (DLS) spectrophotometer (ELS-Z; Otsuka Electronics Co. Ltd., Osaka, Japan). Change of particle size (nm) in DDW and 50% (v/v) FBS was also measured according to the incubation time (0.5, 1, 1.5, 2, 4, 6, 24, 48, and 72 h). The morphology of nanoparticles was observed by transmission electron microscopy (TEM; LIBRA 120; Carl Zeiss, Oberkochen, Germany). Samples were stained with 2% (w/v) phosphotungstic acid, loaded on a copper grid coated with carbon film, and dried at 20 °C. To determine the encapsulation efficiency (EE) of the drug, aliquots of samples (0.1 ml of each nanoparticle suspension) were diluted with a 100× volume of DMSO to disrupt the nanoparticles. DOX content was analyzed by a high-performance liquid chromatography (HPLC) method using a Waters HPLC system (Waters Co., Milford, MA, USA) equipped with a reversed-phase (RP) C-18 column (Xbridge, RP-18, 250 mm × 4.6 mm, 5 μm; Waters Co.), a separation module (Waters e2695), and a fluorescence detector (Waters 2475). The mobile phase consisted of 10 mM K_2HPO_4 (pH 2.5) and 0.01% (v/v) triethylamine in acetonitrile (71:29, v/v) with a flow rate of 1 ml/min. The excitation and emission wavelengths were 470 and 565 nm, respectively. The injection volume was 20 μl. The inter-day and intra-day variances were within the acceptable range. The EE value of DOX in nanoparticles was determined by the following equation:

$$\text{EE}\ (\%) = \frac{\text{actual amount of drug in nanoparticles}}{\text{theoretical amount of drug in nanoparticles}} \times 100 \quad (1)$$

2.4. In vitro DOX release test

DOX-loaded CSOAA or CSOAA-PEG nanoparticles (150 μl) were loaded in a mini GeBA-flex tube (molecular weight cut-off: 12–14 kDa, Gene Bio-Application Ltd., Kfar Hanagide, Israel) and placed in 15 ml of phosphate-buffered saline (PBS: pH 5.5, 6.8, and 7.4, adjusted with phosphoric acid). The drug release test was conducted in a shaking bath at 37 °C and 50 rpm rotation speed. Aliquots of release medium (200 μl) were collected at set times (1, 2, 3, 4, 6, 9, 12, 24, 48, 72, 96, and 120 h), and an equivalent volume of fresh medium was replaced. The amount (%) of DOX released was determined by the HPLC method described above.

2.5. In vitro cytotoxicity of CSOAA and CSOAA-PEG

Human leukemia K562 cells were purchased from the Korean Cell Line Bank (Seoul, Korea). The cells were cultured in RPMI 1640 medium containing 10% FBS, 100 U/ml penicillin, and 100 μg/ml streptomycin at 37 °C in a 5% CO_2 atmosphere and 95% relative humidity. The cytotoxicities of CSOAA and CSOAA-PEG to K562 cells were determined using a 3-(4,5-dimethylthiazol-2-yl)-5(3-carboxymethonyphenol)-2-(4-sulfophenyl)-2H-tetrazolium (MTS)-based assay. Various concentrations (~100 μg/ml) of CSOAA and CSOAA-PEG were added to 1×10^4 cells suspended in 100-μl culture media and incubated for 24, 48, and 72 h. Then, the cells were treated with the MTS-based CellTiter 96 AQ_{ueous} One Solution Cell Proliferation Assay Reagent (Promega Corp., Madison, WI, USA) at 37 °C for 4 h, according to the manufacturer's protocol. The absorbance at 490 nm was measured using a microplate reader (EMax, Molecular Devices, Sunnyvale, CA).

2.6. In vitro cellular uptake study

K562 cells at a density of 6×10^5 per well were treated with free DOX, DOX-loaded CSOAA nanoparticles, or CSOAA-PEG nanoparticles at an equivalent DOX concentration (15 μg/ml). After the cells were incubated for 1 h, they were washed with PBS (pH 7.4) and resuspended in medium with 2% (v/v) FBS. DOX uptake efficiency was evaluated by flow cytometry using a FACSCalibur equipped with the CELLQuest software (Becton Dickinson Biosciences, San Jose, CA, USA).

2.7. In vivo pharmacokinetics in rats

Animal study protocol was approved by the Institutional Animal Care and Use Committee of Seoul National University (Seoul, Korea). Male Sprague-Dawley (SD) rats, weighing 250–300 g (Orient Bio, Inc., Seongnam, Korea), were used. The rats were housed under standard room (Animal Center for Pharmaceutical Research, College of Pharmacy, Seoul National University) at a temperature of 20–23 °C and a relative humidity of 50 ± 5%. A polyethylene tube (PE-50; Clay Adams, Parsippany, NJ, USA) was cannulated into the femoral veins and arteries of rats under ketamine anesthesia (50 mg/kg, intramuscular injection). Each group was administered at a single dose of 4 mg/kg DOX intravenously *via* the femoral vein. Blood samples (300 μl) were then collected *via* the femoral artery at 0, 2, 5, 15, 30, 60, 90, 120, 180, 240, 360, and 480 min and centrifuged (16,000 × *g*, 5 min). Aliquots (150 μl) of plasma were stored at −20 °C until the quantitative analysis of DOX. The DOX concentration in plasma was analyzed by a reported HPLC method (Cho et al., 2012b) with slight modifications. An aliquot of plasma sample (150 μl) with propranolol solution (internal standard, 50 μl, 1 μg/ml) was mixed with acetonitrile (400 μl). After vortexing and centrifuging (16,000 × *g*, 10 min), supernatant (300 μl) was transferred to a clean tube and evaporated under a gentle stream of nitrogen at 40 °C. The residue was reconstituted with 60-μl mobile phase (a mixture of 10 mM K_2HPO_4 (pH 2.5) and 0.01% (v/v) triethylamine in acetonitrile, 73:27, v/v). After vortexing and centrifuging, a 10-μl aliquot was subjected to HPLC analysis. The samples were injected into the RP-HPLC column as described above. The fluorescence intensity was monitored at excitation/emission wavelengths of 470/565 nm for DOX, and 230/540 nm for propranolol. The lower limit of quantification (LLOQ) value of DOX in rat plasma was 0.01 μg/ml. The intra-day and inter-day coefficients of variation were within the acceptable range. The total area under the plasma concentration–time curve from time zero to infinity (AUC), terminal half-life ($t_{1/2}$), time-averaged total body clearance (CL), apparent volume of distribution at steady state (V_{ss}), and mean residence time (MRT) were calculated using the WinNonlin software (Pharsight, Mountain View, CA, USA).

2.8. Statistical analysis

Statistical analysis was conducted using *t*-test and analysis of variance (ANOVA). All experiments were performed at least three times. The data are shown as means ± standard deviation (SD).

3. Results and discussion

3.1. Synthesis of CSOAA-PEG

PEGylated CSOAA was synthesized to develop nanoparticles for DOX delivery. The synthetic method for CSOAA was reported in our previous study (Termsarasab et al., 2013a). Briefly, CSOAA was synthesized by a coupling reaction between the amine groups of CSO and carboxyl groups of AA using EDC and NHS as coupling reagents. EDC was introduced into the carboxyl groups of AA, and an AA-NHS intermediate was formed by adding NHS to EDC active ester. This intermediate was reacted with the amine group of CSO to generate CSOAA. Then, mPEG-SS was introduced to the remaining amine groups of CSOAA. To characterize the structure of CSOAA and CSOAA-PEG, ^{1}H NMR analyses of mPEG-SS, CSOAA, and CSOAA-PEG were performed; their spectra are shown in Fig. 1. The proton peaks of the alkyl chain and methyl group of AA appeared at 1.2 and 0.8 ppm, respectively. The specific proton peaks for the oxyethylene group (—CH_2CH_2O—) and methoxy group (CH_3O—) of mPEG appeared at 3.5–3.7 ppm and 3.3 ppm, respectively. The proton peaks between 2.5 and 3.0 ppm were corresponded to the succinimidyl succinate group of mPEG-SS. Compared with CSOAA and mPEG-SS, the ^{1}H NMR spectrum of CSOAA-PEG exhibited the specific proton peaks of CSOAA and mPEG, while the proton peak of the succinimidyl succinate group shifted to 2.2 ppm. These results confirmed PEG conjugation to CSOAA. A homogeneous physical mixture of CSOAA and PEG was prepared and each component was analyzed by ^{1}H NMR to calculate the molar substitution (MS) of PEG to CSOAA, according to a modified method reported previously (Termsarasab et al., 2013a). The molar substitution of PEG to CSOAA was calculated using the linear regression line, which was plotted between the integration ratio of the methoxy group of PEG (δ = 3.3; CH_3O—) to the N-acetyl proton group of CSO (δ = 1.8; CH_3CONH—), and the molar ratio of mPEG-SS to CSOAA prepared from standard samples (data not shown). The molar substitution (mole of mPEG-SS/mole of CSOAA) of PEG to CSOAA was 1.8 in this investigation.

3.2. Preparation and characterization of DOX-loaded nanoparticles

Based on the CSOAA-PEG synthesized, nanoparticles loaded with DOX were prepared using a solvent evaporation method (Termsarasab et al., 2013a). In this study, CSOAA/DOX and CSOAA-PEG/DOX, at a weight ratio of 7.5–1.5 (polymer to drug), nanoparticles were prepared. The mean diameters of the CSOAA/DOX and CSOAA-PEG/DOX nanoparticles were 124.17 ± 2.58 and 165.75 ± 6.75 nm, respectively (Table 1). As shown in Fig. 2, TEM image of the CSOAA-PEG/DOX nanoparticles showed a spherical shape and similar particle size to that measured by ELS. The hydrophilic PEG, conjugated to CSOAA, constituted the outer shell of the nanoparticles (Fig. 2). Because of this PEG shell, the mean diameter of drug-loaded CSOAA/PEG nanoparticles was increased *versus* drug-loaded CSOAA nanoparticles. This phenomenon was also reported by us previously (Cho et al., 2012b) for amphiphilic hyaluronic acid oligomer-based nanoparticles. Despite the outer hydrophilic PEG shell on the CSOAA-based nanoparticles, the mean

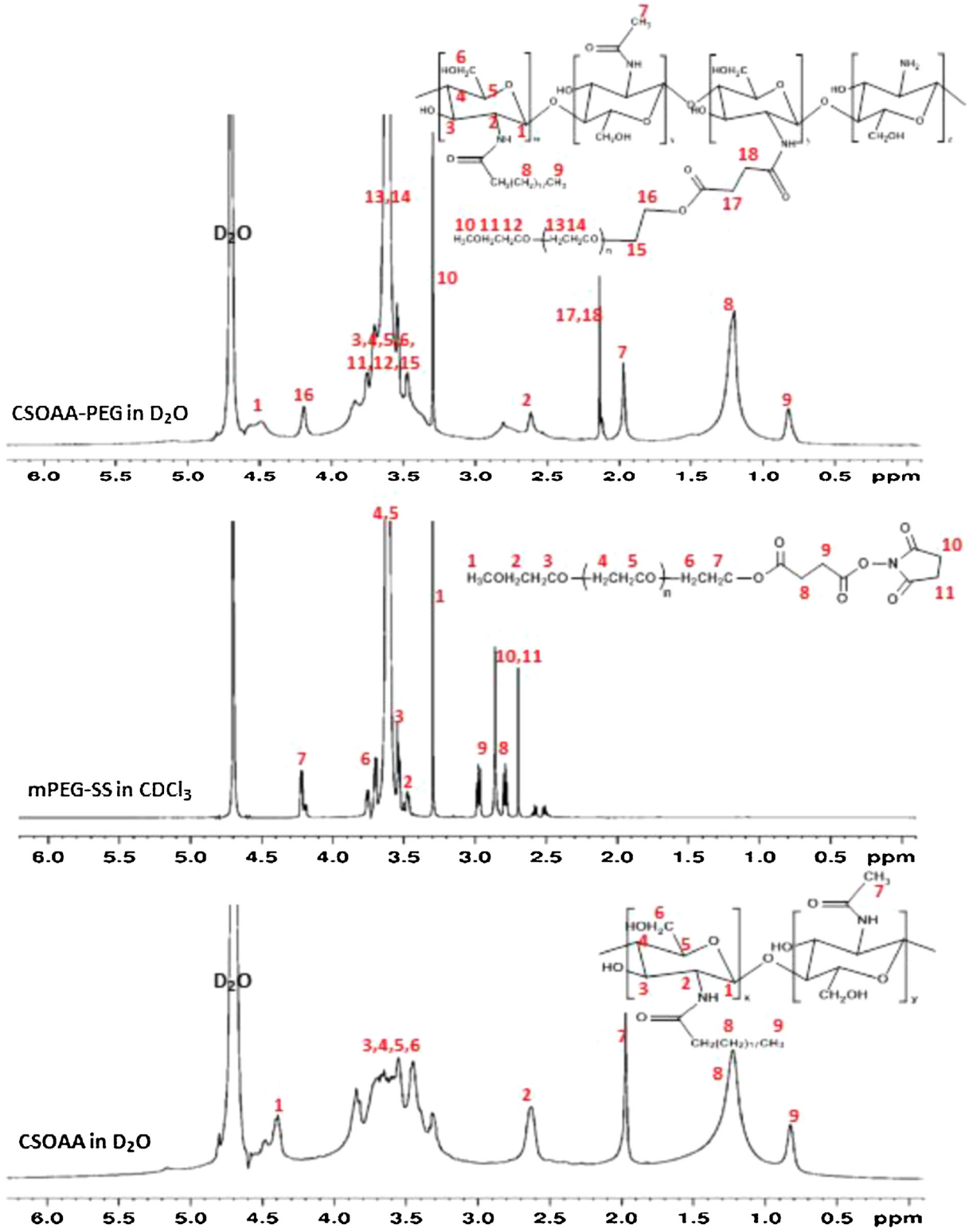

Fig. 1. ^{1}H NMR spectra of CSOAA, mPEG-SS, and CSOAA-PEG. CSOAA and CSOAA-PEG were solubilized in D_2O, and mPEG-SS was dissolved in $CDCl_3$.

Table 1
Characteristics of DOX-loaded CSOAA and CSOAA-PEG nanoparticles ($n \geq 3$).

Formulations (w/w)	Mean diameter (nm)	Polydispersity index	Zeta potential (mV)	Encapsulation efficiency (%)
CSOAA/DOX (7.5/1.5)	124.17 ± 2.58	0.20 ± 0.04	27.28 ± 1.50	60.03 ± 2.14
CSOAA-PEG/DOX (7.5/1.5)	165.75 ± 6.75	0.19 ± 0.03	21.47 ± 2.05	63.80 ± 3.19

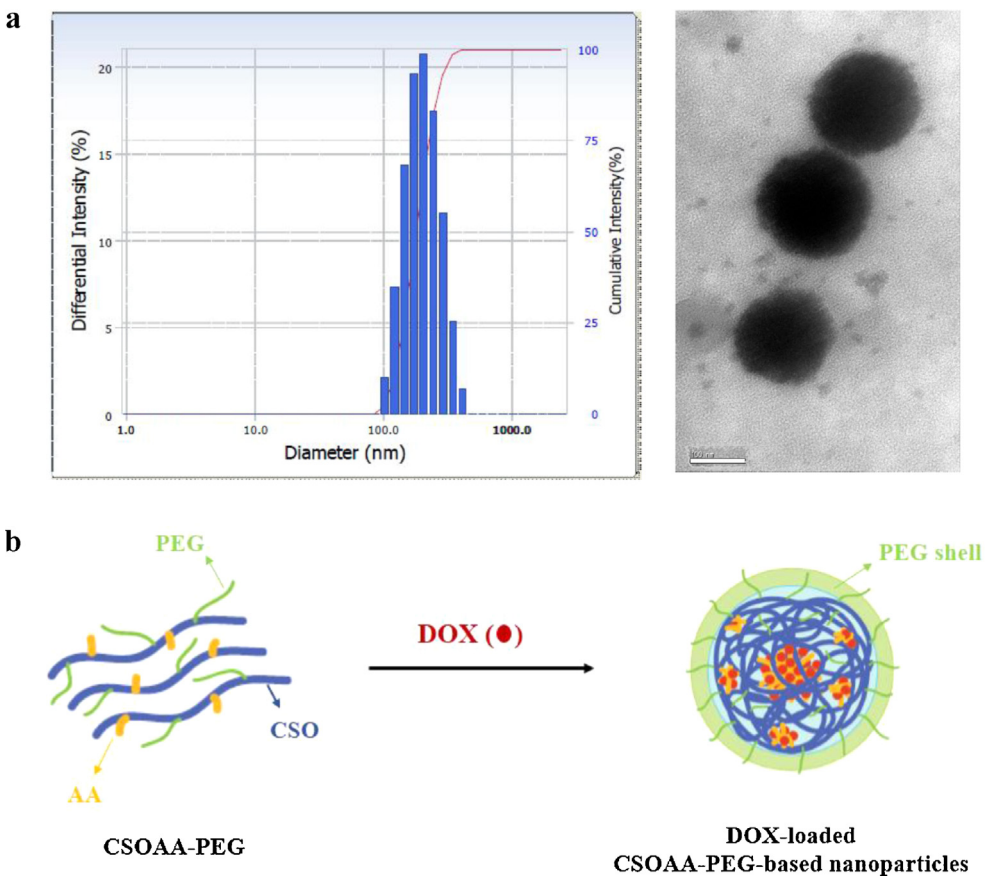

Fig. 2. Characterization and illustration of CSOAA-PEG/DOX nanoparticles. (a) Size distribution (left panel) and TEM image (right panel) of CSOAA-PEG/DOX nanoparticles are shown. Differential intensity (%) of the diameter of CSOAA-PEG/DOX nanoparticles is presented. The bar in the TEM image represents 100 nm. (b) Schematic illustration of DOX-loaded CSOAA-PEG nanoparticles is shown.

diameter was less than 200 nm, indicating a low probability of reticuloendothelial system (RES) clearance (Gaucher et al., 2005). The polydispersity index of PEGylated CSOAA-based nanoparticles containing DOX was 0.19 ± 0.03, indicating a narrow size distribution (Fig. 2). The zeta potential value of the CSOAA-PEG/DOX nanoparticles was lower than that of the CSOAA/DOX nanoparticles ($p < 0.05$), possibly due to the presence of the outer PEG shell.

The mean diameters of drug-loaded CSOAA and CSOAA-PEG nanoparticles were measured in DDW and those values of both nanoparticle groups were constantly maintained for 72 h (Fig. 3a). However, they are not enough to reflect the actual particle size in the blood stream. Additionally, *in vivo* pharmacokinetic and pharmacodynamic performances cannot be predicted precisely from particle size measurements in DDW. Nanoparticles administered by the intravenous route can interact with blood components and form large aggregates or complexes (Liu et al., 2012; Rausch et al., 2010). These unwanted aggregates can inhibit normal blood circulation and are readily eliminated by RES organs (liver and spleen). Thus, changes in particle size in the presence of serum (50%, v/v) were monitored according to the incubation time. As shown in Fig. 3b, the mean diameter of CSOAA-PEG/DOX nanoparticles increased by 20.92% over 72 h, while CSOAA/DOX nanoparticles showed a 223.16% increase in mean diameter during the same period. The hydrophilic PEG shell of CSOAA-PEG/DOX nanoparticles hampered the interaction between blood constituents and the chitosan-based surface, and thus reduced the aggregation of nanoparticles in the presence of serum. Maintaining the initial mean diameter of PEGylated nanoparticles under serum conditions can lead to the improved stability by "stealth effect" (Qu et al., 2009; Zhang et al., 2013), and thereby prolonging circulation of the nanoparticles in the blood stream.

3.3. *In vitro drug release*

DOX release *in vitro* from the nanoparticle formulations was monitored at pH 5.5, 6.8, and 7.4 (Fig. 4). DOX release profiles from CSOAA-based nanoparticles under several pH conditions have been reported previously (Termsarasab et al., 2013a). Despite different weight ratios between CSOAA and DOX compared with the current study, DOX release was improved in acidic pH condition. In this investigation, the proportions (%) of DOX released from CSOAA and CSOAA-PEG nanoparticles after 24 h were 56.69 ± 4.04% and 31.19 ± 0.95%, respectively. After a steady increase in DOX release from the CSOAA-PEG nanoparticles, the two values reached 56.02 ± 2.07% and 50.77 ± 5.88%, respectively, at day 5. Although the proportions of DOX released from both nanoparticle formulations were similar at steady state (around day 5), a sustained pattern of DOX release from the CSOAA-PEG nanoparticles was observed. Thus the PEG shell may delay drug diffusion and dissolution from the reservoir. Sustained drug release from PEGylated nanoparticle formulations has been reported previously (Cho et al., 2012b; Jain et al., 2012). Additionally, pH-dependent DOX release from CSOAA-PEG nanoparticles was observed. The proportions of DOX released from CSOAA-PEG nanoparticles at pH 7.4 and 5.5 on day 5 were 50.77 ± 5.88% and 83.57 ± 0.24%, respectively. This can be explained by the higher solubility of DOX under acidic pH conditions and changes in the binding strength between the drug and nanoparticle structure (Jin et al., 2012; Nukolova et al., 2011; Termsarasab et al., 2013a). Enhanced DOX release at pH 5.5 and 6.8,

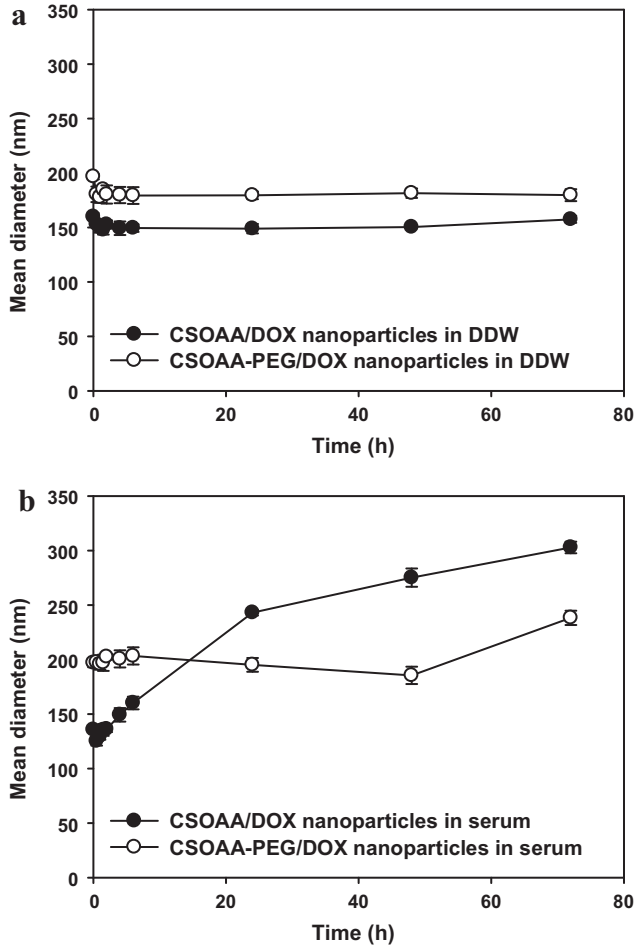

Fig. 3. The change in mean diameter (nm) of the nanoparticles in (a) DDW and (b) 50% (v/v) serum according to incubation time. CSOAA/DOX and CSOAA-PEG/DOX nanoparticles were incubated at 37 °C for various periods. Each point represents the mean ± SD ($n = 3$).

which reflects the conditions in endocytic compartments (endosomes and lysosomes, pH 5.5) and the tumor microenvironment (pH 6.8), may facilitate DOX uptake into cancer cells and so enhance its anti-tumor effect.

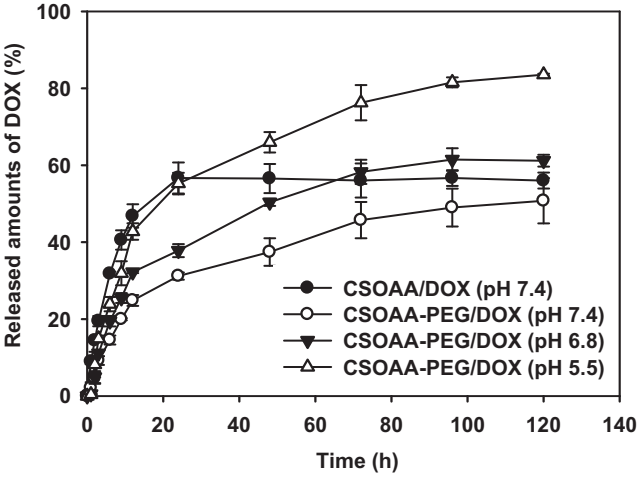

Fig. 4. *In vitro* DOX release profiles of CSOAA and CSOAA-PEG-based nanoparticles. Drug release profiles of DOX-loaded CSOAA nanoparticles (pH 7.4) and CSOAA-PEG nanoparticles at pH 5.5, 6.8, and 7.4 are shown. Each point represents the mean ± SD ($n = 3$).

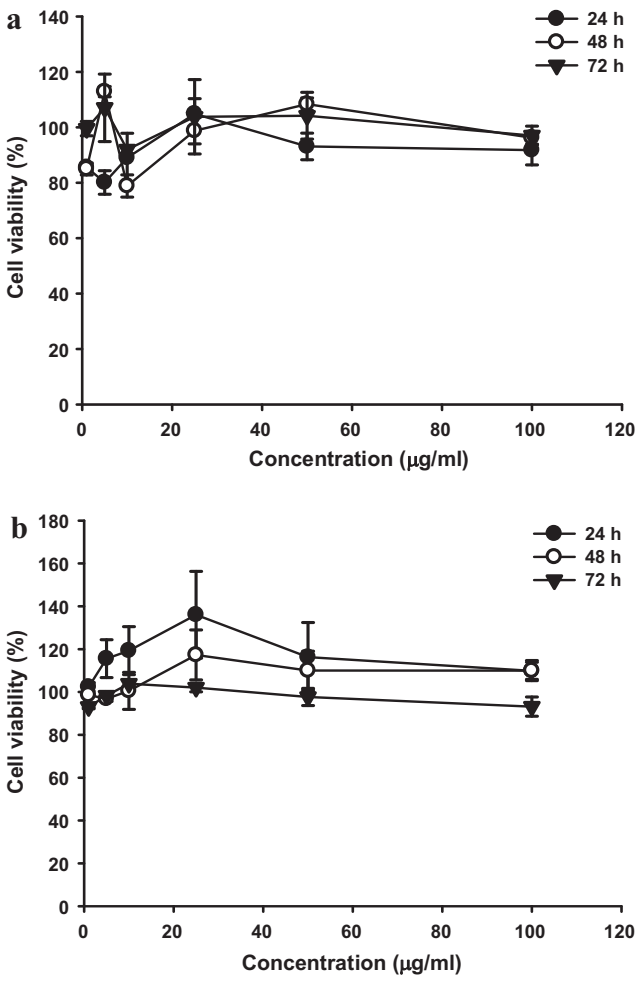

Fig. 5. *In vitro* cytotoxicity test of CSOAA (a) and CSOAA-PEG (b) in K562 cells. Each conjugate at various concentrations was incubated for 24, 48, and 72 h in the presence of K562 cells. Each point represents the mean ± SD ($n = 4$).

3.4. In vitro cytotoxicity

The cytotoxicity of CSOAA and CSOAA-PEG was assessed against K562 cells, human erythromyeloblastoid leukemia cells (Laroche-Clary et al., 2000), using an MTS-based assay. Cell viability (%) is presented after 24, 48, and 72 h of incubation with various concentrations of both conjugates (Fig. 5). One of the indications for DOX is leukemia; thus, K562 cells were used for determination of the cytotoxicity of the conjugates synthesized. Neither CSOAA nor CSOAA-PEG induced serious toxic effects in K562 cells at the concentrations tested after incubation for 24–72 h. In our previous study (Termsarasab et al., 2013a), CSOAA also showed no significant cytotoxicity in head and neck cancer cell line (FaDu cell). Our results here suggest that CSOAA-PEG can be used safely for the preparation of drug delivery vehicle.

3.5. In vitro cellular uptake

The cellular uptake efficiency of DOX from the nanoparticles developed was assessed using flow cytometry. In this investigation, the K562 cell was selected as a model cell line of human leukemia. DOX has been used in leukemia therapy in the clinic; thus, its uptake into K562 cells could be related to its anti-tumor efficacy. As shown in Fig. 6, DOX uptake was higher in the nanoparticle-treated groups than the DOX solution-treated group. This might be due to the electrostatic interaction between the positive charge of the

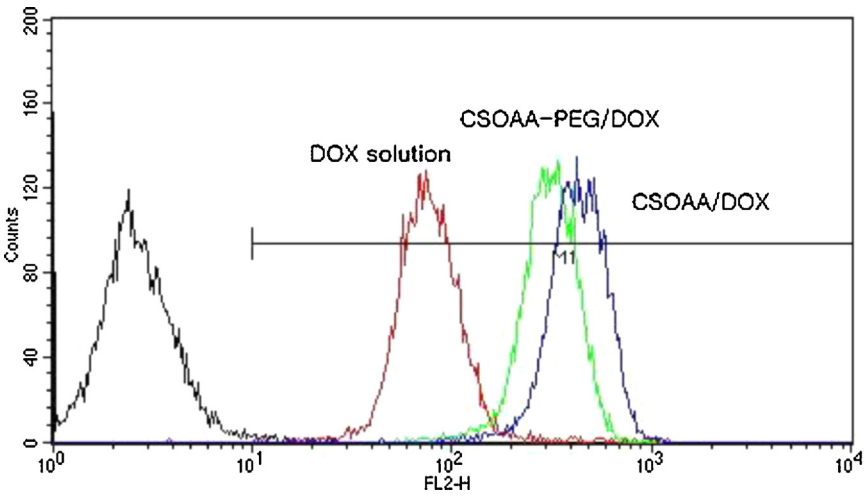

Fig. 6. Flow cytometry analysis of DOX uptake by K562 cells. DOX solution (red), DOX-loaded CSOAA nanoparticles (blue), and DOX-loaded CSOAA-PEG nanoparticles (green) were incubated for 1 h. (For interpretation of the references to color in this figure legend, the reader is referred to the web version of the article.)

chitosan molecules and the negative charge of the cell membrane (Chavanpatil et al., 2006; Termsarasab et al., 2013a; Zauner et al., 1998). As reported in other cell line (Termsarasab et al., 2013a), DOX uptake from CSOAA-based nanoparticle was enhanced compared with DOX solution in K562 cells. However, the cellular uptake of DOX from the PEGylated CSOAA-based nanoparticles was lower than from CSOAA-based nanoparticles. This may be explained by the outer PEG shell reducing the electrostatic force between chitosan and the cell membrane, blocking interactions between the fatty acids in the minor hydrophobic core of the nanoparticles and the cell membrane, thus delaying drug release. Notwithstanding the lower cellular uptake efficiency of PEGylated CSOAA nanoparticles, they may exert a stealth effect, due to the prolonged circulation time in the blood stream after intravenous injection.

3.6. *In vivo* pharmacokinetics in rats

DOX-loaded nanoparticles were administered intravenously at a dose of 4 mg/kg to rats to investigate their effects on the pharmacokinetic properties of DOX. The DOX concentration in plasma according to time is shown in Fig. 7, and the pharmacokinetic parameters are listed in Table 2. The pharmacokinetic parameters of a DOX solution (4 mg/kg dose)-treated group reported in our previous study (Cho et al., 2012b) were used as the control. CL values of CSOAA and CSOAA-PEG nanoparticle groups were decreased, to 11.17% and 2.09% of the value of DOX solution. AUC values of CSOAA and CSOAA-PEG nanoparticle groups exhibited 8.64- and 48.00-fold increases compared with that of the DOX solution group, respectively. Half-life ($t_{1/2}$) values in both groups were increased to 173.50% and 899.82%, respectively, compared with that of the DOX solution group. Additionally, MRT values showed 10.52- and 47.58-fold increases compared to the DOX solution group. These data

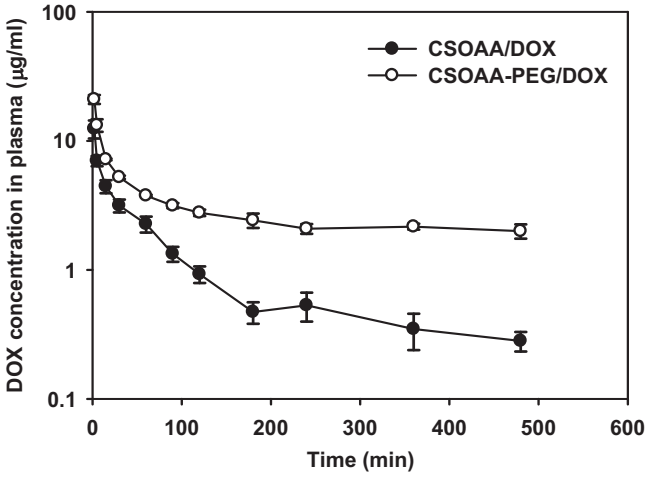

Fig. 7. *In vivo* pharmacokinetic profiles of DOX in rats. Nanoparticles were administered intravenously at a dose of 4 mg/kg (DOX). Each point represents the mean ± SD ($n \geq 3$).

indicated that the nanoparticles developed here exhibited lower *in vivo* clearance of DOX and prolonged circulation of nanoparticles in the blood stream. The PEGylated nanoparticles also showed decreased *in vivo* clearance, and increased AUC, half-life, and MRT values, compared with CSOAA-based nanoparticles ($p < 0.05$). It has been reported that nanoparticles modified with PEG exhibited enhanced systemic exposure of the drug after intravenous injection (Qu et al., 2009; Zhang et al., 2013). The decreased *in vivo* clearance of DOX in the PEGylated CSOAA nanoparticles seems to be based on their greater stability in the presence of serum

Table 2
Pharmacokinetic parameters of DOX in rats after intravenous administration at a dose of 4 mg/kg.

Parameter	DOX solution[a]	CSOAA/DOX	CSOAA-PEG/DOX
AUC (μg·min/ml)	65.18 ± 16.47[#]	563.24 ± 33.34[#]	3128.65 ± 621.52[#]
Terminal $t_{1/2}$ (min)	76.37 ± 8.83[#]	132.50 ± 32.80[#]	687.19 ± 221.97[#]
CL (ml/min/kg)	63.76 ± 14.18[#]	7.12 ± 0.41[#]	1.33 ± 0.31[#]
V_{ss} (ml/kg)	1189.49 ± 204.99	1195.81 ± 192.67	1117.43 ± 207.24
MRT (min)	18.82 ± 1.14[#]	197.94 ± 64.87[#]	895.41 ± 319.77[#]

Data present as mean ± SD ($n \geq 3$).
[a] Data were cited from our previous report (Cho et al., 2012b).
[#] $p < 0.05$, significantly different from the other groups.

(Fig. 3) and sustained drug release (Fig. 4). The stealth effect of the PEG shell likely contributes to the longer dosing interval and improved anti-tumor efficacy. In particular, prolonged circulation of the CSOAA-PEG nanoparticles developed may be appropriate for the therapy of hematological malignancies, such as leukemia and lymphoma.

4. Conclusions

PEGylated CSOAA-based nanoparticles containing DOX were developed to achieve a prolonged circulation time of the drug in the blood stream. Synthesis of the CSOAA-PEG conjugate was confirmed by ^{1}H NMR analysis. DOX-loaded CSOAA-PEG nanoparticles with a ~166-nm mean diameter and positive zeta potential were prepared and a sustained pattern of drug release from the CSOAA-PEG nanoparticles was observed. The cytotoxicity of CSOAA-PEG in K562 cells seemed negligible in the concentration range tested, and the cellular uptake efficiency of the drug from nanoparticles was improved compared with DOX in solution. Decreased *in vivo* clearance and a longer DOX half-life in the blood stream in the CSOAA-PEG nanoparticles group was demonstrated in a pharmacokinetic study. The CSOAA-PEG nanoparticle developed may be a useful candidate of anti-cancer drug delivery system, especially for the treatment of blood cancers.

Acknowledgements

This research was supported by the National Research Foundation of Korea (NRF) funded by the Korean Government (MSIP) (Nos. 2009-0083533 and NRF-2012R1A1A1038944).

References

Bae, Y., Diezi, T.A., Zhao, A., Kwon, G.S., 2007. Mixed polymeric micelles for combination cancer chemotherapy through the concurrent delivery of multiple chemotherapeutic agents. J. Control. Release 122, 324–330.

Chavanpatil, M.D., Khdair, A., Panyam, J., 2006. Nanoparticles for cellular drug delivery: mechanisms and factors influencing delivery. J. Nanosci. Nanotechnol. 6, 2651–2663.

Cho, H.J., Yoon, H.Y., Koo, H., Ko, S.H., Shim, J.S., Lee, J.H., Kim, K., Kwon, I.C., Kim, D.D., 2011. Self-assembled nanoparticles based on hyaluronic acid-ceramide (HA-CE) and Pluronic® for tumor-targeted delivery of docetaxel. Biomaterials 32, 7181–7190.

Cho, H.J., Yoon, H.Y., Koo, H., Ko, S.H., Shim, J.S., Cho, J.H., Park, J.H., Kim, K., Kwon, I.C., Kim, D.D., 2012a. Hyaluronic acid-ceramide-based optical/MR dual imaging nanoprobe for cancer diagnosis. J. Control. Release 162, 111–118.

Cho, H.J., Yoon, I.S., Yoon, H.Y., Koo, H., Jin, Y.J., Ko, S.H., Shim, J.S., Kim, K., Kwon, I.C., Kim, D.D., 2012b. Polyethylene glycol-conjugated hyaluronic acid-ceramide self-assembled nanoparticles for targeted delivery of doxorubicin. Biomaterials 33, 1190–1200.

Chung, C.W., Chung, K.D., Jeong, Y.I., Kang, D.H., 2013. 5-Aminolevulinic acid-incorporated nanoparticles of methoxy poly(ethylene glycol)–chitosan copolymer for photodynamic therapy. Int. J. Nanomedicine 8, 809–819.

ElBayoumi, T.A., Torchilin, V.P., 2009. Tumor-targeted nanomedicines: enhanced antitumor efficacy in vivo of doxorubicin-loaded, long-circulating liposomes modified with cancer-specific monoclonal antibody. Clin. Cancer Res. 15, 1973–1980.

Gaucher, G., Dufresne, M.H., Sant, V.P., Kang, N., Maysinger, D., Leroux, J.C., 2005. Block copolymer micelles: preparation, characterization and application in drug delivery. J. Control. Release 109, 169–188.

Jain, V., Swarnakar, N.K., Mishra, P.R., Verma, A., Kaul, A., Mishra, A.K., Jain, N.K., 2012. Paclitaxel loaded PEGylated gleceryl monooleate based nanoparticulate carriers in chemotherapy. Biomaterials 33, 7206–7220.

Jin, Y.J., Termsarasab, U., Ko, S.H., Shim, J.S., Chong, S., Chung, S.J., Shim, C.K., Cho, H.J., Kim, D.D., 2012. Hyaluronic acid derivative-based self-assembled nanoparticles for the treatment of melanoma. Pharm. Res. 29, 3443–3454.

Kaminskas, L.M., Ascher, D.B., McLeod, V.M., Herold, M.J., Le, C.P., Sloan, E.K., Porter, C.J., 2013. PEGylation of interferon α2 improves lymphatic exposure after subcutaneous and intravenous administration and improves antitumour efficacy against lymphatic breast cancer metastases. J. Control. Release 168, 200–208.

Laroche-Clary, A., Larrue, A., Robert, J., 2000. Down-regulation of bcr-alb and bcl-x_L expression in a leukemia cell line and its doxorubicin-resistant variant by topoisomerase II inhibitors. Biochem. Pharmacol. 60, 1823–1828.

Lee, S.J., Koo, H., Jeong, H., Huh, M.S., Choi, Y., Jeong, S.Y., Byun, Y., Choi, K., Kim, K., Kwon, I.C., 2011. Comparative study of photosensitizer loaded and conjugated glycol chitosan nanoparticles for cancer therapy. J. Control. Release 152, 21–29.

Liu, Z., Jiao, Y., Wang, T., Zhang, Y., Xue, W., 2012. Interactions between solubilized polymer molecules and blood components. J. Control. Release 160, 14–24.

Lv, P.P., Ma, Y.F., Yu, R., Yue, H., Ni, D.Z., Wei, W., Ma, G.H., 2012. Targeted delivery of insoluble cargo (paclitaxel) by PEGylated chitosan nanoparticles grafted with Arg-Gly-Asp (RGD). Mol. Pharm. 9, 1736–1747.

Mu, C.F., Balakrishnan, P., Cui, F.D., Yin, Y.M., Lee, Y.B., Choi, H.G., Yong, C.S., Chung, S.J., Shim, C.K., Kim, D.D., 2010. The effects of mixed MPEG-PLA/Pluronic copolymer micelles on the bioavailability and multidrug resistance of docetaxel. Biomaterials 31, 2371–2379.

Nogueira, D.R., Tavano, L., Mitjans, M., Pérez, L., Infante, M.R., Vinardell, M.P., 2013. In vitro antitumor activity of methotrexate via pH-sensitive chitosan nanoparticles. Biomaterials 34, 2758–2772.

Nukolova, N.V., Oberoi, H.S., Cohen, S.M., Kabanov, A.V., Bronich, T.K., 2011. Folate-decorated nanogels for targeted therapy of ovarian cancer. Biomaterials 32, 5417–5426.

Owens 3rd, D.E., Peppas, N.A., 2006. Opsonization, biodistribution, and pharmacokinetics of polymeric nanoparticles. Int. J. Pharm. 307, 93–102.

Qu, G., Yao, Z., Zhang, C., Wu, X., Ping, Q., 2009. PEG conjugated N-octyl-O-sulfate chitosan micelles for delivery of paclitaxel: in vitro characterization and in vivo evaluation. Eur. J. Pharm. Sci. 37, 98–105.

Rausch, K., Reuter, A., Fischer, K., Schmidt, M., 2010. Evaluation of nanoparticle aggregation in human blood serum. Biomacromolecules 11, 2836–2839.

Termsarasab, U., Cho, H.J., Kim, D.H., Chong, S., Chung, S.J., Shim, C.K., Moon, H.T., Kim, D.D., 2013a. Chitosan oligosaccharide-arachidic acid-based nanoparticles for anti-cancer drug delivery. Int. J. Pharm. 441, 373–380.

Termsarasab, U., Cho, H.J., Moon, H.T., Park, J.H., Yoon, I.S., Kim, D.D., 2013b. Self-assembled magnetic resonance imaging nanoprobes based on arachidyl chitosan for cancer diagnosis. Colloids Surf. B: Biointerfaces 109, 280–286.

Veronese, F.M., Schiavon, O., Pasut, G., Mendichi, R., Andersson, L., Tsirk, A., Ford, J., Wu, G., Kneller, S., Davies, J., Duncan, R., 2005. PEG–doxorubicin conjugates: influence of polymer structure on drug release, in vitro cytotoxicity, biodistribution, and antitumor activity. Bioconjug. Chem. 16, 775–784.

Xiao, Z., Levy-Nissenbaum, E., Alexis, F., Lupták, A., Teply, B.A., Chan, J.M., Shi, J., Digga, E., Cheng, J., Langer, R., Farokhzad, O.C., 2012. Engineering of targeted nanoparticles for cancer therapy using internalizing aptamers isolated by cell-uptake selection. ACS Nano 6, 696–704.

Yadav, K.S., Jacob, S., Sachdeva, G., Chuttani, K., Mishra, A.K., Sawant, K.K., 2011. Long circulating PEGylated PLGA nanoparticles of cytarabine for targeting leukemia. J. Microencapsul. 28, 729–742.

Yang, T., Choi, M.K., Cui, F.D., Kim, J.S., Chung, S.J., Shim, C.K., Kim, D.D., 2007. Preparation and evaluation of paclitaxel-loaded PEGylated immunoliposome. J. Control. Release 120, 169–177.

Zauner, W., Ogris, M., Wagner, E., 1998. Polylysine-based transfection systems utilizing receptor-mediated delivery. Adv. Drug Deliv. Rev. 30, 97–113.

Zhang, L., Zhao, Z.L., Wei, X.H., Liu, J.H., 2013. Preparation and in vitro and in vivo characterization of cyclosporin A-loaded, PEGylated chitosan-modified, lipid-based nanoparticles. Int. J. Nanomedicine 8, 601–610.